Master's Programme in Electronics and Nanotechnology

Invisible Cavity Resonators

Francisco Cuesta

Aalto University

MASTER'S
THESIS

Aalto University
MASTER'S THESIS 2018

Invisible Cavity Resonators

Francisco Cuesta

Thesis submitted in partial fulfillment of the requirements for the degree of Master of Science in Electronics and Nanotechnology.
Otaniemi, 17th Sep 2018

Supervisor: Prof. Sergei Tretyakov
Advisor: D. Sc. Viktar Asadchy

Aalto University
School of Electrical Engineering
Master's Programme in Electronics and Nanotechnology

Author
Francisco Cuesta

Title
Invisible Cavity Resonators

School School of Electrical Engineering

Master's programme Electronics and Nanotechnology

Major Radio Science and Engineering **Code** ELEC3038

Supervisor Prof. Sergei Tretyakov

Advisor D. Sc. Viktar Asadchy

Level Master's thesis **Date** 17 Sep 2018 **Pages** 89 **Language** English

Abstract

This thesis studies one-dimensional structures based on a volume bounded by two metasurfaces. The main objective is to determine the properties of the metasurfaces such that under illumination by a normally incident plane wave the whole structure does not scatter; while the electromagnetic fields inside the bounded volume are not zero and can be tailored. Such invisible resonators are analysed from different perspectives: standing wave ratio, convergence, bandwidth, impact of dissipation losses, reciprocity, and effect of different objects inside the resonator. This thesis also introduces some concepts related to volumes bounded by multiple metasurfaces and some examples. Some applications for these resonators include cloaking and enhancing of low-power sensors.

Keywords sensing, cloaking, bounded volume, metasurface, resonance, Fabry-Perot resonator

Preface

I would like to thank:
All the people I love too much that hurts...
All the people I left behind, with the promise of seeing them again...
All the people I met during this time, who made me feel so powerless...
All the people who teached me, as I wanted to become their rival...

Because in order to go beyond my dreams:
I had to sacrifice all I had...
To start from zero, so I can achieve everything...
The only way I found to face my fate...
Was by accepting my crimes...

As this was the plan I made...
In order to show everyone, to proof myself...
That, no matter what can happen...

Life is beautiful.

At this point of my life, I have achieved the conclusion that there won't be enough words, sentences, and pages to express my thoughts and feeling to the persons whom I have met until now. On the other hand, it becomes completely natural, like a reflex, my desire to acknowledge (and forget about the previous sentence) all these special persons.

First of all, I want to thank my family but I have to say sorry to them, because they have to support the crazy ideas and dreams of their knuclehead relative.

I would like to thank my advisor, Viktar, for answering everyone of my questions (dummy, philosophical, abstract, and sometimes important) while he was patience and comprehensive. In the same way, I would like to express my gratitude to my supervisor, Sergei, for accepting a shy person of broad spectrum as a thesis student; also for not killing me after each thesis revision. I want to thank my friends at Sergei group, specially Sajjad, for showing interest in my research and giving valuable information and experience to continue forward. I want to acknowledge Prof. Ari Sihvola for reviewing my thesis at the last moment.

At the end, and as a strange way of acknowledgement, I would like to thank to whomever who reached this part of the preface without laughing. Also for not commenting the present preface.

Espoo, 16.7.2018

Francisco Cuesta

Contents

Symbols, notations and abbreviations

Symbols

$\lvert\mathrm{A}\rvert^2$	Absorbance of a resonator
$\lvert\tilde{\mathrm{A}}\rvert^2$	Absorbance of a single metasurface
a	Incoming travelling wave
B	Backward wave transfer coefficient
b	Outgoing travelling wave
d	Distance between metasurfaces
$\mathbf{E}$	Electric field
F	Forward wave transfer coefficient
f	Frequency
$\mathbf{H}$	Magnetic field
$\mathbf{J}_\mathrm{e}$	Electric surface current density
$\mathbf{J}_\mathrm{m}$	Magnetic surface current density
k	Medium wavenumber
k_0	Vacuum wavenumber
$\tilde{k}$	Normalized wavenumber k with respect to that in vacuum k_0
k_Δ	Wavenumber at the cutoff frequency
$\mathbf{M}$	Magnetic surface polarization density

$\mathrm{m}_{90\%}$	Convergent cycle (using a criterion of 90%)
$\mathbf{n}$	Normal unitary vector to a given surface
$\mathbf{P}$	Electric surface polarization density
P_{im}	Reactive power
P_{re}	Active power
Q	Quality factor
R_{e}	Electric grid resistance
R_{m}	Magnetic grid resistance
$[S]$	Scattering matrix
S_{e}	Normalized standing wave function
$[T]$	T-parameter matrix
X_{e}	Electric grid reactance
X_{m}	Magnetic grid reactance
$\bar{\bar{Y}}_{\mathrm{e}}$	Electric sheet admittance dyadic
Y_{e}	Electric grid admittance
Y_{m}	Magnetic grid admittance
Y_{eq}	Equivalent admittance
$\bar{\bar{Z}}_{\mathrm{m}}$	Magnetic sheet impedance dyadic
Z_{e}	Electric grid impedance
Z_{m}	Magnetic grid impedance
$[Z]$	Impedance matrix, Z-matrix
Z_{eq}	Equivalent impedance
Γ	Reflection coefficient of a resonator
$\tilde{\Gamma}$	Reflection coefficient of a single metasurface
γ	Propagation constant
δ_d	Position of an object inside an invisible cavity resonator

ε	Medium permittivity
ε_0	Vacuum permittivity
ε_r	Medium relative permittivity
$\mathcal{E}_\mathrm{f}$	Enhancement factor
η	Medium characteristic impedance
η_0	Vacuum characteristic impedance
$\bar{\bar{\kappa}}$	Magnetoelectric coupling dyadic
λ	Medium wavelength
λ_0	Vacuum wavelength
μ	Medium permeability
μ_0	Vacuum permeability
μ_r	Medium relative permeability
$\bar{\bar{\xi}}$	Electromagnetic coupling dyadic
ρ_e	Electric charge density
ρ_m	Magnetic charge density
τ	Transmission coefficient of a resonator
$\tilde{\tau}$	Transmission coefficient of a single metasurface
ϕ	Phase factor
$\bar{\bar{\chi}}_\mathrm{ee}$	Metasurface surface suceptibility electric/electric coupling dyadic
$\bar{\bar{\chi}}_\mathrm{em}$	Metasurface surface suceptibility electric/magnetic coupling dyadic
$\bar{\bar{\chi}}_\mathrm{me}$	Metasurface surface suceptibility magnetic/electric coupling dyadic
$\bar{\bar{\chi}}_\mathrm{mm}$	Metasurface surface suceptibility magnetic/magnetic coupling dyadic
Ψ	Resonance factor

ω_0	Angular frequency at resonance
$\Delta\omega$	Half-power bandwidth

Operators

a^*	Complex conjugate of variable a
∇a	Gradient of variable a
$\tilde{Z}$	Normalized impedance Z with respect to vacuum impedance η_0
$\hat{\mathbf{A}}$	Arithmetic average value of field $\mathbf{A}$ at a discontinuity
$\mathbf{A}_{\parallel}$	Tangential component of vector $\mathbf{A}$ with respect to a given surface
A_n	Normal component of vector $\mathbf{A}$ with respect to a given surface
$\mathbf{A} \cdot \mathbf{B}$	Dot product of vectors $\mathbf{A}$ and $\mathbf{B}$
$\nabla \cdot \mathbf{A}$	Divergence of vector $\mathbf{A}$
$\nabla \times \mathbf{A}$	Curl of vector $\mathbf{A}$

Notation

$\mathbf{A}$	Vector $\mathbf{A}$
a	Variable a
a_+	Value of variable a at $z > 0$
a_-	Value of variable a at $z < 0$
$\bar{\bar{\alpha}}$	Dyadic $\bar{\bar{\alpha}}$
$[T]$	Matrix $[T]$
T_{ij}	Matrix $[T]$ element at the i-th row and j-th column

Abbreviations

B	Backward (subindex)
BIC	Bound state in the continuum
DER	Double-electric resonator
ds	Fabry-Perot resonator with a dielectric slab (subindex)
EPM	Electrically polarizable metasurface
EMPM	Electrically and magnetically polarizable metasurface
F	Forward (subindex)
fs	Free space (subindex)
FPR	Fabry-Perot resonator
GSTC	Generalized sheet transition conditions
I	Incident (subindex)
ICR	Invisible cavity resonator
MER	Magnetic-electric resonator
MLR	Matryoshka-like resonator
MPM	Magnetically polarizable metasurface
PEC	Perfect electric conductor
PMC	Perfect magnetic conductor
S	Standing (subindex)
s	Current sheet, sensor
SWR	Standing wave ratio
T	Transmitted (subindex)
TER	Triple-electric resonator
ws	Fabry-Perot resonator with two conductive plates (subindex)

1. Introduction

Flatland is a book written by Edwin A. Abbott in 1885 [1]. In that literature work, the main character "A Square" tries to understand and to explain the complexities of lower and higher dimensions (the book also comments about Victorian hierarchical society). The relation between Flatland and Spaceland, or between "A Square" and "Sphere", is used by Rudy Rucker as an analogy to understand the complexities related with the fourth dimension [2]. At some point, Rucker starts discussing about the form of the space, and the case when a region of the space could be "pinched-off" and disconnected from the rest. This scenario implies that there is a part of the space that cannot be seen by the rest, in other words, a hidden region. Unfortunately, we cannot take apart regions of space; but the idea of making them invisible (and hiding them) is still fascinating.

Figure 1.1. A Square, as seen in [2].

Expanding this concept, we can imagine how an object (like a box) could be invisible. We can think that an invisible box could be like a piece of "solid" air: we can see through it, without seeing the box, we can interact with it (e.g., mechanically) but not observe it. Let us consider the case when another visible object is inside the box. Thanks to the properties of the box, we are able to see "through" both objects, the box and the object. At this point, two scenarios could occur if the object inside the box is moved: first, the box and the object are still not visible; second, we can see a distorted version of the box and the object. In the first scenario, we say that the box is a *"cloaking device"* [3–6], because it can make the whole region inside it invisible. But, in the second case, the box is called an *"invisibility device"*, because it operates only under some specific conditions

(like the position or the shape of the objects inside and their interaction with the box). To summarize, a cloaking device is able to create an electromagnetically void region, remaining invisible regardless of the object inside the region. On the other hand, an invisibility device cannot create this void, producing internal fields inside it, but invisible from the outside. This thesis will be focused on the second case, where the box is an invisibility device.

Linked with the previous example, it is convinient to think about different phenomena happening outside and inside an invisibility device. Outside of the device, there are no scattered fields and the incident waves remain unchanged, as if the device was not there. To realize this scenario, the device not only requires total transparency to become invisible, but also that the phases of the transmitted waves remain unchanged. For most applications, this phase constrain is not even considered, but from the formal point of view, it is compulsory that there is no change in magnitude nor in phase. Therefore, this invisibility device can be considered as nonscattering. There are examples of how these structures can be realized in the optical range for a fixed incident wave, as shown in [7], and extending the concept to obtain a non-radiating scatterer supporting multiple incident directions [8]; unfortunately, it has been shown that there are no isotropic scatters [9]. This thesis will consider only one incident wave with an one-dimensional invisibility device (which bounds an invisible region). Opposite to the cloaking device (which creates an electromagnetic void), it is reasonable to think that there are fields inside the invisibility device. Because the device does not produce any scattering, the energy of the inner fields cannot flow away and it remains confined inside. In that case, the region inside the device can be also considered as a bound state in the continuum (BIC) [10]. The first proposal of BICs was published in von Neumann and Wigner's work [11]; which has been used as a starting point for following studies, covering different physics branches: photonics, quantum, acoustics and others [10, 12–18]. In each field, the research of BICs is promising but it also deals with the disadvantages of each technology. For example, acoustic-wave devices are sensitive to a large number of physical parameters (temperature, pressure, stress) [19]; or, like in the case of photonic crystals, to the internal losses produced by multiple reflections [20]. In this respect, it is convenient to think of optical devices which can be modified to become a BIC.

In optics, a well-known device is the laser (light amplification by stimulated emission of radiation), which uses two mirrors to increase the number of photons excited in the active medium by an external source [21]. The generated light can go outside the gain medium through one of the mirrors, which is semitransparent. If we take only the mirrors, and we make both semitransparent, we can

obtain a structure that can support a BIC. This structure is known as a Fabry-Perot resonator (FPR), which was developed by Charles Fabry and Alfred Perot in 1899 [22, 23]. There are at least three different kinds of FPRs: two parallel plates placed at a given distance in a homogeneous medium (e.g. free space), two parallel plates separated by a dielectric spacer, and a single dielectric slab (interferences are produced by the difference of the refraction index between the slab and the surrounding medium) [24]. Due to their high quality factor, the most common use of FPRs is in spectroscopy, in particular for interferometers [25]. Due to that, analysis of FPRs was mostly focussed on the transmitted and reflected powers (transmittance and reflectance, respectively), without considering the phase of the transmitted wave, in other words, scattering. It can be shown that FPRs based on dielectric slab can achieve zero-phase transmission. A disadvantage of the dielectric slab is the need of a trade-off between obtaining high internal reflection (by using dielectrics with high permittivity [13]) and the propagation through the slab, as it cannot be used to enhance the magnitude of the internal fields. In that case, it is necessary to use low-loss metal coating layers (or metallic plates in the free-space case) to increase the reflection coefficient without compromising the propagation through the resonator. It is a common practice to use two identical metallic layers. However, a FPR without a dielectric slab cannot achieve zero-phase transmission. Considering that the presence or absence of metallic layers and dielectric slab can be interpreted as extreme cases of their physical properties, it is reasonable to think that achieving zero-phase transmission with a dielectric-based FPR is possible. In that case, it could be possible that the resonator characteristics (dimensions, metallic layers) differ to a slab-based resonator. Therefore, it is compulsory to analyse the general case where a resonator formed by two plates with well-defined properties, with or without a dielectric slab, can achieve an invisibility state with zero-phase transmission. But, what kind of plates should be used for this purpose? Due to the limited properties of conventional materials, probably the best candidates are metamaterials.

X, the mathematical variable which represents limitless possibilities [26]; used to represent something that can be definded or changed at will. In science and engineering, metamaterials have become this variable to achieve new and fascinating applications. Defined as “an arrangement of artificial structural elements, called meta-atoms, designed to achieve advantageous and unusual electromagnetic properties” [27], metamaterials can be the adequate approach for designing an invisibility device. More specifically, metasurfaces (optically thin two-dimensional analogues of metamaterials) can be used to create such “open” cavity resonators, or invisible cavity resonators (ICRs). There are interesting applications for ICRs,

as using them to reduce the scattering cross section of a given object or to increase the captured power of a small sensor. In order to explore the possibilities of this kind of structures, the objective of this thesis is to determine the conditions to create an invisible cavity resonator, with zero-phase transmission, while tailoring the fields inside it. For simplicity, this study will consider an one-dimensional scenario, where a region is bounded by two metasurfaces; and a normal-incidence wave illuminates the structure.

This thesis is structured as follows. After this introductory section, a theoretical analysis of metasurfaces will be performed. The main purpose of Chapter 2 is to develop a basic model of isotropic metasurfaces (in the plane), which considers the interactions of meta-atoms with the fields around them. Additionally, this section will define the primary conditions of the three kinds of metasurfaces used in this study: Electrically Polarizable Metasurfaces, Magnetically Polarizable Metasurfaces, and Electrically and Magnetically Porlarizable Metasurfaces. In Chapter 3, the invisibility conditions are found for ICRs for two cases: when the region is bounded by two electrically polarizable metasurfaces, and also when this region is bounded by a magnetically polarizable metasurface and an electrically polarizable metasurface. In order to have a deeper understanding of its invisibility properties, Chapters 4 and 5 evaluate the structure performance under different scenarios through a detailed theoretical analysis. Chapter 4 considers some basic aspects related with these structures, focused on developing design criteria related with its properties. Finally, Chapters 5 considers the effects of placing objects with different properties inside the resonator: active, lossy and reactive objects. These analyses will help us to determine the capabilities of this invisible structure related to sensing enhancement and cloaking.

2. Scattered fields produced by thin surfaces

2.1 Generalized sheet transition conditions

The properties of a periodic mesurface are defined by the composition and arrangement of its meta-atoms over the host material. The meta-atoms can be modelled as electrically and magentically polarizable entitites, making possible to define electric and magnetic surface polarization densities $\mathbf{P}$ and $\mathbf{M}$, respectively [28]. These polarization densities depend on the surrounding electromagnetic fileds, as shown in Figure 2.1, and on metasurface properties:

$$\mathbf{P} = \varepsilon \bar{\bar{\chi}}_{\mathrm{ee}} \cdot \hat{\mathbf{E}} + \bar{\bar{\chi}}_{\mathrm{em}} \cdot \sqrt{\varepsilon\mu}\hat{\mathbf{H}}, \tag{2.1a}$$

$$\mathbf{M} = \bar{\bar{\chi}}_{\mathrm{mm}} \cdot \hat{\mathbf{H}} + \bar{\bar{\chi}}_{\mathrm{me}} \cdot \sqrt{\frac{\varepsilon}{\mu}}\hat{\mathbf{E}}, \tag{2.1b}$$

where $\bar{\bar{\chi}}$ are the metasurface transverse susceptiblity polarization responses written in dyadic form: for the electric/electric 'ee', electric/magnetic 'em', magnetic/magnetic 'mm', and magnetic/electric 'mm' couplings [29]. $\hat{\mathbf{E}}$ and $\hat{\mathbf{H}}$ are the average electric and magnetic fields, respectively, around the metasurface:

$$\hat{\mathbf{E}} = \frac{\mathbf{E}_+ + \mathbf{E}_-}{2}, \qquad \hat{\mathbf{H}} = \frac{\mathbf{H}_+ + \mathbf{H}_-}{2}, \tag{2.2}$$

where $\mathbf{E}_-$ is the total tangential electrical field "before" the metasurface ($z = -0$ if the metasurface is placed at origin), and $\mathbf{E}_+$ is the total electrical field "after" the metasurface ($z = +0$).

Since the metasurface thickness is assumed to be negligible, it must be considered as an electromagentic discontinuity in space [28], and because metasurfaces can be polarized also in the normal direction, conventional boundary conditions cannot be used. Instead, the generalized sheet transition conditions (GSTCs) (for

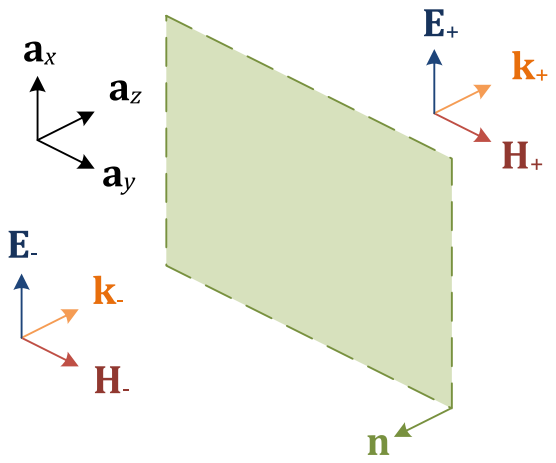

Figure 2.1. Electromagnetic fields around a metasurface placed in free space

time harmonic fields with $\exp(j\omega t)$) [28] must be applied:

$$\mathbf{n} \times (\mathbf{E}_+ - \mathbf{E}_-) = -\left(j\omega\mu\mathbf{M}_\parallel - \mathbf{n} \times \nabla_\parallel \frac{P_n}{\varepsilon}\right), \tag{2.3a}$$

$$\mathbf{n} \times (\mathbf{H}_+ - \mathbf{H}_-) = j\omega\mathbf{P}_\parallel + \mathbf{n} \times \nabla_\parallel M_n, \tag{2.3b}$$

$$\mathbf{n} \cdot (\mathbf{D}_+ - \mathbf{D}_-) = \nabla \cdot \mathbf{P}_\parallel, \tag{2.3c}$$

$$\mathbf{n} \cdot (\mathbf{B}_+ - \mathbf{B}_-) = \mu\nabla \cdot \mathbf{M}_\parallel, \tag{2.3d}$$

where $\mathbf{n}$ is the unitary vector orthogonal to the metasurface, $\parallel$ denotes the components parallel to the metasurface (in the u-v plane), ∇ by itself denotes the gradient function and $\nabla\cdot$ correspond to the divergence. ε and μ correspond to the permittivity and permeability of the supporting medium where the meta-atoms are placed.

The use of the GSTCs is a straight-forward method to define the field jumps if the polarization vectors are known. One method to simplify the GSTCs is by using Huygens equivalent principle and the duality theorem [30–36], and characterize the metasurface by its effective electric and magnetic charges and currents ($\mathbf{J}_\mathrm{e}$, $\mathbf{J}_\mathrm{m}$, ρ_e and ρ_m, respectively):

$$\mathbf{J}_\mathrm{m} = -\left(j\omega\mu\mathbf{M}_\parallel - \mathbf{n} \times \nabla_\parallel \frac{P_n}{\varepsilon}\right), \qquad \mathbf{J}_\mathrm{e} = j\omega\mathbf{P}_\parallel + \mathbf{n} \times \nabla_\parallel M_n, \tag{2.4a}$$

$$\rho_\mathrm{e} = \nabla \cdot \mathbf{P}_\parallel, \qquad \rho_\mathrm{m} = \mu\nabla \cdot \mathbf{M}_\parallel. \tag{2.4b}$$

Then, the GSTCs can be written as conventional boundary conditions:

$$\mathbf{n} \times (\mathbf{E}_+ - \mathbf{E}_-) = \mathbf{J}_\mathrm{m}, \qquad \mathbf{n} \times (\mathbf{H}_+ - \mathbf{H}_-) = -\mathbf{J}_\mathrm{e}, \tag{2.5a}$$

$$\mathbf{n} \cdot (\mathbf{D}_+ - \mathbf{D}_-) = \rho_\mathrm{e}, \qquad \mathbf{n} \cdot (\mathbf{B}_+ - \mathbf{B}_-) = \rho_\mathrm{m}. \tag{2.5b}$$

In general, as the effective charges (Equation (2.4b)) are already considered in

the analysis of the GSTCs (as done in [37, 38]), the relations shown in (2.5b) are not considered in some problems.

2.2 Anisotropic metasurfaces supporting electric and magnetic currents

The simplified approach of the GSTCs, shown in Equation (2.4), shows that it is possible to define the metasurface properties using equivalent induced electric and magnetic surface current densities. But the relationship between these currents and the electromagnetic fields around the metasurface is not so straightforward. Because of that, it is more convient to relate these currents to the fields:

$$\mathbf{J}_{\mathrm{e}} = \bar{\bar{Y}}_{\mathrm{e}} \cdot \hat{\mathbf{E}} + \bar{\bar{\kappa}} \cdot \hat{\mathbf{H}}, \tag{2.6a}$$

$$\mathbf{J}_{\mathrm{m}} = \bar{\bar{\xi}} \cdot \hat{\mathbf{E}} + \bar{\bar{Z}}_{\mathrm{m}} \cdot \hat{\mathbf{H}}, \tag{2.6b}$$

where $\bar{\bar{Y}}_{\mathrm{e}}$ is the electric sheet admittance dyadic, $\bar{\bar{Z}}_{\mathrm{m}}$ is the magnetic sheet impedance dyadic, $\bar{\bar{\kappa}}$ and $\bar{\bar{\xi}}$ corresponds to the dimentionless magnetoelectric and electromagnetic coupling dyadics, respectively [29]. This thesis will be focused on a specific kind of metasurfaces, reffered to as anisotropic, whose meta-atoms does not produce any electromangetic coupling ($\bar{\bar{\kappa}} = \bar{\bar{\xi}} = 0$) [39]. From this group of metasurfaces, it is still possible to classify them according to their polarization's nature: Electrically Polarizable Metasurfaces (EPMs), Magnetically Polarizable Metasurfaces (MPMs), and Electrically and Magnetically Polarizable Metasurfaces (EMPMs). EPMs are characterized for the presence of only superficial electric currents densities, produced by meta-atoms which are not effective-loops, such as metal patches or strips of different shapes [39]. On the other hand, MPMs have only superficial magnetic current densities, produced by the antisymetric component of the induced electric-current distribution, which can be obtained using effective loops [39], such two layers of patch array sheets with different induced electrical currents. In both cases, the GSTCs can be simplified even more; unlike EMPMs, which preserve both kind of superficial current densities. In the next part, we'll consider the properties these different kind of metasurfaces.

2.2.1 Electrically polarizable metasurfaces

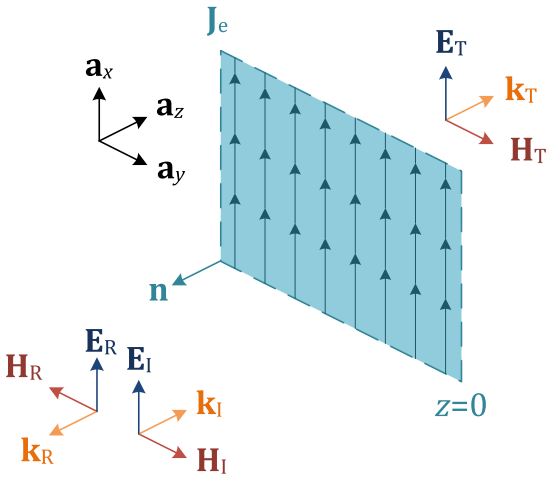

Figure 2.2. Normal-incidence scenario for an EMP.

If we consider the case where a metasurface can be modelled only by electric current densities, the GSTCs can be simplified:

$$\mathbf{E}_+ - \mathbf{E}_- = 0, \tag{2.7a}$$

$$\mathbf{n} \times (\mathbf{H}_+ - \mathbf{H}_-) = -\mathbf{J}_\mathrm{e}. \tag{2.7b}$$

From the definition of the electric and magnetic currents of (2.6), EPMs are the ones which is characterized by only the electric sheet admittance dyadic. Because of that, the electric induced current density is proportional to the average electrical field, expressed in Equation (2.2), as shown in Equation (2.8), where $\bar{\bar{Z}}_\mathrm{e}$ is the metasurface grid impedance (equivalent to the inverse dyadic of the electric sheet admittance dyadic). Also, because of the conditions of Equation (2.7a), the electric surface current density can be defined by the electric field located at one side of the metasurface:

$$\bar{\bar{Z}}_\mathrm{e} \cdot \mathbf{J}_\mathrm{e} = \hat{\mathbf{E}} = \mathbf{E}_+ = \mathbf{E}_-. \tag{2.8}$$

Let us consider the scenario shown in Figure 2.2, where an infinite EPM, placed at the origin, is illuminated by an incident plane wave with the wavevector normal to the metasurface. Based on the general case, we can assume different media before and after the metasurface, characterized by their wavenumber k and characteristic impedance η. The medium before the metasurface is denoted by the minus "$-$" subindex, and the plus "$+$" is used for the medium after the metasurface. The interaction between the metasurface and the incident wave produces two scattering waves: one with the same direction as the incident wave and another one with the opposite direction. We will call the first one the transmitted wave, and the second one as the reflected wave. The mathematical expressions for these

three waves are written as

$$\mathbf{E}_{\mathrm{I}} = E_{\mathrm{I}} e^{-jk_- z}\mathbf{a}_{\mathrm{x}}, \qquad \mathbf{H}_{\mathrm{I}} = H_{\mathrm{I}} e^{-jk_- z}\mathbf{a}_{\mathrm{y}}, \tag{2.9a}$$

$$\mathbf{E}_{\mathrm{R}} = E_{\mathrm{R}} e^{jk_- z}\mathbf{a}_{\mathrm{x}}, \qquad \mathbf{H}_{\mathrm{R}} = -H_{\mathrm{R}} e^{jk_- z}\mathbf{a}_{\mathrm{y}}, \tag{2.9b}$$

$$\mathbf{E}_{\mathrm{T}} = E_{\mathrm{T}} e^{-jk_+ z}\mathbf{a}_{\mathrm{x}}, \qquad \mathbf{H}_{\mathrm{T}} = H_{\mathrm{T}} e^{-jk_+ z}\mathbf{a}_{\mathrm{y}}. \tag{2.9c}$$

We can consider the grid impedance as isotropic in the x-y plane, so the dyadic form $\bar{\bar{Z}}_{\mathrm{e}}$ can be replaced by the scalar form Z_{e}. Under this conditions, the GSTCs can be written as

$$E_{\mathrm{I}} + E_{\mathrm{R}} = E_{\mathrm{T}}, \tag{2.10a}$$

$$E_{\mathrm{T}}\left(\frac{1}{\eta_+} + \frac{1}{Z_{\mathrm{e}}}\right) = \frac{1}{\eta_-}\left(E_{\mathrm{I}} - E_{\mathrm{R}}\right). \tag{2.10b}$$

Then, this equation system is solved by defining two transfer functions:

$$\tilde{\tau} = \frac{E_{\mathrm{T}}}{E_{\mathrm{I}}} = \frac{2}{1 + \eta_-\left(\dfrac{1}{Z_{\mathrm{e}}} + \dfrac{1}{\eta_+}\right)}, \tag{2.11a}$$

$$\tilde{\Gamma} = \frac{E_{\mathrm{R}}}{E_{\mathrm{I}}} = \frac{1 - \eta_-\left(\dfrac{1}{Z_{\mathrm{e}}} + \dfrac{1}{\eta_+}\right)}{1 + \eta_-\left(\dfrac{1}{Z_{\mathrm{e}}} + \dfrac{1}{\eta_+}\right)}, \tag{2.11b}$$

$$\tilde{J}_{\mathrm{e}} = \frac{J_{\mathrm{e}}}{E_{\mathrm{I}}} = \frac{2}{Z_{\mathrm{e}} + \eta_-\left(1 + \dfrac{Z_{\mathrm{e}}}{\eta_+}\right)}, \tag{2.11c}$$

$$1 = \tilde{\tau} - \tilde{\Gamma} \tag{2.11d}$$

where $\tilde{\Gamma}$ is the transfer function for the reflected wave and $\tilde{\tau}$ is the transfer function for the transmitted wave. Additionally, Equation (2.11c) gives the induced current $\tilde{J}_{\mathrm{e}}$ at the metasurface. By comparing both scattering coefficients, the primal relation of Equation (2.11d) is achieved; independent of the grid impedance and the surrounding media.

If we consider the case when the metasurface is placed in free space ($\eta_- = \eta_+ = \eta_0$), the expressions of Equation (2.11) can be reduced even more. For ease of use, we can denote by $\tilde{Z}_{\mathrm{e}}$ the normalized version of the grid impedance with respect to the free-space characteristic impedance η_0

$$Z_{\mathrm{e}} = \tilde{Z}_{\mathrm{e}}\eta_0. \tag{2.12}$$

Thanks to that, the transfer functions can be reduced to

$$\tilde{\tau} = \frac{2\tilde{Z}_\mathrm{e}}{2\tilde{Z}_\mathrm{e}+1}, \tag{2.13a}$$

$$\tilde{\Gamma} = -\frac{1}{2\tilde{Z}_\mathrm{e}+1}, \tag{2.13b}$$

$$\tilde{J}_\mathrm{e} = \frac{2}{\eta_0\left(2\tilde{Z}_\mathrm{e}+1\right)}. \tag{2.13c}$$

To understand the properties of the metasurface, it is convenient to split the grid impedance into its resistive and reactive components: $Z_\mathrm{e} = R_\mathrm{e} + jX_\mathrm{e}$. A figure of merit is the scattered power, characterized by the transmittance and reflectance. These parameters are defined as the squared values of the magnitude of the transmission and reflection coefficient, respectively:

$$|\tilde{\tau}|^2 = \frac{4\left(\tilde{R}_\mathrm{e}^2+\tilde{X}_\mathrm{e}^2\right)}{\left(2\tilde{R}_\mathrm{e}+1\right)^2+4\tilde{X}_\mathrm{e}^2}, \tag{2.14a}$$

$$|\tilde{\Gamma}|^2 = \frac{1}{\left(2\tilde{R}_\mathrm{e}+1\right)^2+4\tilde{X}_\mathrm{e}^2}. \tag{2.14b}$$

Absorbance $|\tilde{A}|^2$ measures the power which was not reflected nor transmitted by the metasurface. In the case of EPMs, the analytical expression for the combined reflected and transmitted powers and the absorbance are written as:

$$|\tilde{\tau}|^2 + |\tilde{\Gamma}|^2 = \frac{4\left(\tilde{R}_\mathrm{e}^2+\tilde{X}_\mathrm{e}^2\right)+1}{\left(2\tilde{R}_\mathrm{e}+1\right)^2+4\tilde{X}_\mathrm{e}^2}, \tag{2.15a}$$

$$|\tilde{A}|^2 = 1 - \left(|\tilde{\tau}|^2 + |\tilde{\Gamma}|^2\right) = \frac{4\tilde{R}_\mathrm{e}}{\left(2\tilde{R}_\mathrm{e}+1\right)^2+4\tilde{X}_\mathrm{e}^2}. \tag{2.15b}$$

Analysing Equation (2.15), allows us to extract certain properties of EPMs, based on the grid resistance R_e. The metasurface is called “active” when the grid resistance has a negative value, because the absorbance has a negative value, corresponding to a radiating surface. On the other hand, the metasurface is called “lossy” when the grid resistance has a positive value, as the absorbance has a positive value. It is only at the absence of grid resistance that the metasurface is “lossless”, and the total scattered power is equal to the incident power, meaning that the metasurface has zero absorbance. In the previous cases, the metasurface properties are not defined by the grid reactance. From (2.15b), it can be extracted another scenario where absorbance could reach values close to zero, when the grid impedance has high values. This particular result is achieved because the

meta-atoms are difficult to excite and, considering this scenario in Equation (2.13), the metasurface becomes transparent.

2.2.2 Magnetically polarizable metasurfaces

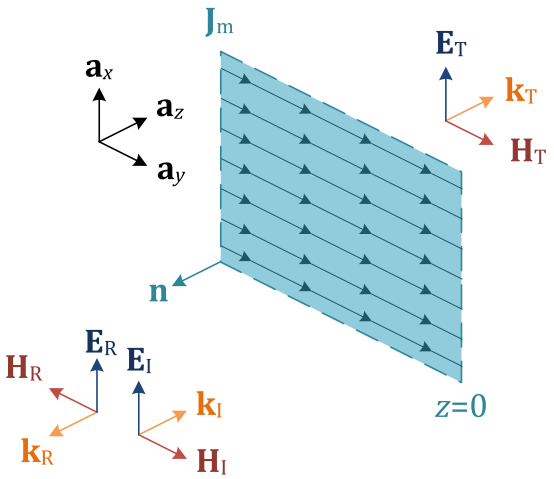

Figure 2.3. Normal-incidence scenario for an MPM.

Based on a similar analysis, the GSTCs for an MPM, where there is only induced magnetic current density

$$\mathbf{n} \times (\mathbf{E}_+ - \mathbf{E}_-) = \mathbf{J}_\mathrm{m}, \tag{2.16a}$$

$$\mathbf{H}_+ - \mathbf{H}_- = 0. \tag{2.16b}$$

Similarly to the EPM case, the induced magnetic current density $\mathbf{J}_\mathrm{m}$ can be expressed as proportional to the average magnetic field around the metasurface

$$\bar{\bar{Y}}_\mathrm{m} \cdot \mathbf{J}_\mathrm{m} = \hat{\mathbf{H}} = \mathbf{H}_+ = \mathbf{H}_-, \tag{2.17}$$

where $\bar{\bar{Y}}_\mathrm{m}$ represents the magnetic grid admittance (equivalent to the inverse dyadic of the magnetic sheet impedance dyadic). Due to the continuity of the magnetic field across the metasurface, as shown in (2.16b), the induced magnetic current density can be also defined as proportional to the net magnetic field located at one side of the metasurface. Let us consider the scenario shown in Figure 2.3, with similar conditions used with an infinite size EPM, hence the scattered fields, shown in Equation (2.9), with an isotropic grid impedance remain valid for this analysis. Under these conditions, the GSTCs can be written as

$$E_\mathrm{I} + E_\mathrm{R} = E_\mathrm{T}\left(1 + \frac{Z_\mathrm{m}}{\eta_+}\right), \tag{2.18a}$$

$$\frac{1}{\eta_-}\left(E_\mathrm{I} - E_\mathrm{R}\right) = \frac{E_\mathrm{T}}{\eta_+}. \tag{2.18b}$$

This equation system can be solved by defining the transfer function corresponding to the reflected wave $\tilde{\Gamma}$, the transmitted wave $\tilde{\tau}$, and the induced current density $\tilde{J}_\mathrm{m}$:

$$\tilde{\tau} = \frac{E_\mathrm{T}}{E_\mathrm{I}} = \frac{2\eta_+}{\eta_+ + \eta_- + Z_\mathrm{m}}, \tag{2.19a}$$

$$\tilde{\Gamma} = \frac{E_\mathrm{R}}{E_\mathrm{I}} = \frac{\eta_+ - \eta_- + Z_\mathrm{m}}{\eta_+ + \eta_- + Z_\mathrm{m}}, \tag{2.19b}$$

$$\tilde{J}_\mathrm{m} = \frac{J_\mathrm{m}}{H_\mathrm{I}} = \frac{2Z_\mathrm{m}\eta_-}{\eta_+ + \eta_- + Z_\mathrm{m}}, \tag{2.19c}$$

$$1 = \tilde{\tau} + \tilde{\Gamma}. \tag{2.19d}$$

Similarly to an EPM, the relation between the metasurface transmission and reflection coefficient is shown in Equation (2.19d). As the EPM case, a normalized grid impedance $\tilde{Z}_\mathrm{m}$ can be defined as

$$Z_\mathrm{m} = \tilde{Z}_\mathrm{m}\eta_0. \tag{2.20}$$

Then, the transfer functions for free space can be developed into

$$\tilde{\tau} = \frac{2}{2 + \tilde{Z}_\mathrm{m}}, \tag{2.21a}$$

$$\tilde{\Gamma} = \frac{\tilde{Z}_\mathrm{m}}{2 + \tilde{Z}_\mathrm{m}}, \tag{2.21b}$$

$$\tilde{J}_\mathrm{m} = \frac{2\tilde{Z}_\mathrm{m}\eta_0}{2 + \tilde{Z}_\mathrm{m}}. \tag{2.21c}$$

To understand the properties of the metasurface, it is convenient to split the grid impedance into its resistive and reactive components: $Z_\mathrm{m} = R_\mathrm{m} + jX_\mathrm{m}$. Like in the EPM case, it is possible to find the transmittance and reflectance:

$$|\tilde{\tau}|^2 = \frac{4}{\left(\tilde{R}_\mathrm{m} + 2\right)^2 + \tilde{X}_\mathrm{m}^2}, \tag{2.22a}$$

$$|\tilde{\Gamma}|^2 = \frac{\tilde{R}_\mathrm{m}^2 + \tilde{X}_\mathrm{m}^2}{\left(\tilde{R}_\mathrm{m} + 2\right)^2 + \tilde{X}_\mathrm{m}^2}. \tag{2.22b}$$

Both values are used to determine the total power and the absorbance, which can be reduced to

$$|\tilde{\tau}|^2 + |\tilde{\Gamma}|^2 = \frac{4 + \tilde{R}_\mathrm{m}^2 + \tilde{X}_\mathrm{m}^2}{\left(\tilde{R}_\mathrm{m} + 2\right)^2 + \tilde{X}_\mathrm{m}^2}, \tag{2.23a}$$

$$|\tilde{A}|^2 = \frac{4\tilde{R}_\mathrm{m}}{\left(\tilde{R}_\mathrm{m} + 2\right)^2 + \tilde{X}_\mathrm{m}^2}. \tag{2.23b}$$

By analysing the metasurface absorbance, it is possible to reach the same conclusions related to the metasurface properties in terms of the grid resistance. The metasurface is active when the grid resistance has a negative value, lossy when it has a positive value, and lossless when there the value of the grid resistance is zero. In all cases, this property is independent of the value of the grid reactance.

2.2.3 Electrically and magnetically polarizable metasurfaces

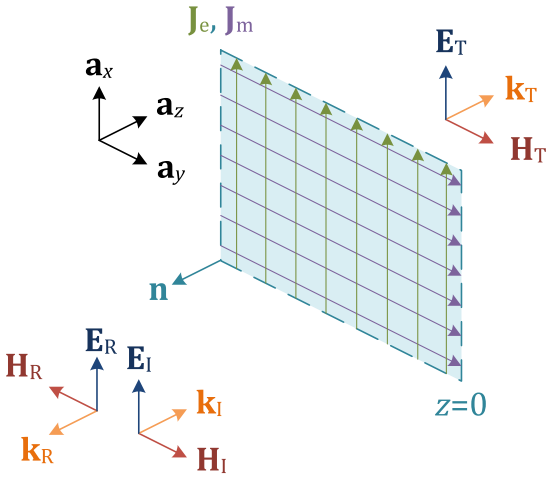

Figure 2.4. Normal-incidence scenario for an EMPM.

In a more general approach, the GSTCs for a generic metasurface can be written as

$$\mathbf{n} \times (\mathbf{E}_+ - \mathbf{E}_-) = \mathbf{J}_\mathrm{m}, \tag{2.24a}$$

$$\mathbf{n} \times (\mathbf{H}_+ - \mathbf{H}_-) = -\mathbf{J}_\mathrm{e}. \tag{2.24b}$$

The induced electric and magnetic current densities can be defined as shown in Equations (2.8) and (2.17); but given the GSTCs, it is not possible to consider the fields from only one side, and the averaged fields must be used. Using similar conditions as in the previous analysis, based on Figure 2.4, the GSTCs can be reduced to

$$E_\mathrm{I}\left(1 - \frac{Z_\mathrm{m}}{2\eta_-}\right) = E_\mathrm{T}\left(1 + \frac{Z_\mathrm{m}}{2\eta_+}\right) - E_\mathrm{R}\left(1 + \frac{Z_\mathrm{m}}{2\eta_-}\right), \tag{2.25a}$$

$$E_\mathrm{I}\left(\frac{2Z_\mathrm{e}}{\eta_-} - 1\right) = E_\mathrm{T}\left(\frac{2Z_\mathrm{e}}{\eta_+} + 1\right) + E_\mathrm{R}\left(\frac{2Z_\mathrm{e}}{\eta_-} + 1\right). \tag{2.25b}$$

This equation system is solved, as in the previous cases, by defining the transmission coefficient $\tilde{\tau}$, the reflection coefficient $\tilde{\Gamma}$, the electric $\tilde{J}_\mathrm{e}$ and the magnetic

normalized surface current $\tilde{J}_\mathrm{m}$:

$$\Delta = \left(1+\frac{Z_\mathrm{m}}{2\eta_-}\right)\left(\frac{2Z_\mathrm{e}}{\eta_+}+1\right)+\left(1+\frac{Z_\mathrm{m}}{2\eta_+}\right)\left(\frac{2Z_\mathrm{e}}{\eta_-}+1\right), \tag{2.26a}$$

$$\tilde{\tau} = \Delta^{-1}\left[\left(1+\frac{Z_\mathrm{m}}{2\eta_-}\right)\left(\frac{2Z_\mathrm{e}}{\eta_-}-1\right)+\left(1-\frac{Z_\mathrm{m}}{2\eta_-}\right)\left(\frac{2Z_\mathrm{e}}{\eta_-}+1\right)\right], \tag{2.26b}$$

$$\tilde{\Gamma} = \Delta^{-1}\left[\left(1+\frac{Z_\mathrm{m}}{2\eta_+}\right)\left(\frac{2Z_\mathrm{e}}{\eta_-}-1\right)-\left(1-\frac{Z_\mathrm{m}}{2\eta_-}\right)\left(\frac{2Z_\mathrm{e}}{\eta_+}+1\right)\right], \tag{2.26c}$$

$$\tilde{J}_\mathrm{e} = \frac{1}{2Z_\mathrm{e}}\left[1+\tilde{\Gamma}+\tilde{\tau}\right] \tag{2.26d}$$

$$\tilde{J}_\mathrm{m} = \frac{Z_\mathrm{m}\eta_-}{2}\left[\frac{1}{\eta_-}-\frac{\tilde{\Gamma}}{\eta_-}+\frac{\tilde{\tau}}{\eta_+}\right]. \tag{2.26e}$$

Because of the number of degrees of freedom, given by the electric and magnetic grid resistance and reactance, the analysis through the total power and absorbance is not useful to characterize properly a generic metasurface. Instead, it is more convenient to find out the dependency of the grid impedance for given transfer functions $\tilde{\tau}$ and $\tilde{\Gamma}$. In that case, the GSTCs of Equation (2.24) can be written as

$$1+\tilde{\Gamma}-\tilde{\tau} = \frac{Z_\mathrm{m}}{2}\left(\frac{1}{\eta_-}-\frac{\tilde{\Gamma}}{\eta_-}+\frac{\tilde{\tau}}{\eta_+}\right), \tag{2.27a}$$

$$\frac{1}{\eta_-}-\frac{\tilde{\Gamma}}{\eta_-}-\frac{\tilde{\tau}}{\eta_+} = \frac{1}{2Z_\mathrm{e}}\left(1+\tilde{\Gamma}+\tilde{\tau}\right). \tag{2.27b}$$

Then, the values of Z_e and Z_m are obtained directly:

$$Z_\mathrm{e} = \frac{\eta_-}{2}\frac{1+\tilde{\tau}+\tilde{\Gamma}}{1-\dfrac{\eta_-}{\eta_+}\tilde{\tau}-\tilde{\Gamma}}, \tag{2.28a}$$

$$Z_\mathrm{m} = 2\eta_-\frac{1-\tilde{\tau}+\tilde{\Gamma}}{1+\dfrac{\eta_-}{\eta_+}\tilde{\tau}-\tilde{\Gamma}}. \tag{2.28b}$$

In free-space conditions, the transfer functions for scattered waves and induced currents can be reduced to

$$\tilde{\tau} = \frac{1}{2}\left[\frac{2\tilde{Z}_\mathrm{e}-1}{2\tilde{Z}_\mathrm{e}+1}+\frac{2-\tilde{Z}_\mathrm{m}}{2+\tilde{Z}_\mathrm{m}}\right], \tag{2.29a}$$

$$\tilde{\Gamma} = \frac{1}{2}\left[\frac{2\tilde{Z}_\mathrm{e}-1}{2\tilde{Z}_\mathrm{e}+1}-\frac{2-\tilde{Z}_\mathrm{m}}{2+\tilde{Z}_\mathrm{m}}\right], \tag{2.29b}$$

$$\tilde{J}_\mathrm{e} = \frac{2}{\eta_0\left(2\tilde{Z}_\mathrm{e}+1\right)}, \tag{2.29c}$$

$$\tilde{J}_\mathrm{m} = \frac{2\tilde{Z}_\mathrm{m}\eta_0}{2+\tilde{Z}_\mathrm{m}}. \tag{2.29d}$$

Also, values of normalized grid impedances can be obtained based of the transfer

Surface	$\tilde{\tau}$	$\tilde{\Gamma}$	$\lvert\tilde{A}\rvert^2$	$\tilde{Z}_{\mathrm{e}}$	$\tilde{Z}_{\mathrm{m}}$
Invisible	1	0	0	∞	0
PEC	0	-1	0	0	0
PMC	0	1	0	∞	∞
Absorbing	0	0	1	$1/2$	2
Partially Transmitting	α	0	$1-\alpha^2$	$\frac{1}{2}\frac{\alpha+1}{1-\alpha}$	$2\frac{1-\alpha}{1+\alpha}$
Partially Reflecting	0	α	$1-\alpha^2$	$\frac{1}{2}\frac{\alpha+1}{1-\alpha}$	$2\frac{1+\alpha}{1-\alpha}$

Table 2.1. Grid impedances for certain types of surfaces

coefficients:

$$\tilde{Z}_{\mathrm{e}} = \frac{1}{2}\frac{1+\tilde{\tau}+\tilde{\Gamma}}{1-\tilde{\tau}-\tilde{\Gamma}}, \tag{2.30a}$$

$$\tilde{Z}_{\mathrm{m}} = 2\frac{1-\tilde{\tau}+\tilde{\Gamma}}{1+\tilde{\tau}-\tilde{\Gamma}}. \tag{2.30b}$$

Table 2.1 shows the equivalent grid impedances for some surfaces placed in a free-space environment.

If equations (2.15b) and (2.23b) are analysed, it is possible to conclude that it is not possible to obtain total absorption ($|\tilde{A}|^2 = 1$) by inducing only electric or only magnetic currents, because that would contradict to the results of (2.11d) and (2.19d). Instead, it is required both types of induced currents to create an absorbing surface, obtained by inducing electrical and magnetic coupling [40].

2.3 Metasurface as a two-port device

In the previous section it was shown that different kinds of metasurfaces can be characterized by their grid impedances and scattering coefficients, without the use of GSTCs. Because of that, it is really useful to perform a general extension of this abstraction level, based on scattering coeffients, such that more complex scenarios can be solved using the same approach. Some of these new possible scenarios assume that the metasurface could be illuminated from both sides, such as the presence of a second radiating source or when a reflective object is placed behind the metasurface. For that cases, it is appropriate to model the metasurface as a two-port device, as show in Figure 2.5.

In this approach, the outgoing waves $\mathbf{E}_{\mathrm{OUT}-}$ and $\mathbf{E}_{\mathrm{OUT}+}$ and incoming waves

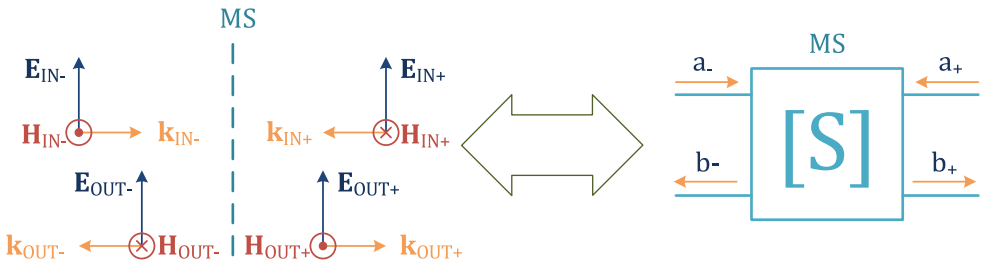

Figure 2.5. Equivalent model for a two-side illumimated metasurface.

$\mathbf{E}_{\mathrm{IN}-}$ and $\mathbf{E}_{\mathrm{IN}+}$ are represented by parameters a_-, a_+, b_- and b_+ written as

$$a_- = \frac{E_{\mathrm{N}-} + \eta_- H_{\mathrm{N}-}}{2\sqrt{\eta_-}}, \quad b_- = \frac{E_{\mathrm{N}-} - \eta_- H_{\mathrm{N}-}}{2\sqrt{\eta_-}}, \tag{2.31a}$$

$$a_+ = \frac{E_{\mathrm{N}+} - \eta_+ H_{\mathrm{N}+}}{2\sqrt{\eta_+}}, \quad b_+ = \frac{E_{\mathrm{N}+} + \eta_+ H_{\mathrm{N}+}}{2\sqrt{\eta_+}}, \tag{2.31b}$$

where $E_{\mathrm{N}-}$, $E_{\mathrm{N}+}$, $H_{\mathrm{N}-}$and $H_{\mathrm{N}+}$ are the net electric and magnetic fields before and after the metasurface [35, 41, 42]. Both net fields are written as

$$E_{\mathrm{N}-} = E_{\mathrm{IN}-} + E_{\mathrm{OUT}-}, \quad H_{\mathrm{N}-} = \frac{E_{\mathrm{IN}-} - E_{\mathrm{OUT}-}}{\eta_-}, \tag{2.32a}$$

$$E_{\mathrm{N}+} = E_{\mathrm{IN}+} + E_{\mathrm{OUT}+}, \quad H_{\mathrm{N}+} = \frac{E_{\mathrm{OUT}+} - E_{\mathrm{IN}+}}{\eta_+}. \tag{2.32b}$$

If the net fields are replaced into the parameters of (2.31), they can be simplified as

$$a_- = \frac{E_{\mathrm{IN}-}}{\sqrt{\eta_-}}, \quad b_- = \frac{E_{\mathrm{OUT}-}}{\sqrt{\eta_-}}, \tag{2.33a}$$

$$a_+ = \frac{E_{\mathrm{IN}+}}{\sqrt{\eta_+}}, \quad b_+ = \frac{E_{\mathrm{OUT}+}}{\sqrt{\eta_+}}. \tag{2.33b}$$

In terms of the power waves, the scattering matrix is written as

$$\begin{bmatrix} b_- \\ b_+ \end{bmatrix} = \begin{bmatrix} S_{11} & S_{12} \\ S_{21} & S_{22} \end{bmatrix} \begin{bmatrix} a_- \\ a_+ \end{bmatrix}. \tag{2.34}$$

By replacing the values of the power waves, it is possible to establish the relation between the outgoing waves with respect to the incoming waves:

$$\begin{bmatrix} \dfrac{E_{\mathrm{OUT}-}}{\sqrt{\eta_-}} \\ \dfrac{E_{\mathrm{OUT}+}}{\sqrt{\eta_+}} \end{bmatrix} = \begin{bmatrix} S_{11} & S_{12} \\ S_{21} & S_{22} \end{bmatrix} \begin{bmatrix} \dfrac{E_{\mathrm{IN}-}}{\sqrt{\eta_-}} \\ \dfrac{E_{\mathrm{IN}+}}{\sqrt{\eta_+}} \end{bmatrix}. \tag{2.35}$$

Because the GSTCs of Equation (2.5) consider the fields around the metasurfaces regardless of their propagation direction, it is possible to expand the results obtained for single-source metasurfaces analysis using the superposition principle.

In that case, the relations between the incoming fields and outgoing fields can be written using the scattering coefficients:

$$\begin{bmatrix} E_{\mathrm{OUT}-} \\ E_{\mathrm{OUT}+} \end{bmatrix} = \begin{bmatrix} \tilde{\Gamma}_- & \tilde{\tau}_+ \\ \tilde{\tau}_- & \tilde{\Gamma}_+ \end{bmatrix} \begin{bmatrix} E_{\mathrm{IN}-} \\ E_{\mathrm{IN}+} \end{bmatrix}, \tag{2.36}$$

where the scattering coefficient subindex is defined so that the "$-$" corresponds to the scattering coefficients for the illuminating source $\mathbf{E}_{\mathrm{IN}-}$, which propagates from the $-z$ half-space with $\mathbf{a}_\mathrm{z}$ propagation direction. Likewise, "$+$" subindex corresponds to the illuminating source $\mathbf{E}_{\mathrm{IN}+}$ of the $+z$ half-space and the propagation direction $-\mathbf{a}_\mathrm{z}$. Hence, the relationship between the scattering matrix and the metasurface scattering coefficients can be written as

$$\begin{bmatrix} S_{11} & S_{12} \\ S_{21} & S_{22} \end{bmatrix} = \begin{bmatrix} \tilde{\Gamma}_- & \sqrt{\frac{\eta_+}{\eta_-}}\tilde{\tau}_+ \\ \sqrt{\frac{\eta_-}{\eta_+}}\tilde{\tau}_- & \tilde{\Gamma}_+ \end{bmatrix}. \tag{2.37}$$

It can be shown (doing the same analysis using Equation 2.24 with illumination from $+z$ half-space) that for an EMPM placed between two different media, the reflection and transmission coefficients corresponding to $E_{\mathrm{IN}-}$ ($\tilde{\Gamma}_-$ and $\tilde{\Gamma}_+$) are not equal to their counterparts obtained from $E_{\mathrm{IN}+}$ ($\tilde{\Gamma}_+$ and $\tilde{\tau}_+$); but this result does not imply that reciprocity is broken, since the components S_{12} and S_{21} of the scattering matrix are equal due the additional factors of Equation (2.37). Now consider the scenario where the EMPM is placed in an homogeneous medium (like free space), the transmission and reflection coefficients from both sides become equal. This result can be extended to EPMs and MPMs (forcing the adequate grid impedances values); or for any other anisotropic metasurface. Notice that the scattering coefficients symmetry in homogeneous medium is not true when the magnetoelectric coupling coefficients of Equation (2.6) are not zero, meaning that the analysed metasurface is bianisotropic.

2.4 Impedance matrix and equivalent circuit of a metasurface

Consider an EMPM in free space, as shown in Figure 2.4, with scattering coefficients of Equation (2.29). The scattering matrix can be reduced to

$$\begin{bmatrix} S_{11} & S_{12} \\ S_{21} & S_{22} \end{bmatrix} = \frac{1}{2}\left(\frac{2\tilde{Z}_\mathrm{e} - 1}{2\tilde{Z}_\mathrm{e} + 1} \begin{bmatrix} 1 & 1 \\ 1 & 1 \end{bmatrix} + \frac{\tilde{Z}_\mathrm{m} - 2}{\tilde{Z}_\mathrm{m} + 2} \begin{bmatrix} 1 & -1 \\ -1 & 1 \end{bmatrix} \right). \tag{2.38}$$

Based on the scattering matrix, it is possible to find the impedance matrix [Z] as shown in [42], obtaining

$$\begin{bmatrix} Z_{11} & Z_{12} \\ Z_{21} & Z_{22} \end{bmatrix} = \eta_0 \left(\tilde{Z}_\mathrm{e} \begin{bmatrix} 1 & 1 \\ 1 & 1 \end{bmatrix} + \frac{\tilde{Z}_\mathrm{m}}{4} \begin{bmatrix} 1 & -1 \\ -1 & 1 \end{bmatrix} \right). \tag{2.39}$$

A good electric-circuit analogy for the Z-matrix is the T equivalent circuit shown in [42], which can be implemented for an EMPM as shown in Figure 2.6. As mentioned previously, if the analysed metasurface has bianisotropic properties, it is possible that matrix elements Z_{11} and Z_{22} of Equation (2.39) have different values.

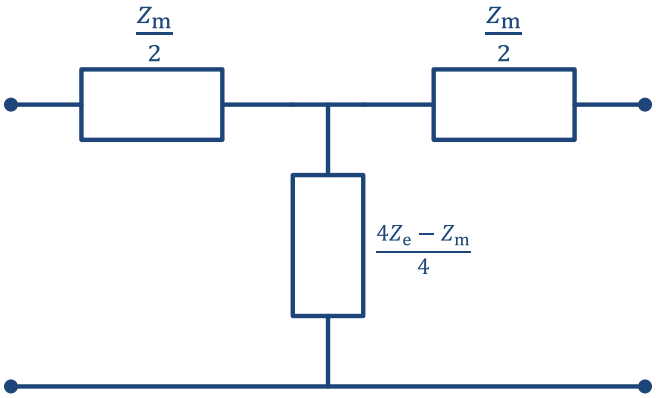

Figure 2.6. Equivalent T-circuit for an EMPM.

If we force the conditions for an EPM ($\tilde{Z}_\mathrm{m} = 0$) in the Z-matrix of (2.39), the equivalent circuit is a load Z_e in a parallel connection with the transmission line. Likewise, forcing the conditions for an MPM ($\tilde{Z}_\mathrm{e} \to \infty$), the equivalent circuit is a load Z_m in a shunt connection with the transmission line. Both representations are shown in Figure 2.7.

This approach is useful to relate the properties of these kinds of metasurfaces with the conventional circuit theory. An extensive analysis of slabs and infinites-

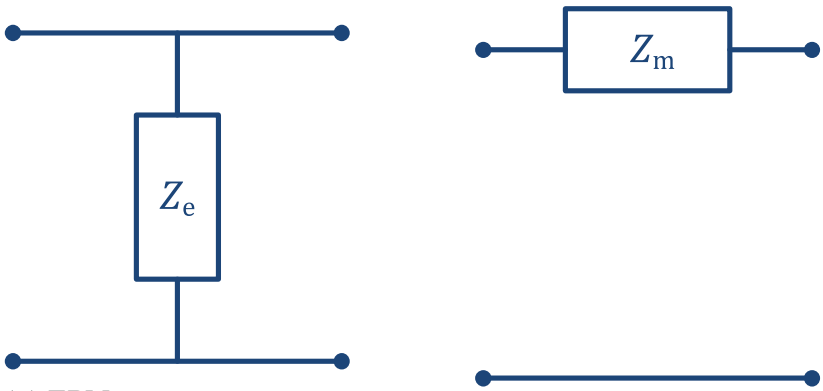

(a) EPM **(b)** MPM

Figure 2.7. Equivalent circuits for EPMs and MPMs.

imally thin sheets of bulk materials using this approach can be found in [38]; these results can also be extended for metasurfaces because of the small size of the meta-atoms with respect to the wavelength. Because the objective of this thesis is to study the scattered fields produced by multiple metasurfaces, this level of abstraction, which uses an approach based on the conventional circuit theory, cannot be used, and the equivalent model based on the scattering matrix will be considered.

3. Invisible cavity resonators based on metasurfaces

3.1 Wave propagation through a double-metasurface resonator

Until this moment, we considered scenarios where only one metasurface was illuminated at normal incidence. Based on the results summarized in Table 2.1, the only possible way to obtain an invisible metasurface is forcing a high-value of electrical grid impedance and zero magnetic grid impedance, implying the absence of the metasurface. In other words, the conditions for invisibility based on a single uniform metasurface, under the assumptions of the previous chapter, are limited. The main objective of this study is to "hide" (in terms of visibility) two parallel metasurfaces, with some control of the fields inside the bounded-volume between them. In order to accomplish this objective, this study will consider the interactions between two metasurfaces, as shown in Figure 3.1.

Both metasurfaces, ideally of infinite area, are separated by an isotropic lossless

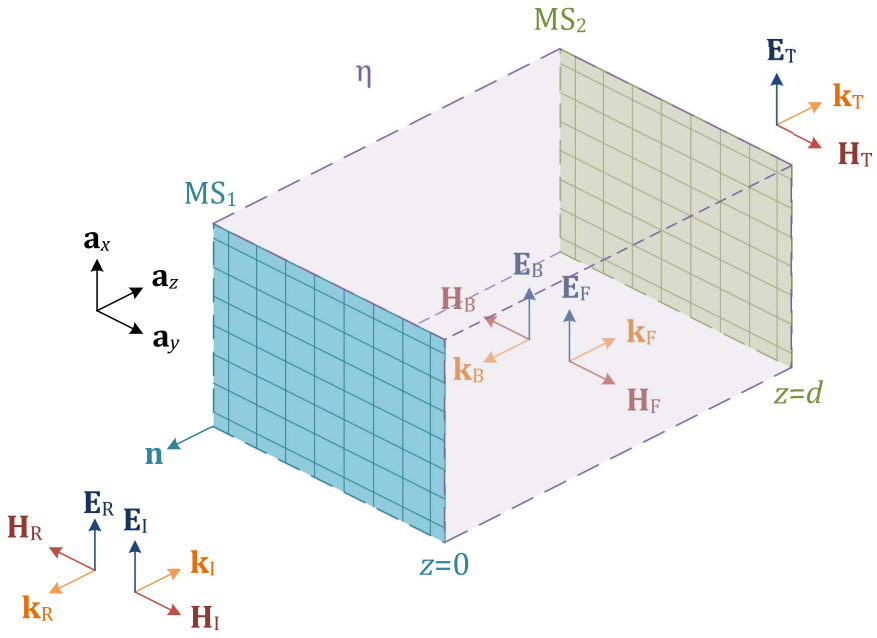

Figure 3.1. Electromagnetic fields across two generic metasurfaces

material slab of thickness d. Because of that, the whole space can be separated into two regions: a bounded volume between the metasurfaces, and the space outside of the volume. If the structure is illuminated by an electromagnetic wave with electric field $\mathbf{E}_{\mathrm{R}}$, with the propagation vector orthogonal to both metasurfaces, the discontinuities introduced by the metasurfaces create scattered waves. These waves can be classified according to their location in space: a reflected wave $\mathbf{E}_{\mathrm{R}}$ and a transmitted wave $\mathbf{E}_{\mathrm{T}}$ allocated outside the structure. Meanwhile, like a resonator, a forward $\mathbf{E}_{\mathrm{F}}$ and a backward $\mathbf{E}_{\mathrm{B}}$ waves are excited inside the bounded-volume. The definitions for the incident, reflected and transmitted waves of (2.9) remains usable in this analysis and, in the same way, the forward and backward waves can be defined as

$$\mathbf{E}_{\mathrm{F}}(z) = E_{\mathrm{F}} e^{-jkz}\mathbf{a}_x, \qquad \mathbf{H}_{\mathrm{F}}(z) = \frac{E_{\mathrm{F}}}{\eta} e^{-jkz}\mathbf{a}_y, \tag{3.1a}$$

$$\mathbf{E}_{\mathrm{B}}(z) = E_{\mathrm{B}} e^{jkz}\mathbf{a}_x, \qquad \mathbf{H}_{\mathrm{B}}(z) = -\frac{E_{\mathrm{B}}}{\eta} e^{jkz}\mathbf{a}_y. \tag{3.1b}$$

In the general case, it is not necessary true that the bounded-volume has the same electromagnetic properties as the space outside the resonator. For simplicity, we can assume that the resonator is located in free space, with η_0 and k_0 as its characteristic impedance and wavenumber, respectively; while the bounded-volume slab is formed by a medium with η and k parameters. Then, using Equation (2.34), it is possible to relate the magnitude of the different electric fields for the first metasurface

$$E_{\mathrm{F}} = S_{21,1}\sqrt{\frac{\eta}{\eta_0}} E_{\mathrm{I}} + S_{22,1} E_{\mathrm{B}}, \tag{3.2a}$$

$$\sqrt{\frac{\eta}{\eta_0}} E_{\mathrm{R}} = S_{11,1}\sqrt{\frac{\eta}{\eta_0}} E_{\mathrm{I}} + S_{12,1} E_{\mathrm{B}}; \tag{3.2b}$$

and for the second one

$$\sqrt{\frac{\eta}{\eta_0}} E'_{\mathrm{T}} = S_{21,2} E'_{\mathrm{F}}, \tag{3.3a}$$

$$E'_{\mathrm{B}} = S_{11,2} E'_{\mathrm{F}}. \tag{3.3b}$$

In the above equations, the scattering matrix coefficients are written as $S_{ij,1}$ and $S_{ij,2}$ for the first and second metasurface, respectively. Also, E'_{T}, E'_{F} and E'_{B} are the different electric fields when the coordinates reference is located at $z = d$. Notice that the magnitudes of the electric fields in Equation (3.3) are not the same as in Equation (3.2), as the reference is moved to the position of the second metasurface.

The previous analysis determines the scattering matrix for a metasurface, which is independent from the position where the metasurface is located. Because of

that, the scattering matrix remains invariable if the metasurface is displaced to position $z = d$. In that case, new definitions for the forward, backward and transmitted waves must be introduced:

$$\mathbf{E}'_{\mathrm{F}} = E'_{\mathrm{F}} e^{-jk(z-d)} \mathbf{a}_{\mathrm{x}}, \qquad \mathbf{H}'_{\mathrm{F}} = H'_{\mathrm{F}} e^{-jk(z-d)} \mathbf{a}_{\mathrm{y}}, \tag{3.4a}$$

$$\mathbf{E}'_{\mathrm{B}} = E'_{\mathrm{B}} e^{jk(z-d)} \mathbf{a}_{\mathrm{x}}, \qquad \mathbf{H}'_{\mathrm{B}} = -H'_{\mathrm{B}} e^{jk(z-d)} \mathbf{a}_{\mathrm{y}}, \tag{3.4b}$$

$$\mathbf{E}'_{\mathrm{T}} = E'_{\mathrm{T}} e^{-jk_0(z-d)} \mathbf{a}_{\mathrm{x}}, \qquad \mathbf{H}'_{\mathrm{T}} = H'_{\mathrm{T}} e^{-jk_0(z-d)} \mathbf{a}_{\mathrm{y}}. \tag{3.4c}$$

Because the displaced fields of (3.4) are the same as the fields of (3.1) and (2.9c), it is possible to find the relation between the magnitude of the displaced fields and their original counterparts:

$$E'_{\mathrm{F}} = E_{\mathrm{F}} e^{-jkd}, \tag{3.5a}$$

$$E'_{\mathrm{B}} = E_{\mathrm{B}} e^{jkd}, \tag{3.5b}$$

$$E'_{\mathrm{T}} = E_{\mathrm{T}} e^{-jk_0 d}. \tag{3.5c}$$

In fact, these results can be extended for the general case, where all the electromagnetic waves that propagate in the $+\mathbf{a}_{\mathrm{z}}$ direction, like the forward wave, must be corrected by adding the factor e^{-jkd} ; likewise, the backward wave result can be extended to all the electromangetic waves that propagate in the $-\mathbf{a}_{\mathrm{z}}$ direction, by adding the factor e^{jkd}. Thanks to that, the equations of (3.3) can be written in terms of the origin-defined electromagnetic waves as

$$\sqrt{\frac{\eta}{\eta_0}} E_{\mathrm{T}} = S_{21,2} E_{\mathrm{F}} e^{-j(k-k_0)d}, \tag{3.6a}$$

$$E_{\mathrm{B}} = S_{11,2} E_{\mathrm{F}} e^{-2jkd}. \tag{3.6b}$$

After defining the relation between the different electromagnetic fields across the structure, while considering the displacement of the second metasurface, it is possible to find the values of each field as functions of the incident wave and the metasurfaces scattering matrices. The magnitudes of each wave can be solved by defining different transfer function, which involve the use of the resonance factor

Ψ:

$$\Psi = \frac{1}{1 - e^{-2jkd} S_{22,1} S_{11,2}}, \tag{3.7a}$$

$$\Gamma = \frac{E_{\mathrm{R}}}{E_{\mathrm{I}}} = S_{11,1} + S_{11,2} S_{12,1} S_{21,1} e^{-2jkd} \Psi, \tag{3.7b}$$

$$\tau = \frac{E_{\mathrm{T}}}{E_{\mathrm{I}}} = S_{21,1} S_{21,2} e^{-j(k-k_0)d} \Psi, \tag{3.7c}$$

$$F = \frac{E_{\mathrm{F}}}{E_{\mathrm{I}}} = S_{21,1} \sqrt{\frac{\eta}{\eta_0}} \Psi, \tag{3.7d}$$

$$B = \frac{E_{\mathrm{B}}}{E_{\mathrm{I}}} = S_{11,2} S_{21,1} \sqrt{\frac{\eta}{\eta_0}} e^{-2jkd} \Psi. \tag{3.7e}$$

Thanks to the use of the scattering matrices, the results shown in Equation (3.7) can be used to characterize the fields produced by two sheets. For the metasurface family considered in this work, it is possible to consider them as reciprocal (implying that $S_{21,i} = S_{12,i}$). In the specific case when the bounded volume has the same electromagnetic properties as the medium outside the resonator (free space during this analysis), some simplifications can be performed, and the transfer functions of (3.7) can be reduced even more:

$$\Psi_{\mathrm{fs}} = \frac{1}{1 - e^{-2jk_0 d} \tilde{\Gamma}_1 \tilde{\Gamma}_2}, \tag{3.8a}$$

$$\Gamma_{\mathrm{fs}} = \frac{E_{\mathrm{R}}}{E_{\mathrm{I}}} = \tilde{\Gamma}_1 + \tilde{\Gamma}_2 \tilde{\tau}_1^2 e^{-2jk_0 d} \Psi_{\mathrm{fs}}, \tag{3.8b}$$

$$\tau_{\mathrm{fs}} = \frac{E_{\mathrm{T}}}{E_{\mathrm{I}}} = \tilde{\tau}_1 \tilde{\tau}_2 \Psi_{\mathrm{fs}}, \tag{3.8c}$$

$$F_{\mathrm{fs}} = \frac{E_{\mathrm{F}}}{E_{\mathrm{I}}} = \tilde{\tau}_1 \Psi_{\mathrm{fs}}, \tag{3.8d}$$

$$B_{\mathrm{fs}} = \frac{E_{\mathrm{B}}}{E_{\mathrm{I}}} = \tilde{\Gamma}_2 \tilde{\tau}_1 e^{-2jk_0 d} \Psi_{\mathrm{fs}}. \tag{3.8e}$$

3.2 Wave propagation through conventional Fabry-Perot resonators

Before developing the conditions for an ICR, it is convenient to review the transmitted and reflected fields produced by conventional Fabry-Perot resonators (FPRs). There are three different types of FPRs: with two metallic plates, with two metallic plates and a dielectric slab in between; and with only a dielectric slab. First, we can consider the more general case with a dielectric slab covered by two identical high conductive plates.

Fabry-Perot resonators with dielectric slab and two conductive plates
In this case, the inner volume can be bounded by two identical metallic plates made of a good conductor (to obtain high-reflection). Both metallic plates are electrically

thin, meaning that the tangential electric field across each plate is continuous. On the other hand, the induced currents at each plate produce discontinuities in the magnetic field. By combining these two phenomena, it is reasonable to model a metallic plate (based on a good conductor) as an EPM, and reuse the formulations made in Chapter 2. The only condition is that both metallic plates have the same electrical properties, with the consequence that both plates can be defined using the same electrical grid impedance $Z_{\mathrm{e,p}}$. Therefore, the scattering matrix for both metallic plates can be written substituting the transmission and reflection coefficients of Equation (2.11) substituted into the scattering matrix of Equation (2.37), as shown in Equations (3.9) for the first plate and (3.10) for the second one.

$$S_{11,1} = \frac{Z_{\mathrm{e,p}}\left(\eta - \eta_0\right) - \eta\eta_0}{Z_{\mathrm{e,p}}\left(\eta + \eta_0\right) + \eta\eta_0} \qquad S_{12,1} = \frac{2Z_{\mathrm{e,p}}\sqrt{\eta\eta_0}}{Z_{\mathrm{e,p}}\left(\eta + \eta_0\right) + \eta\eta_0} \tag{3.9a}$$

$$S_{21,1} = \frac{2Z_{\mathrm{e,p}}\sqrt{\eta\eta_0}}{Z_{\mathrm{e,p}}\left(\eta + \eta_0\right) + \eta\eta_0} \qquad S_{22,1} = \frac{Z_{\mathrm{e,p}}\left(\eta_0 - \eta\right) - \eta\eta_0}{Z_{\mathrm{e,p}}\left(\eta + \eta_0\right) + \eta\eta_0} \tag{3.9b}$$

$$S_{11,2} = \frac{Z_{\mathrm{e,p}}\left(\eta_0 - \eta\right) - \eta\eta_0}{Z_{\mathrm{e,p}}\left(\eta + \eta_0\right) + \eta\eta_0} \qquad S_{12,2} = \frac{2Z_{\mathrm{e,p}}\sqrt{\eta\eta_0}}{Z_{\mathrm{e,p}}\left(\eta + \eta_0\right) + \eta\eta_0} \tag{3.10a}$$

$$S_{21,2} = \frac{2Z_{\mathrm{e,p}}\sqrt{\eta\eta_0}}{Z_{\mathrm{e,p}}\left(\eta + \eta_0\right) + \eta\eta_0} \qquad S_{22,2} = \frac{Z_{\mathrm{e,p}}\left(\eta - \eta_0\right) - \eta\eta_0}{Z_{\mathrm{e,p}}\left(\eta + \eta_0\right) + \eta\eta_0} \tag{3.10b}$$

The next step is to determine the FPR transmission and reflection coefficients. By inserting the plates scattering matrices into Equation (3.7), both coefficients can be obtained:

$$\Gamma_{\mathrm{FPR}} = \frac{2\eta Z_{\mathrm{e,p}}\left[\eta\eta_0 + Z_{\mathrm{e,p}}(\eta + \eta_0) - e^{2jkd}(\eta\eta_0 + Z_{\mathrm{e,p}}(\eta - \eta_0))\right]}{(\eta\eta_0 + Z_{\mathrm{e,p}}(\eta + \eta_0))^2 - e^{-2jkd}(\eta\eta_0 + Z_{\mathrm{e,p}}(\eta - \eta_0))^2} - 1, \tag{3.11a}$$

$$\tau_{\mathrm{FPR}} = \frac{4\eta\eta_0 Z_{\mathrm{e,p}}^2 e^{-j(k-k_0)d}}{(\eta\eta_0 + Z_{\mathrm{e,p}}(\eta + \eta_0))^2 - e^{-2jkd}(\eta\eta_0 + Z_{\mathrm{e,p}}(\eta - \eta_0))^2}. \tag{3.11b}$$

These general FPRs can be designed for interferometers with total transmission. As it will be shown in Section 3.2, zero phase transmission can be achieved using these FPRs. These results can be used to analyse the other two kinds of resonators.

Fabry-Perot resonators with two conductive plates

For the second kind of FPRs, where the dielectric spacer is removed ($\eta = \eta_0$ and $k = k_0$), the transmission and reflection coefficients can be simplified into

$$\Gamma_{\mathrm{ws}} = -\frac{\eta_0\left[\eta_0 + 2Z_{\mathrm{e,p}} + e^{-2jk_0d}(2Z_{\mathrm{e,p}} - \eta_0)\right]}{(\eta_0 + 2Z_{\mathrm{e,p}})^2 - \eta_0^2 e^{-2jk_0d}}, \tag{3.12a}$$

$$\tau_{\mathrm{ws}} = \frac{4Z_{\mathrm{e,p}}^2}{(\eta_0 + 2Z_{\mathrm{e,p}})^2 - \eta_0^2 e^{-2jk_0d}}, \tag{3.12b}$$

where the subindex "ws" denotes "without slab". Based on these equations, it is possible to conclude that FPRs without spacer can be invisible ($\Gamma_{\mathrm{ws}} = 0$ and $\tau_{\mathrm{ws}} = 1$) only when the metallic plates have infinite grid impedance. This result corresponds to the trivial solution when there are no metallic plates.

If the conditions are relaxed, and only zero-phase unitary transmission is applied ($\tau_{\mathrm{ws}} = 1$),then the required grid impedance and the produced reflection coefficient are written as

$$Z_{\mathrm{e,p}} = \frac{\eta_0}{4}\left(e^{-2jk_0d} - 1\right) \tag{3.13a}$$

$$\Gamma_{\mathrm{ws}} = -2 \tag{3.13b}$$

If Equation (3.13a) is analysed, it is possible to notice that the grid impedance of the metallic plates require active response (except when $Z_{\mathrm{e,p}} = 0$). Also, Equation (3.13b) shows that there is a constant backscattering produced due to the negative grid impedance. Therefore, by combining both analysis, the conclusion is that it is not possible to achieve invisibility with zero-phase transmission using a conventional FPR in a homogeneous medium and with identical metallic plates.

Fabry-Perot resonators with a dielectric slab

The next step is to consider the scenario of an FPR with single dielectric slab (without metallic plates). The expressions of transmission and reflection coefficients can be obtained from Equation (3.11) by forcing $Z_{\mathrm{e,p}} \to \infty$. Then, the scattering coefficients for a dielectric slab are written as

$$\Gamma_{\mathrm{ds}} = \frac{2\eta\left[\eta + \eta_0 - e^{2jkd}(\eta - \eta_0)\right]}{(\eta + \eta_0)^2 - e^{-2jkd}(\eta - \eta_0)^2} - 1, \tag{3.14a}$$

$$\tau_{\mathrm{ds}} = \frac{4\eta\eta_0 e^{-j(k-k_0)d}}{(\eta + \eta_0)^2 - e^{-2jkd}(\eta - \eta_0)^2}, \tag{3.14b}$$

where "ds" denotes "dielectric slab". In this case, zero reflection is obtained when the thickness of the dielectric slab d_{ds} fulfils the condition

$$d_{\mathrm{ds}} = \frac{n\lambda_0}{2\sqrt{\varepsilon_{\mathrm{r}}}}, \tag{3.15}$$

where n is a positive integer, λ_0 is the free-space wavelength and ε_r is the relative permittivity of the slab medium. Under these conditions, the transmission coefficient can be simplified into

$$\tau_\mathrm{ds} = \exp\left[jn\pi\left(\frac{1}{\sqrt{\varepsilon_\mathrm{r}}} - 1\right)\right]. \tag{3.16}$$

This result shows that a dielectric slab resonator can have total transmission, but zero-phase transmission can be achieved only for specific slab permittivities:

$$\varepsilon_\mathrm{r} = \left(\frac{n}{2m+n}\right)^2, \tag{3.17}$$

where m is another integer value.

For this case, the fields inside the dielectric slab (represented by $E_\mathrm{F,ds}$ and $E_\mathrm{B,ds}$) can be simplified into

$$E_\mathrm{F,ds} = \frac{1}{2}\left(1 + \frac{1}{\sqrt{\varepsilon_\mathrm{r}}}\right)E_\mathrm{I}, \tag{3.18a}$$

$$E_\mathrm{B,ds} = \frac{1}{2}\left(1 - \frac{1}{\sqrt{\varepsilon_\mathrm{r}}}\right)E_\mathrm{I}. \tag{3.18b}$$

Therefore, the net field inside the dielectric slab $\mathbf{E}_\mathrm{ds}$ is defined as the sum of the forward and backward waves:

$$\mathbf{E}_\mathrm{ds} = \mathbf{E}_\mathrm{F} + \mathbf{E}_\mathrm{B} = \left(\cos(kz) - j\frac{\sin(kz)}{\sqrt{\varepsilon_\mathrm{r}}}\right)E_\mathrm{I}\mathbf{a}_\mathrm{x}. \tag{3.19}$$

By analysing the net field, it is possible to find out that, for FPRs with $\varepsilon_\mathrm{r} > 0$, the electrical field varies in the range between $[E_\mathrm{I}; E_\mathrm{I}/\sqrt{\varepsilon_\mathrm{r}}]$. According to Equation (3.17), the dielectric slab only offers strong fields inside when $0 < \varepsilon_\mathrm{r} < 1$ materials are used which are not so common in nature. In summary, it is possible to obtain invisibility conditions using a dielectric slab, but this regime requires $\varepsilon_\mathrm{r} < 1$ dielectrics to achieve zero-phase transmission with strong fields inside.

3.3 Wave propagation through a resonator based on two electrically polarizable metasurfaces

In order to simplify the analysis of a volume bounded by two metasurfaces, it is convenient to define some cases when the used metasurfaces have specific properties: when both metasurfaces are EPM (Double-Electric Resonator - DER), and when one metasurface is EPM and the other is MPM (Magnetic-Electric Resonator - MER). In both cases, at first we will assume that the volume has different electrical properties as outside the resonator. Moreover, the free-space

scenarios will be considered for each case.

Dielectric-filled metasurface resonators

The first case is when the resonator is composed by two EPM under general conditions, when the bounded volume has not necessarily the same properties as the medium outside the resonator, like in Figure 3.2.

Based on these conditions, the scattering matrices for both metasurfaces are obtained from the transmission and reflection coefficients given by Equation (2.11), for the first metasurface:

$$S_{11,1} = \frac{Z_{e1}(\eta - \eta_0) - \eta\eta_0}{Z_{e1}(\eta + \eta_0) + \eta\eta_0}, \qquad S_{12,1} = \frac{2Z_{e1}\sqrt{\eta\eta_0}}{Z_{e1}(\eta + \eta_0) + \eta\eta_0}, \tag{3.20a}$$

$$S_{21,1} = \frac{2Z_{e1}\sqrt{\eta\eta_0}}{Z_{e1}(\eta + \eta_0) + \eta\eta_0}, \qquad S_{22,1} = \frac{Z_{e1}(\eta_0 - \eta) - \eta\eta_0}{Z_{e1}(\eta + \eta_0) + \eta\eta_0}; \tag{3.20b}$$

and for the second one:

$$S_{11,2} = \frac{Z_{e2}(\eta_0 - \eta) - \eta\eta_0}{Z_{e2}(\eta + \eta_0) + \eta\eta_0}, \qquad S_{12,2} = \frac{2Z_{e2}\sqrt{\eta\eta_0}}{Z_{e2}(\eta + \eta_0) + \eta\eta_0}, \tag{3.21a}$$

$$S_{21,2} = \frac{2Z_{e2}\sqrt{\eta\eta_0}}{Z_{e2}(\eta + \eta_0) + \eta\eta_0}, \qquad S_{22,2} = \frac{Z_{e2}(\eta - \eta_0) - \eta\eta_0}{Z_{e2}(\eta + \eta_0) + \eta\eta_0}. \tag{3.21b}$$

Before substituting the metasurfaces scattering matrices into the transfer functions, it is convenient to perform some simplifications related to the bounded volume medium. Similarly to the case of the metasurfaces grid impedances in free-space scenarios, the characteristic impedance η and the wavenumber k can be normalized with respect to their free-space counterparts. Also, the value $k_0 d$ can be combined into a phase factor ϕ. All these notations are introduced in Equation

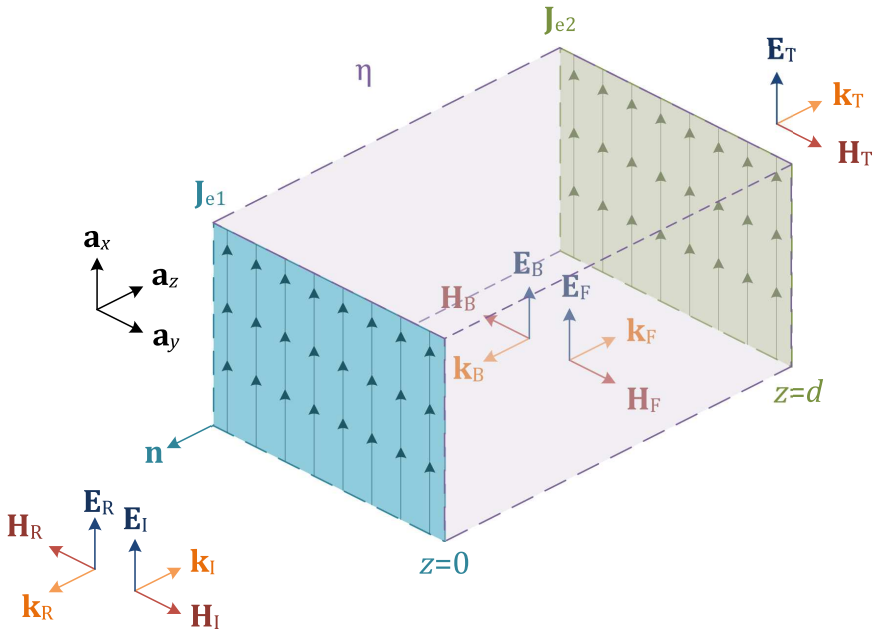

Figure 3.2. Electromagnetic fields across two generic metasurfaces

(3.22).

$$\eta = \tilde{\eta}\eta_0 \tag{3.22a}$$

$$k = \tilde{k}k_0 \tag{3.22b}$$

$$\phi = k_0 d \tag{3.22c}$$

Using the scattering matrices with the normalized values, the transfer functions for each produced wave can be obtained as functions of the grid impedances and the bounded volume parameters:

$$\begin{aligned}\Delta =& e^{2j\tilde{k}\phi}(\tilde{Z}_{\mathrm{e1}}(1+\tilde{\eta})+\tilde{\eta})(\tilde{Z}_{\mathrm{e2}}(1+\tilde{\eta})+\tilde{\eta}) \\ &-(\tilde{Z}_{\mathrm{e1}}(1-\tilde{\eta})-\tilde{\eta})(\tilde{Z}_{\mathrm{e2}}(1-\tilde{\eta})-\tilde{\eta}),\end{aligned} \tag{3.23a}$$

$$\begin{aligned}\Gamma = \frac{E_{\mathrm{R}}}{E_{\mathrm{I}}} =& \Delta^{-1}\Big[e^{2j\tilde{k}\phi}(\tilde{Z}_{\mathrm{e1}}(\tilde{\eta}-1)-\tilde{\eta})(\tilde{Z}_{\mathrm{e2}}(1+\tilde{\eta})+\tilde{\eta}) \\ &+(\tilde{Z}_{\mathrm{e1}}(1+\tilde{\eta})-\tilde{\eta})(\tilde{Z}_{\mathrm{e2}}(1-\tilde{\eta})-\tilde{\eta})\Big],\end{aligned} \tag{3.23b}$$

$$\tau = \frac{E_{\mathrm{T}}}{E_{\mathrm{I}}} = \Delta^{-1}\left[4e^{j(1+\tilde{k})\phi}\tilde{Z}_{\mathrm{e1}}\tilde{Z}_{\mathrm{e2}}\tilde{\eta}\right], \tag{3.23c}$$

$$F = \frac{E_{\mathrm{F}}}{E_{\mathrm{I}}} = \Delta^{-1}\left[2e^{2j\tilde{k}\phi}\tilde{Z}_{\mathrm{e1}}\tilde{\eta}(\tilde{Z}_{\mathrm{e2}}(1+\tilde{\eta})+\tilde{\eta})\right], \tag{3.23d}$$

$$B = \frac{E_{\mathrm{B}}}{E_{\mathrm{I}}} = \Delta^{-1}\left[2\tilde{Z}_{\mathrm{e1}}\tilde{\eta}(\tilde{Z}_{\mathrm{e2}}(1-\tilde{\eta})-\tilde{\eta})\right]. \tag{3.23e}$$

The structure of Figure 3.1 can be considered invisible if the transfer function of (3.23) fulfils the conditions: $\Gamma = 0$ and $\tau = 1$. To achieve these conditions, the corresponding values of the grid impedances can be obtained from Equations (3.23b) and (3.23c) to obtain

$$\tilde{Z}_{\mathrm{e1}} = \frac{e^{j(\tilde{k}+1)\phi}\left(e^{2j\tilde{k}\phi}-1\right)\tilde{\eta}}{e^{2j\tilde{k}\phi}\left(2+e^{j(\tilde{k}+1)\phi}(\tilde{\eta}-1)\right)-e^{j(\tilde{k}+1)\phi}(\tilde{\eta}+1)}, \tag{3.24a}$$

$$\tilde{Z}_{\mathrm{e2}} = \frac{e^{-j(\tilde{k}+1)\phi}\left(1-e^{-2j\tilde{k}\phi}\right)\tilde{\eta}}{e^{-2j\tilde{k}\phi}\left(2+e^{-j(\tilde{k}+1)\phi}(\tilde{\eta}-1)\right)-e^{-j(\tilde{k}+1)\phi}(\tilde{\eta}+1)}, \tag{3.24b}$$

$$\tilde{Z}_{\mathrm{e1}} = -\tilde{Z}^{*}_{\mathrm{e2}}. \tag{3.24c}$$

It is important to remark that the grid impedance of the first metasurface is equal to the negative and complex conjugate (where $*$ denotes the complex conjugate operator) of the second metasurface grid impedance. Figure 3.3 shows the normalized grid impedances for the case when the bounded volume is filled by a dielectric slab (with $\varepsilon_{\mathrm{r}} = 2$ and $\mu_r = 1$, chosen arbitrary).

For our case (considering possible realistic implementations), of special interest is the family of points where both metasurfaces are pure-reactive ($\tilde{R}_{\mathrm{e1}} = \tilde{R}_{\mathrm{e2}} = 0$),

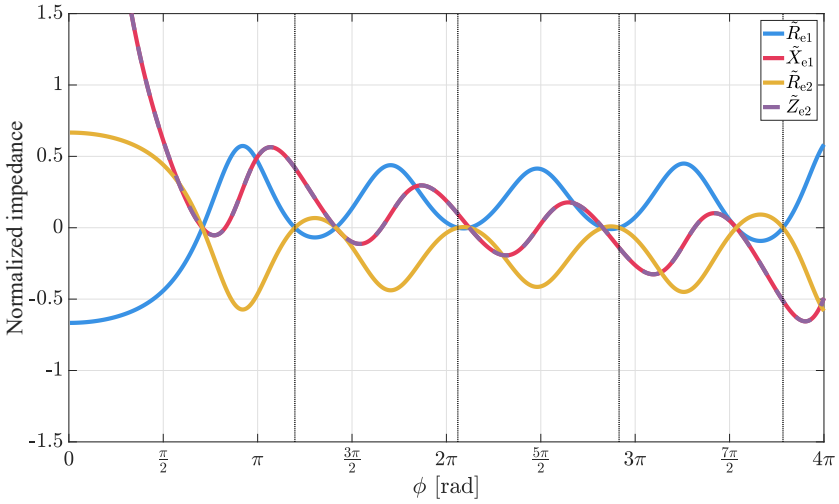

Figure 3.3. Normalized impedances for a DER using a slab of $\varepsilon_r = 2$ and $\mu_r = 1$. Notice that the imaginary parts of both grid impedances are overlapped. The dotted lines show some values of ϕ where both metasurfaces are pure-reactive.

as in the case when $\phi = 11.89\,[\text{rad}]$ and the metasurfaces have pure-capacitive grid impedances ($\tilde{X}_{e1} = \tilde{X}_{e2} = -0.5126$). As it is seen from (3.24), in this lossless case $Z_{el} = Z_{e2}$ and both metasurfaces become identical. Thus, the invisible regime can be achieved also with conventional FPRs consisting of a dielectric slab whose both sides are covered by metal films. It should be noted that usually the regime of invisibility is not desired in FPRs. Nevertheless, this regime is the subject of this thesis. The transfer functions for the forward and backward waves under invisibility conditions are written as

$$F = \frac{e^{j(\tilde{k}-1)\phi}\left(e^{j(\tilde{k}+1)\phi} - 1\right)}{e^{2j\tilde{k}\phi} - 1}, \tag{3.25a}$$

$$B = \frac{e^{j(\tilde{k}-1)\phi} - 1}{e^{2j\tilde{k}\phi} - 1}; \tag{3.25b}$$

which can be used to find the electromagnetic fields across the structure, as shown in Figure 3.4 for the case when $\phi = 11.89\,[\text{rad}]$.

Dielectric-free metasurface resonator

In the particular case when the bounded volume is free space, the transfer functions can be obtained by using Equation (3.8) with the metasurfaces scattering coefficients; or by using the values $\tilde{k}, \tilde{\eta} = 1$ in the transfer function of the general case of Equation (3.23). In both cases, the simplified transfer function for

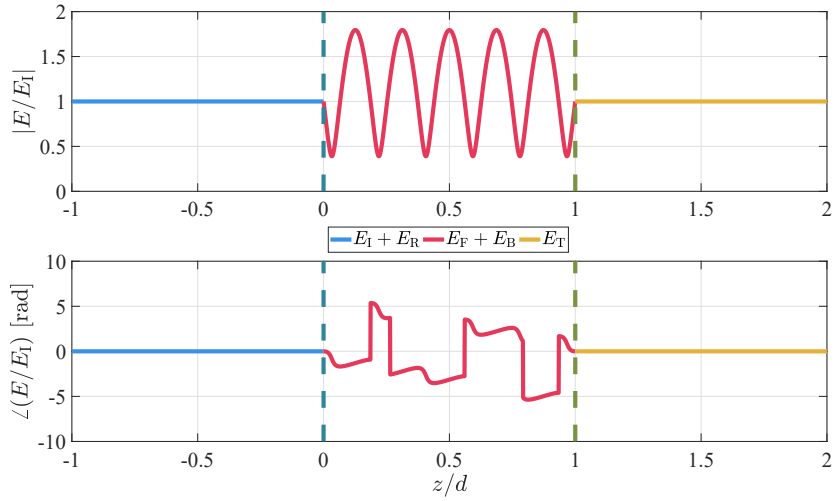

Figure 3.4. Electromagnetic fields across the two electrical sheets structure using a slab of $\varepsilon_\mathrm{r}=2$ and $\mu_r=1$: top - Magnitude, bottom - Phase.

free-space case are written as

$$\Delta_\mathrm{fs} = e^{2j\phi}(1+2\tilde{Z}_\mathrm{e1})(1+2\tilde{Z}_\mathrm{e2})-1, \tag{3.26a}$$

$$\Gamma_\mathrm{fs} = \Delta_\mathrm{fs}{}^{-1}\left[1-2\tilde{Z}_\mathrm{e1}-e^{2j\phi}(1+2\tilde{Z}_\mathrm{e2})\right], \tag{3.26b}$$

$$\tau_\mathrm{fs} = \Delta_\mathrm{fs}{}^{-1}\left[4e^{2j\phi}\tilde{Z}_\mathrm{e1}\tilde{Z}_\mathrm{e2}\right], \tag{3.26c}$$

$$F_\mathrm{fs} = \Delta_\mathrm{fs}{}^{-1}\left[2e^{2j\phi}\tilde{Z}_\mathrm{e1}(1+2\tilde{Z}_\mathrm{e2})\right], \tag{3.26d}$$

$$B_\mathrm{fs} = \Delta_\mathrm{fs}{}^{-1}\left[-2\tilde{Z}_\mathrm{e1}\right]. \tag{3.26e}$$

Because of the media difference between the bounded-volume and the outer space, the invisibility conditions for this case are not the same. The invisibility conditions are achieved when

$$e^{2j\phi}=1, \tag{3.27a}$$

$$d=\frac{n\lambda_0}{2}, \tag{3.27b}$$

$$\tilde{Z}_\mathrm{e1}=-\tilde{Z}_\mathrm{e2}, \tag{3.27c}$$

where n is an integer. Under this condition, the relationship between both grid impedances, shown in Equation (3.27c), is similar to the general case of Equation (3.24c); with the key difference that both grid impedances do not depend directly of the distance between metasurfaces. As a consequence, both grid impedances may be chosen to simplify the structure implementation, like using purely reactive surfaces without requiring active or lossy metasurfaces.

Induced currents in the metasurfaces

The use of the scattering matrix, combined with the metasurfaces transmission and reflection coefficients significantly simplify calculations of the transfer functions of the DER. Unfortunately, a disadvantage of using this method is that some analysis is omitted due the used abstraction level. Because of that, it is convenient to remember that each resonator metasurface has its own induced electric surface current density $\mathbf{J}_{\mathrm{e}1}$ and $\mathbf{J}_{\mathrm{e}2}$ for the first and the second metasurface, respectively:

$$\mathbf{J}_{\mathrm{e}1} = \frac{\mathbf{E}_{\mathrm{I}}(0) + \mathbf{E}_{\mathrm{R}}(0)}{Z_{\mathrm{e}1}}, \tag{3.28a}$$

$$\mathbf{J}_{\mathrm{e}2} = \frac{\mathbf{E}_{\mathrm{T}}(d)}{Z_{\mathrm{e}2}}. \tag{3.28b}$$

Because of the relation between the induced currents and the electromagnetic waves across the resonator, it is reasonable to determine the collective admittance for each metasurface, which can be written as

$$\tilde{J}_{\mathrm{e}1} = \frac{\mathbf{J}_{\mathrm{e}1} \cdot \mathbf{a}_{\mathrm{x}}}{\mathbf{E}_{\mathrm{I}}(0) \cdot \mathbf{a}_{\mathrm{x}}} = \frac{4e^{2j\phi}\tilde{Z}_{\mathrm{e}2} + 2\left(e^{2j\phi} - 1\right)}{\eta_0 \Delta_{\mathrm{fs}}}, \tag{3.29a}$$

$$\tilde{J}_{\mathrm{e}2} = \frac{\mathbf{J}_{\mathrm{e}2} \cdot \mathbf{a}_{\mathrm{x}}}{\mathbf{E}_{\mathrm{I}}(0) \cdot \mathbf{a}_{\mathrm{x}}} = \frac{4e^{2j\phi}\tilde{Z}_{\mathrm{e}1}}{\eta_0 \Delta_{\mathrm{fs}}} e^{-j\phi}. \tag{3.29b}$$

If also the invisibility conditions of Equation (3.27) are considered, the collective admittances can be simplified into

$$\tilde{J}_{\mathrm{e}1} = (-1)^{n+1}\tilde{J}_{\mathrm{e}2} = \frac{1}{Z_{\mathrm{e}1}}. \tag{3.30}$$

These results can be seen as the scenario where two current sheets with equal phases are separated at a distance of $\lambda_0/2$. In that case, the fields radiated by both current sheets cancel each others and no radiated field is seen in front and behind the current sheets. This conclusion means that the radiated fields produced outside the bounded volume by one metasurface is cancelled by the other one. Therefore, when the invisibility conditions of Equation (3.27) are applied, the ICR acts as a non-scattering system.

3.4 Wave propagation through a resonator based on mangetically polarizable and electrically polarizable metasurfaces

Dielectric-filled metasurface resonators

In previous analyses, the invisibility conditions for a DER were found. The next step is to analyse a Magnetic-Electic Resonator (MER), obtained by replacing the

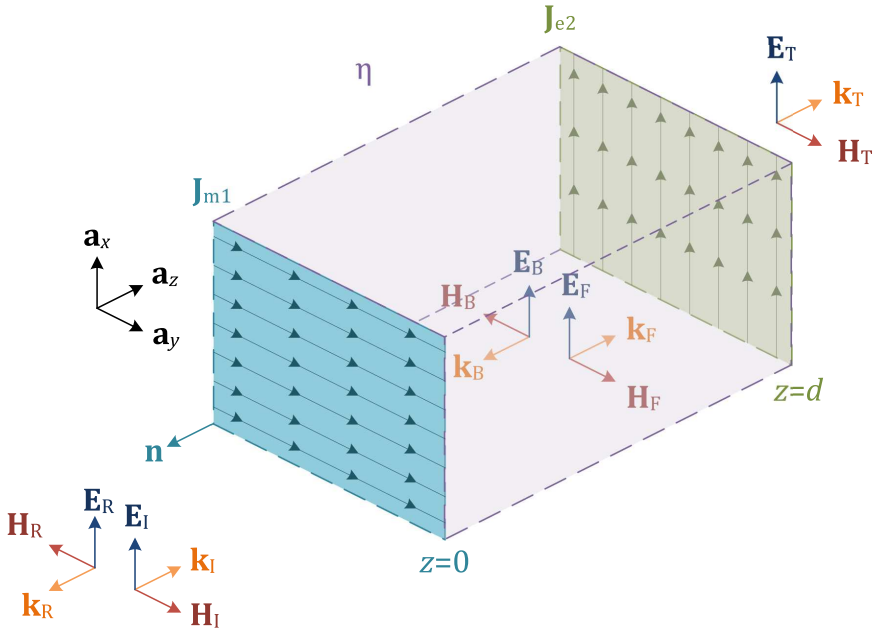

Figure 3.5. Electromagnetic fields, produced by an external incident wave, across a MER.

first metasurface with a MPM, as shown in Figure 3.5.

Therefore, the scattering matrix for the first metasurface must be based on the transmission and reflection coefficients of Equation (2.19):

$$S_{11,1} = \frac{\eta - \eta_0 + Z_{\mathrm{m1}}}{\eta + \eta_0 + Z_{\mathrm{m1}}}, \qquad S_{12,1} = \frac{2\sqrt{\eta\eta_0}}{\eta + \eta_0 + Z_{\mathrm{m1}}}, \tag{3.31a}$$

$$S_{21,1} = \frac{2\sqrt{\eta\eta_0}}{\eta + \eta_0 + Z_{\mathrm{m1}}}, \qquad S_{22,1} = \frac{\eta_0 - \eta + Z_{\mathrm{m1}}}{\eta + \eta_0 + Z_{\mathrm{m1}}}. \tag{3.31b}$$

On the other hand, the second metasurface remains the same, so that the scattering matrix showed in Equation (3.21), based on EPM model of Equation (2.11), is still usable for this case.

Using the same normalization as shown in Equation (3.22), the transfer functions for this case can be achieved by substituting both scattering matrices into the general transfer function expressions of Equation (3.7). Then, a simplified version can be obtained for the general case:

$$\begin{aligned}\Delta =& e^{2j\tilde{k}\phi}(1 + \tilde{Z}_{\mathrm{m1}} + \tilde{\eta})(\tilde{Z}_{\mathrm{e2}}(\tilde{\eta} + 1) + \tilde{\eta}) \\ &+ (1 + \tilde{Z}_{\mathrm{m1}} - \tilde{\eta})(\tilde{Z}_{\mathrm{e2}}(\tilde{\eta} - 1) + \tilde{\eta}),\end{aligned} \tag{3.32a}$$

$$\begin{aligned}\Gamma =& \Delta^{-1}\Big[(-1 + \tilde{Z}_{\mathrm{m1}} - \tilde{\eta})(\tilde{Z}_{\mathrm{e2}}(\tilde{\eta} - 1) + \tilde{\eta}) \\ &+ e^{2j\tilde{k}\phi}(-1 + \tilde{Z}_{\mathrm{m1}} + \tilde{\eta})(\tilde{Z}_{\mathrm{e2}}(\tilde{\eta} + 1) + \tilde{\eta})\Big],\end{aligned} \tag{3.32b}$$

$$\tau = \Delta^{-1}\left[4e^{j(1+\tilde{k})\phi}\tilde{\eta}\tilde{Z}_{\mathrm{e2}}\right], \tag{3.32c}$$

$$F = \Delta^{-1}\left[2e^{2j\tilde{k}\phi}\tilde{\eta}(\tilde{Z}_{\mathrm{e2}}(\tilde{\eta} + 1) + \tilde{\eta})\right], \tag{3.32d}$$

$$B = \Delta^{-1}\left[-2\tilde{\eta}(\tilde{Z}_{\mathrm{e2}}(\tilde{\eta} - 1) + \tilde{\eta})\right]. \tag{3.32e}$$

Then, it is possible to find an analytical expression for the grid impedances required to grant invisibility ($\Gamma = 0$, $\tau = 1$):

$$\tilde{Z}_{\mathrm{m1}} = \frac{1 + \tilde{\eta} + (1 - \tilde{\eta})e^{2j\tilde{k}\phi} - 2e^{j(\tilde{k}-1)\phi}}{1 + e^{2j\tilde{k}\phi}}, \tag{3.33a}$$

$$\tilde{Z}_{\mathrm{e2}} = \frac{\tilde{\eta}\left(1 + e^{2j\tilde{k}\phi}\right)}{1 - \tilde{\eta} - (1 + \tilde{\eta})e^{2j\tilde{k}\phi} + 2\tilde{\eta}e^{j(\tilde{k}+1)\phi}}, \tag{3.33b}$$

where both grid impedances are quite similar (especially when the grid admittance of the MPM $\tilde{Y}_{\mathrm{m1}}$ is compared to the grid impedance of the EPM $\tilde{Z}_{\mathrm{e2}}$). Figure 3.6 shows the required grid impedances as a function of the distance between metasurfaces, as done previously, considering a bounded volume composed by a dielectric slab (using arbitrarily taken values of $\varepsilon_{\mathrm{r}} = 2$ and $\mu_{\mathrm{r}} = 1$).

While the DER of Figure 3.3 shows a symmetric relation between the grid resistances, this case has some more complex relations between them. In order to improve the readability, Figure 3.6 depicts the normalized grid admittance for the MPM. Due to that, it is possible to notice that MPM grid suceptance follows closely the EPM grid reactance for values of ϕ greater than 2. In the case of resistance and conductance, they show a similar behaviour as observed in DER case, showing a quasi-mirror pattern. Also, it should be noted that both metasurfaces become purely reactive at some discrete points, and like in the previous case, they are interesting for possible future implementations. One example of this family of solutions is found at $\phi = 10.41\,[\mathrm{rad}]$ where $\tilde{X}_{\mathrm{m1}} = 2.5761$ and $\tilde{X}_{\mathrm{e2}} = -0.2745$, Figure 3.7 shows the fields across this resonator under this condition.

As a complementary information, the transfer functions of the inner fields can

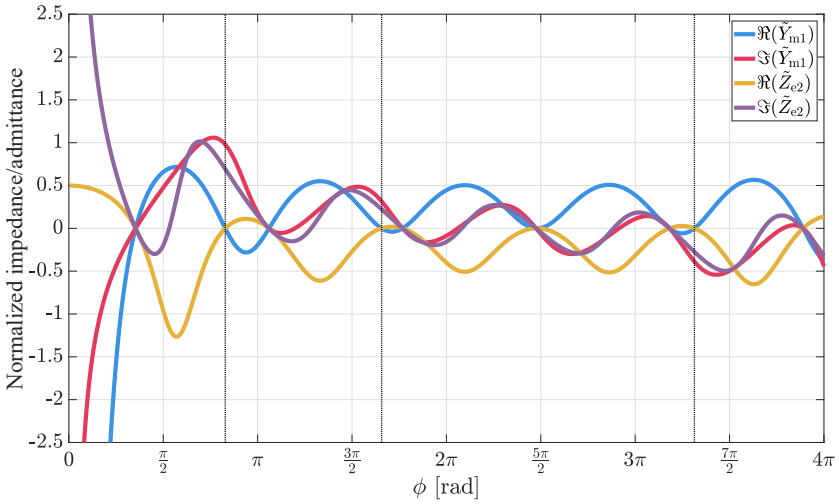

Figure 3.6. Normalized electric impedance and magnetic admittance for the resonator based on one MPM and one EPM using a slab of $\varepsilon_{\mathrm{r}} = 2$ and $\mu_r = 1$. The dotted lines show some values of ϕ where both metasurfaces are pure-reactive.

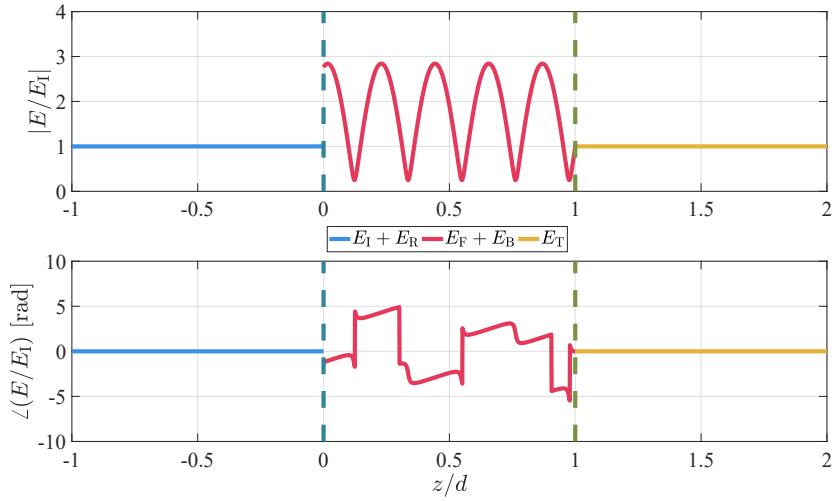

Figure 3.7. Electromagnetic fields across the magnetic and electric sheets structure using a slab of $\varepsilon_\mathrm{r}=2$ and $\mu_r=1$: top - Magnitude, bottom - Phase

be derived for invisible conditions:

$$F=\frac{e^{2j\tilde{k}\phi}\left(e^{-j(\tilde{k}+1)\phi}+\tilde{\eta}\right)}{e^{2j\tilde{k}\phi}+1}, \tag{3.34a}$$

$$B=\frac{e^{j(\tilde{k}-1)\phi}-\tilde{\eta}}{e^{2j\tilde{k}\phi}+1}. \tag{3.34b}$$

Dielectric-free metasurface resonator

As found previously, by forcing free-space conditions in (3.32) or by using the free-space scattering coefficients in the transfer functions of (3.8), the transfer functions for each electromagnetic field component is simplified:

$$\Delta_\mathrm{fs}=\tilde{Z}_\mathrm{m1}+e^{2j\phi}(2+\tilde{Z}_\mathrm{m1})(1+2\tilde{Z}_\mathrm{e2}), \tag{3.35a}$$

$$\Gamma_\mathrm{fs}=\Delta_\mathrm{fs}{}^{-1}\left[\tilde{Z}_\mathrm{m1}-2+e^{2j\phi}\tilde{Z}_\mathrm{m1}(1+2\tilde{Z}_\mathrm{e2})\right], \tag{3.35b}$$

$$\tau_\mathrm{fs}=\Delta_\mathrm{fs}{}^{-1}\left[4e^{2j\phi}\tilde{Z}_\mathrm{e2}\right], \tag{3.35c}$$

$$F_\mathrm{fs}=\Delta_\mathrm{fs}{}^{-1}\left[2e^{2j\phi}(1+2\tilde{Z}_\mathrm{e2})\right] \tag{3.35d}$$

$$B_\mathrm{fs}=-2\Delta_\mathrm{fs}{}^{-1}. \tag{3.35e}$$

To find the invisibility conditions, $\Gamma=0$ and $\tau=1$, two conditions must be obtained from Equation (3.35):

$$e^{2j\phi}=-1 \tag{3.36a}$$

$$d=\lambda\left(\frac{1}{4}+\frac{n}{2}\right), \tag{3.36b}$$

$$\tilde{Z}_\mathrm{m1}=-\frac{1}{\tilde{Z}_\mathrm{e2}}. \tag{3.36c}$$

Induced currents in the metasurfaces

As mentioned in description of the DER case, the induced currents can be related to the fields at metasurface planes. In the case of the MPM, magnetic current density $\mathbf{J}_{\mathrm{m1}}$ is due to the magnetic fields; while the EPM has an electric current density $\mathbf{J}_{\mathrm{e2}}$, due to the electric fields. The relations between the induced currents and the fields are written as

$$\mathbf{J}_{\mathrm{m1}} = Z_{\mathrm{m1}} \left(\mathbf{H}_{\mathrm{I}}(0) + \mathbf{H}_{\mathrm{R}}(0) \right), \tag{3.37a}$$

$$\mathbf{J}_{\mathrm{e2}} = \frac{\mathbf{E}_{\mathrm{T}}(d)}{Z_{\mathrm{e2}}}. \tag{3.37b}$$

Similarly to the previous case, the collective impedance for the MPM and the collective admitance for the EPM can be calculated for the free space scenario as

$$\tilde{J}_{\mathrm{m1}} = \frac{\mathbf{J}_{\mathrm{m1}} \cdot \mathbf{a}_{\mathrm{y}}}{\mathbf{H}_{\mathrm{I}}(0) \cdot \mathbf{a}_{\mathrm{y}}} = \eta_0 \frac{\tilde{Z}_{\mathrm{m1}}}{\Delta_{\mathrm{fs}}} \left[2(e^{2j\phi} + 1) + 4\tilde{Z}_{\mathrm{e2}} e^{2j\phi} \right], \tag{3.38a}$$

$$\tilde{J}_{\mathrm{e2}} = \frac{\mathbf{J}_{\mathrm{e2}} \cdot \mathbf{a}_{\mathrm{x}}}{\mathbf{E}_{\mathrm{I}}(0) \cdot \mathbf{a}_{\mathrm{x}}} = \frac{4e^{2j\phi}}{\eta_0 \Delta_{\mathrm{fs}}} e^{-j\phi}. \tag{3.38b}$$

Under the invisibility conditions of (3.36), both collective impedance/admitance can be simplified even more:

$$\tilde{J}_{\mathrm{m1}} = Z_{\mathrm{m1}}, \tag{3.39a}$$

$$\tilde{J}_{\mathrm{e2}} = (-1)^n \frac{1}{Z_{\mathrm{e2}}}, \tag{3.39b}$$

$$\tilde{J}_{\mathrm{m1}} = (-1)^{n+1} \eta_0^2 \tilde{J}_{\mathrm{e2}}. \tag{3.39c}$$

It is possible to show that this pair of surface currents act as a non-radiating source (showing that this resonator is a non-scattering system), but this must be demostrated by solving the radiated fields of each current sheet; unlike the DER which current transfer functions can be compared directly.

4. General properties of invisible cavity resonators

Until now, transfer functions for two different resonators were developed. In this chapter, some analyses will be performed in order to understand their general properties. Most of the analysis will be done so that the conclusions can be applied for both cases, choosing the first case based on DER just for results interpretation. All the analysis will assume that the bounded volume has the same electromagnetic properties as the space outside the resonator, because of that, most of the free-space subindexes "fs" *will be omitted*.

4.1 Standing waves inside the structure

Previously, two conditions were found to grant invisibility: one related with the distance between the metasurfaces and the second related with the grid impedances. The first condition is achieved at discrete distance values (see (3.27b)), where the phase shift is fixed (see (3.27a)). Therefore, these discrete distance values do not change the magnitude nor the phase of the fields inside the resonator. On the other hand, the grid impedances can modify the amplitude and phase of the scattered waves, with the only restriction shown in equations (3.27c) or (3.36c). As mentioned previously, these kinds of structures produces inner fields (see Equation (3.1)), which combines into a standing wave $\mathbf{E}_{\mathrm{S}}$

$$\mathbf{E}_{\mathrm{S}} = \mathbf{E}_{\mathrm{F}}(z) + \mathbf{E}_{\mathrm{B}}(z) = \mathbf{E}_{\mathrm{I}}(z)\left(F + Be^{2jk_0 z}\right), \tag{4.1}$$

where the definition given in Equations (2.9a) and (3.1) were used. One important parameter of a standing wave is the Standing Wave Ratio (SWR), which is the ratio between the maximum and the minimum values of the field amplitude in the standing wave [35, 42, 43]. Therefore, the SWR can be defined as

$$\mathrm{SWR} = \frac{1 + |\Gamma_{\mathrm{int}}|}{1 - |\Gamma_{\mathrm{int}}|}, \tag{4.2}$$

where Γ_{int} corresponds to the internal reflection coefficient:

$$\Gamma_{\text{int}} = \frac{\mathbf{E}_{\text{B}} \cdot \mathbf{a}_x}{\mathbf{E}_{\text{F}} \cdot \mathbf{a}_x}. \tag{4.3}$$

It is possible to express the SWR based on the transfer functions defined for both structures, by combining the equations (4.2), (4.3), and (3.1):

$$\text{SWR} = \frac{|\text{F}| + |\text{B}|}{|\text{F}| - |\text{B}|}. \tag{4.4}$$

Resonator formed by two electrically polarizable metasurfaces

First, let us consider a DER. Its transfer functions corresponding to the inner fields of Equation (3.26) can be reduced to

$$F = 1 - \frac{1}{2\tilde{Z}_{\text{e1}}} = 1 + \frac{j}{2\tilde{X}_{\text{e1}}}, \tag{4.5a}$$

$$B = \frac{1}{2\tilde{Z}_{\text{e1}}} = -\frac{j}{2\tilde{X}_{\text{e1}}}. \tag{4.5b}$$

Thanks to Equations (4.4), it is possible to determine the SWR of a given DER:

$$\text{SWR} = \frac{|2\tilde{Z}_{\text{e1}} - 1| + 1}{|2\tilde{Z}_{\text{e1}} - 1| - 1}. \tag{4.6}$$

Figure 4.1 shows how the SWR can be increased by reducing the magnitude of metasurfaces grid reactances. A theoretically infinite SWR can be obtained in the limit when the impedances of both metasurfaces tend to zero (from the positive and negative sides). If both impedances reach zero, the standing wave inside the

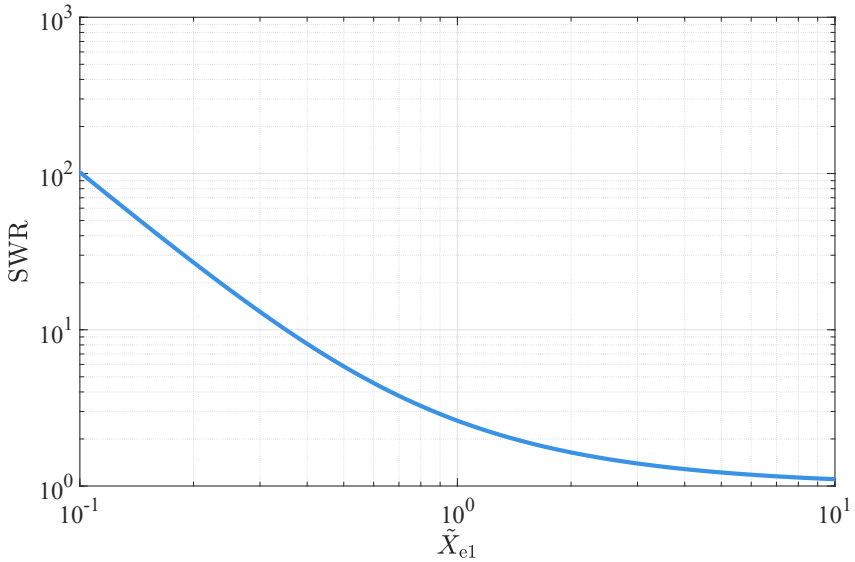

Figure 4.1. SWR as a function of the first metasurface reactance for a DER with pure reactive metasurfaces.

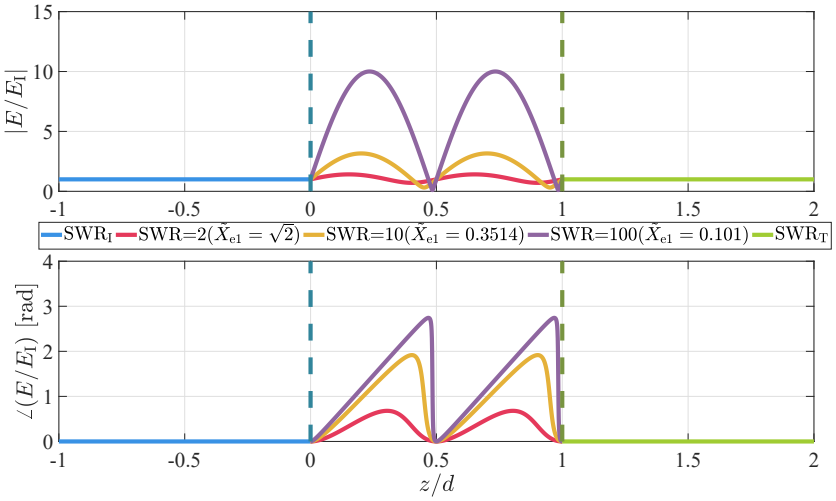

Figure 4.2. Standing waves across a DER for different SWR values, using a distance $d = \lambda$ and $\tilde{X}_{e1} > 0$: top - Magnitude, bottom - Phase.

resonator cannot be excited and it behaves as a PEC wall. In the opposite limit, when the metasurfaces have infinite grid impedance, no standing wave is produced and the SWR becomes equal to 1.

Likewise, it is also possible to determine the grid reactance required to achieve a specific SWR:

$$\tilde{X}_{e1} = \frac{1}{2}\sqrt{\left(\frac{\mathrm{SWR}+1}{\mathrm{SWR}-1}\right)^2 - 1}. \tag{4.7}$$

Figure 4.2 provides a view of the electromagnetic fields inside a structure with $d = \lambda_0$ for different values of SWR, considering the case when the first metasurface has inductive properties ($\tilde{X}_{e1} > 0$).

An additional characteristic of standing waves is the position of the field critical points, maxima and minima, which can be found using the first and second derivatives of the magnitude of the amplitude of the standing field $\mathbf{E}_S$, shown in (4.1). It is convenient to define z_0 as the location of maxima/minima, written for lossless metasurfaces as

$$z_0 = \frac{\lambda_0}{4}\left(p - \frac{\arctan(2\tilde{X}_{e1})}{\pi}\right), \tag{4.8a}$$

$$(-1)^p \overset{?}{\underset{<}{>}} 0. \tag{4.8b}$$

Notice that z_0 are a set of points (denoted by the integer p) separated by $\lambda_0/4$. The exact locations of these points also depend on the grid reactance, as shown in Figure 4.3. For low grid reactance values, the offset produced by the resonator becomes equal to zero, placing the locations for maxima and minima as multiples of $\lambda_0/4$, like the standing waves inside a conventional cavity resonator. In the opposite case, infinite grid impedances will create an offset of $\lambda_0/8$ but without

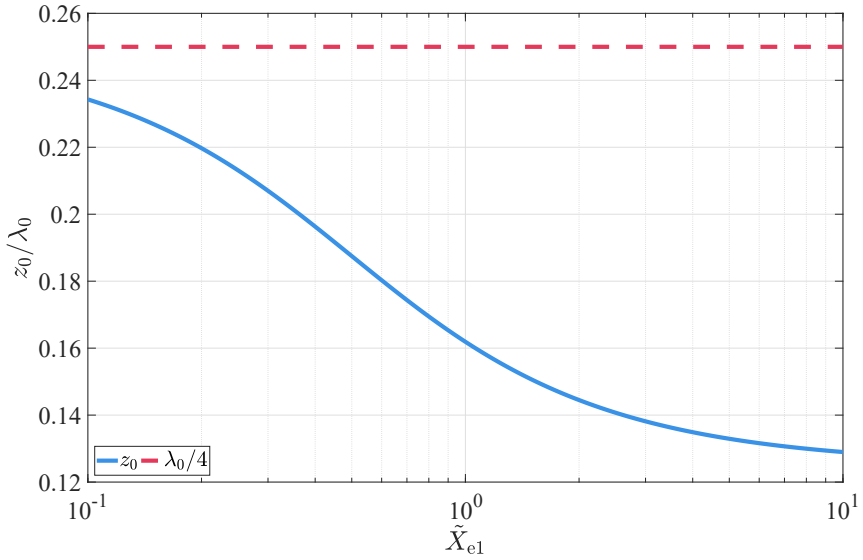

Figure 4.3. Location of first z_0 ($p = 1$) as a function of the grid reactance.

any significance since both metasurfaces become transparent.

The criteria which determines if a certain z_0 is a local maximum/minimum is shown in (4.8b), based on concavity; where a negative value means a local maximum, and a positive value corresponds to a local minimum (showed as $\overset{?}{>}_{<}$). Additionally, the sequence of maxima/minima is determined by the reactance type of the first metasurface: If the first metasurface has an inductive reactance, then the first critical point will be a local maximum; and, on the other hand, if the metasurface has a capacitive reactance, the first critical point will be a local minimum. Given the condition shown in (3.27c), inverting the grid reactance signs implies that the standing waves profile is also inverted.

In order to understand the relation between the electric field of the standing wave $\mathbf{E}_\mathrm{S}$ and the incident field $\mathbf{E}_\mathrm{I}$, it is convenient to define the normalized standing wave function S_e:

$$S_\mathrm{e}(z) = \frac{\mathbf{E}_\mathrm{S} \cdot \mathbf{a}_\mathrm{x}}{E_\mathrm{I}} = Fe^{-jk_0 z} + Be^{jk_0 z} \tag{4.9}$$

By substituting the transfer functions of Equations (4.5), and considering pure-reactive metasurfaces, the absolute value of S_e can be reduced to

$$|S_\mathrm{e}(z)| = \frac{1}{|\tilde{X}_{e1}|}\sqrt{\tilde{X}_{e1}^2 + \tilde{X}_{e1}\sin(2k_0 z) + \sin^2(k_0 z)}. \tag{4.10}$$

The magnitudes of field's maxima and minima are found at the values of $z = z_0$ specified in Equation (4.8), such that the field maxima and minima are written, respectively, as

$$|S_\mathrm{e}|_\mathrm{max} = \sqrt{\mathrm{SWR}}, \quad |S_\mathrm{e}|_\mathrm{min} = \frac{1}{\sqrt{\mathrm{SWR}}}. \tag{4.11}$$

Resonator formed by a magnetically polarizable and an electrically polarizable metasurfaces

In the case of an MER, Equation (4.4) can be reused, but considering the transfer function of the inner fields for this resonator:

$$F = 1 + \frac{1}{2\tilde{Z}_{e2}} = 1 - \frac{j}{2\tilde{X}_{e2}}, \tag{4.12a}$$

$$B = \frac{1}{2\tilde{Z}_{e2}} = -\frac{j}{2\tilde{X}_{e2}}. \tag{4.12b}$$

Similar SWR equations can be obtained for this case:

$$\mathrm{SWR} = \frac{|2\tilde{Z}_{e2} + 1| + 1}{|2\tilde{Z}_{e2} + 1| - 1}, \tag{4.13}$$

$$\tilde{X}_{e2} = \frac{1}{2}\sqrt{\left(\frac{\mathrm{SWR} + 1}{\mathrm{SWR} - 1}\right)^2 - 1}, \tag{4.14}$$

where the first one corresponds to the SWR as a function of the EMP grid impedance and the second equation gives us the required reactance for the second metasurface when the lossless/passive case is considered. Figure 4.4 shows electromagnetic fields across the two metasurfaces when they are separated by the distance $d = 3\lambda_0/4$, for different values of SWR, and considering the EPM as purely inductive ($\tilde{X}_{e2} > 0$).

As in the scenario where a DER was considered, it is possible to find the critical points of the standing wave of Equation (4.1) using the first and second derivatives. The location of the critical points z_0 and its maxima/minima criteria are written

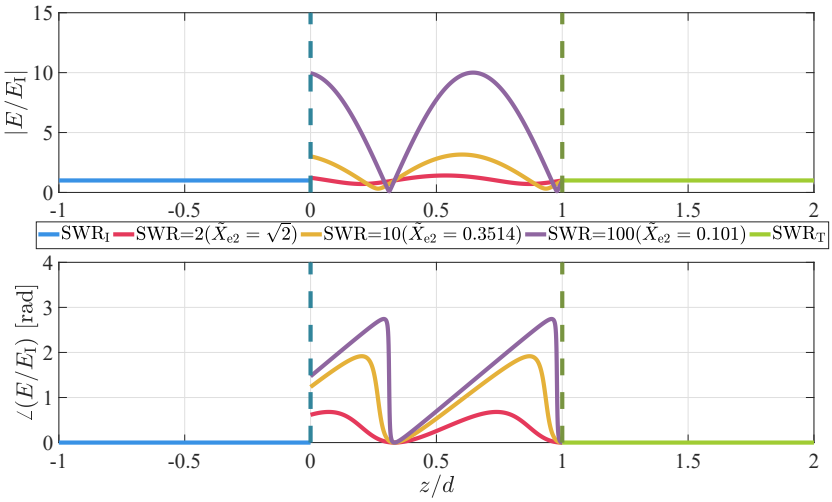

Figure 4.4. Standing waves across the magnetic and electric sheet structure for different SWR values for a distance $d = 3\lambda_0/4$ and $\tilde{X}_{e2} > 0$: top - Magnitude, bottom - Phase.

as

$$z_0 = \frac{\lambda}{4}\left(q + \frac{\arctan(2\tilde{X}_{e2})}{\pi}\right), \tag{4.15a}$$

$$(-1)^{q+1} \overset{?}{\underset{<}{>}} 0, \tag{4.15b}$$

using the integer q as an analogue of p in (4.8). An important difference between the DER case and this case is that the maxima/minima sequence is not altered by the nature of the second metasurface grid impedance; as the first point will always be a maximum. As mentioned in the previous case, inverting the metasurfaces order (the EMP before the MPM) will produce a mirror image of the standing waves for the original case.

The amplitude of the standing wave can be obtained by substituting the free-space transfer functions of (4.12) into Equation (4.9), considering pure reactive metasurfaces. The simplified expression for the standing wave's magnitude is written as

$$|S_e(z)| = \frac{1}{|\tilde{X}_{e2}|}\sqrt{\tilde{X}_{e2}^2 + \tilde{X}_{e2}\sin(2k_0 z) + \cos^2(k_0 z)}, \tag{4.16}$$

which peak values at $z = z_0$ of (4.15) lead us to the same expressions of (4.11).

Until now, we analysed each resonator separately, but since their properties and performance are quite similar, it is better to focus on one kind of structure in order to reduce redundancy in the following analysis. Due to its simplicity, the selected resonator is DER.

4.2 Multiple-reflection analysis

The analysis which lead us to the transfer functions corresponding to each scattered field was performed considering the total value of each scattered field. This kind of analysis is useful to understand the structure performance under nominal conditions, but the structure behaviour as a function of each contributors is hidden. Because of that, it is useful to perform a multiple reflection analysis, which considers the scattered fields produced by the incidence of a single plane wave.

Consider the scattered fields of Figure 4.5, where the reflections produced by a plane wave inside the structure are decomposed. Each metasurface is characterized by its transmission coefficient $\tilde{\tau}$ and reflection coefficient $\tilde{\Gamma}$, as defined in (2.13), (2.21) and (2.29) for EPM, MPM and EMPM, respectively. As mentioned earlier, the use of the scattering coefficients in the second metasurface is neccesary to consider the effect of displacement shown in Equation (3.5). This analysis

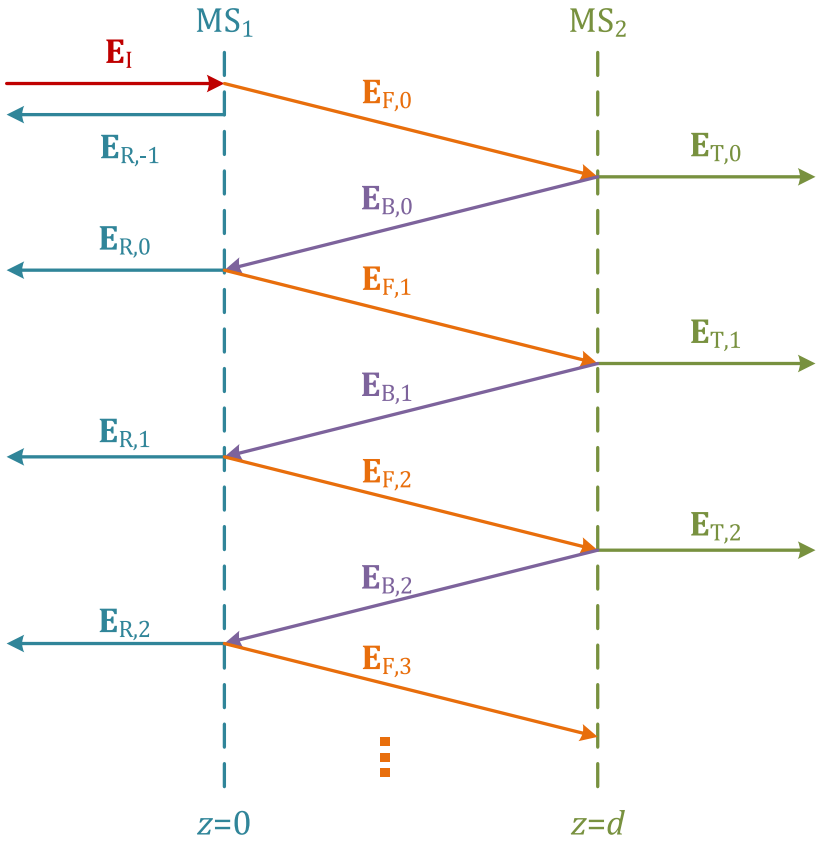

Figure 4.5. Decomposed scattered fields produced in a volume bounded by two arbitrary metasurfaces. The scattered waves are show as oblique only for visual clarify.

considers that the metasurfaces grid impedances are frequency-invariant, and the results of this analysis cannot be considered directly as a transient analysis. On the other hand, there are some concepts that can be related to a transient analysis.

Due to the multiple reflected and transmitted waves, the net scattered fields are the sums of all reflected/transmitted components. Hence, each resonator's transfer function (F, B, τ and Γ) can be determined for the m-th cycle. A cycle is defined as the period of time between the generation of two consecutive scattered components of the same scattered wave, or as the round-trip time between the two metasurfaces. Under these considerations, the transfer functions after the m-th cycle:

$$F_{\mathrm{m}} = \tilde{\tau}_1 \left[1 + \tilde{\Gamma}_1\tilde{\Gamma}_2 e^{-2jk_0d} + \ldots + \left(\tilde{\Gamma}_1\tilde{\Gamma}_2 e^{-2jk_0d}\right)^{\mathrm{m}}\right], \tag{4.17a}$$

$$B_{\mathrm{m}} = \tilde{\tau}_1\tilde{\Gamma}_2 e^{-2jk_0d}\left[1 + \tilde{\Gamma}_1\tilde{\Gamma}_2 e^{-2jk_0d} + \ldots + \left(\tilde{\Gamma}_1\tilde{\Gamma}_2 e^{-2jk_0d}\right)^{\mathrm{m}}\right], \tag{4.17b}$$

$$\tau_{\mathrm{m}} = \tilde{\tau}_1\tilde{\tau}_2 \left[1 + \tilde{\Gamma}_1\tilde{\Gamma}_2 e^{-2jk_0d} + \ldots + \left(\tilde{\Gamma}_1\tilde{\Gamma}_2 e^{-2jk_0d}\right)^{\mathrm{m}}\right], \tag{4.17c}$$

$$\Gamma_{\mathrm{m}} = \tilde{\Gamma}_1 + \tilde{\tau}_1^2\tilde{\Gamma}_2 e^{-2jk_0d}\left[1 + \tilde{\Gamma}_1\tilde{\Gamma}_2 e^{-2jk_0d} + \ldots + \left(\tilde{\Gamma}_1\tilde{\Gamma}_2 e^{-2jk_0d}\right)^{\mathrm{m}}\right], \tag{4.17d}$$

where $\tilde{\tau}_1$ and $\tilde{\Gamma}_1$ correspond to the transmission and reflection coefficients of the first metasurface, while $\tilde{\tau}_2$ and $\tilde{\Gamma}_2$ correspond to the second metasurface.

All the transfer functions of Equation (4.17) contains a geometric series, defined as Ψ_{m} (the stepped resonant factor), which can be reduced to

$$\Psi_{\mathrm{m}} = \sum_{l=0}^{\mathrm{m}} \left(\tilde{\Gamma}_1\tilde{\Gamma}_2 e^{-2jk_0d}\right)^l = \frac{1-\left(\tilde{\Gamma}_1\tilde{\Gamma}_2 e^{-2jk_0d}\right)^{\mathrm{m}+1}}{1-\tilde{\Gamma}_1\tilde{\Gamma}_2 e^{-2jk_0d}}. \tag{4.18}$$

In theory, the geometric series of Equation (4.18) converges only when $|\tilde{\Gamma}_1\tilde{\Gamma}_2| < 1$. Due to that, the transient component could diverge when active metasurfaces are used. In a realistic scenario, this function never diverges since active metasurfaces are nonlinear at high amplitudes of the fields. On the other hand, when lossy or pure reactive metasurfaces are used, the steeped resonant ractor can be reduced to

$$\Psi = \lim_{\mathrm{m}\to\infty} \Psi_{\mathrm{m}} = \frac{1}{1-\tilde{\Gamma}_1\tilde{\Gamma}_2 e^{-2jk_0d}}, \quad \left(|\tilde{\Gamma}_1\tilde{\Gamma}_2| < 1\right), \tag{4.19}$$

which corresponds to the resonance factor Ψ shown in Equation (3.8a). In fact, all the transfer functions converge at infinite cycles to the transfer functions of Equation (3.8).

Figure 4.6 shows that all the transfer functions converge evenly as the cycles pass. Additionaly, because of the same convergence, the SWR does not depend on the current cycle. From these results, there are two conclusions to be considered: First, the SWR cannot be used as a figure of merit of the structure in a multiple reflection analysis, instead, the figure of merit must be based on Ψ_{m}. In that case, the convergent cycle must be defined as the m-cycle at which the absolute value of its instance function $|\Psi_{\mathrm{m}}|$ is at least 90% of $|\Psi|$. Because of the complex nature of the reflection coefficients in (4.18), the definition of convergent cycle cannot be applied directly, but instead we consider only the absolute value of the reflection

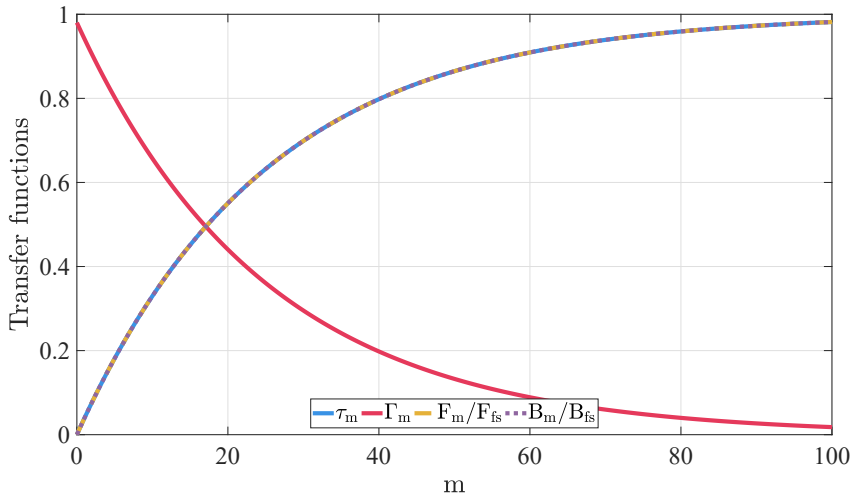

Figure 4.6. Evolution of transfer functions depending of the number of cycles, for the case of a DER with SWR $= 100$.

coefficients product. With this minor change, the expression for the convergent cycle can be written as

$$\mathrm{m}_{90\%} = \left\lceil \frac{\ln\left(1-0.9\right)}{\ln|\tilde{\Gamma}_1\tilde{\Gamma}_2|} - 1 \right\rceil, \tag{4.20}$$

where the ceiling function is used to obtain an integer value closer to the nominal stage of the resonator.

Figure 4.7 shows the dependency of the convergent cycle as a function of the grid impedance for a DER. This figure show the first tradeoff in this kind of structures: The convergent cycle is inversely proportional to the absolute value of the grid reactance, meaning that low reactive grid impedances can create high-SWR standing waves but it requires more reflections to achieve its nominal state. On the other hand, resonators with high reactive grid impedances produce low SWR with high convergence. It is especially interesting to consider the case when $\mathrm{m}_{90\%} = 1$, meaning that the resonator is invisible after one cycle (with “direct" convergence). This case is obtained using Equation (4.21), where $\tilde{X}_{\mathrm{e,crit}}$ is referred to the first metasurface in the case when DER is used or referred to the EPM when a MER is used. In both cases, the normalized grid impedance is approximately 0.7352, corresponding to SWR of 3.5698.

$$\tilde{X}_{\mathrm{e,crit}} = \frac{1}{2}\sqrt{\sqrt{\frac{1}{1-0.9}} - 1} \tag{4.21}$$

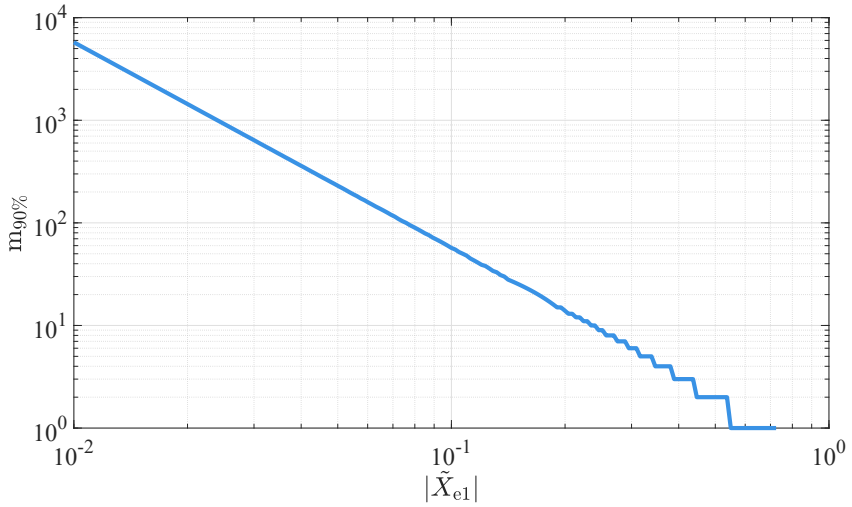

Figure 4.7. Convergent cycle as a function of the grid reactace for the case of a DER with pure reactive metasurfaces.

4.3 Performance in frequency domain

The invisibility conditions for a volume bounded by metasurfaces can be classified by their nature: The first condition is given by the relation between the metasurfaces grid impedances, and the second condition requires that a fixed electric distance between the metasurfaces. The grid impedances condition was used previously as a design's parameter to engineer the resonant fields inside the bounded volume based on the equivalent SWR. But, the second condition was only represented as a collection of fixed distances between the metasurfaces. This criterion is only applicable when a monochromatic wave illuminates the bounded volume. Because of that, it is important to characterize the performance of this kind of structures when they are illuminated by a source with variable frequency. This analysis does not consider the effect of the wave's wavelength over the metasurfaces, because different metasurfaces designs can lead to different grid impedance's models. In order to characterize only the effects of frequency into the structure design, the grid impedances of each metasurface are considered constant in the selected frequency range. Therefore, as the frequency of the incident wave changes, the wavenumber k becomes different from k_0 found in (3.22c), changing the magnitude and phase of the transfer functions of Equation (3.26).

Figure 4.8 shows the effect of the source's wavelength over the transmission coefficient of a DER, where λ_0 is the wavelength corresponding to the first Fabry-Perot mode ($n = 1$). This figure shows that the resonator becomes invisible only at the frequencies related to different resonant modes, modifying the effective bandwidth as a function of the grid impedance. Figure 4.8 also reminds the Airy distribution of the transmitted wave from a FPR, where highly reflective bounds (dielectric

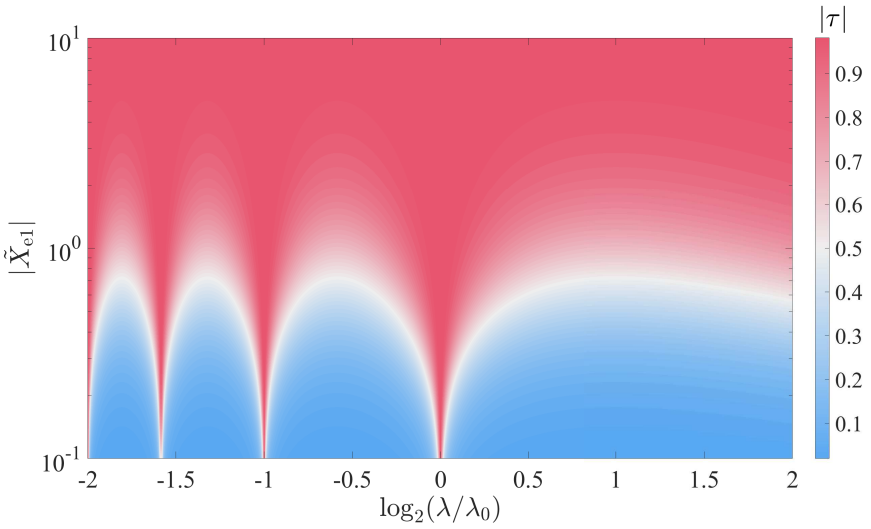

Figure 4.8. Transmission coefficient as a function of the grid reactance and the normalized wavelength for a DER.

interfaces or metallic plates) lead to a narrow transmission in the frequency domain. Like in RLC circuits, the quality factor can be used as a figure of merit for this frequency-related behaviour. The Q-factor is defined as the ratio of the resonance frequency and the half-power bandwidth with respect to the structure transmittance:

$$Q = \frac{\omega_0}{\Delta\omega}, \quad |\tau(\omega_0 \pm \Delta\omega/2)|^2 = \frac{1}{2}|\tau|^2_{\max}, \tag{4.22}$$

where the half-power bandwidth ($\Delta\omega$) is defined as the frequency range where the transmittance is at least half of the maximum value, which in the case of ideal invisibility is equal to 1.

In the scenario where a DER is considered, the invisibility conditions related with the impedance in (3.27c) and the resonance phase ($e^{2jk_0d} = 1$, which leads to $d = n\lambda_0/2$) are considered into the transmission coefficient in free space of Equation (3.26c). Then, applying the quality factor definition of (4.22), the expression of Equation (4.23) is achieved:

$$|e^{2jk_\Delta d}\left(1 - 4\tilde{Z}^2_{\mathrm{e1}}\right) - 1|^2 = 32|\tilde{Z}^2_{\mathrm{e1}}|^2 \tag{4.23}$$

The variable k_Δ represents the wavenumber at the cutoff frequency: $k_\Delta = k_0 \pm (\Delta\omega\sqrt{\varepsilon_0\mu_0})/2$. If the phase product $k_\Delta d$ is considered, the expression can be reduced to $k_\Delta d = n\pi\,(1 \pm \Delta\omega/2\omega_0)$. The first component of the sum will vanish after substituting it into the exponent in (4.23), while the second component will lead us to the quality factor. The solution of Equation (4.23) requires the complex expansion of the grid impedance ($\tilde{Z}_{\mathrm{e}} = \tilde{R}_{\mathrm{e}} + j\tilde{X}_{\mathrm{e}}$) and the complex exponential $e^{2jk_\Delta d}$:

$$\begin{aligned} &32\left[\left(\tilde{R}^2_{\mathrm{e1}} - \tilde{X}^2_{\mathrm{e1}}\right)^2 + \left(2\tilde{R}_{\mathrm{e1}}\tilde{X}_{\mathrm{e1}}\right)^2\right] \\ &= \left[\cos\left(\frac{n\pi}{Q}\right)\left(1 - 4\tilde{R}^2_{\mathrm{e1}} + 4\tilde{X}^2_{\mathrm{e1}}\right) \pm 8\sin\left(\frac{n\pi}{Q}\right)\tilde{R}_{\mathrm{e1}}\tilde{X}_{\mathrm{e1}} - 1\right]^2 \\ &\quad + \left[8\cos\left(\frac{n\pi}{Q}\right)\tilde{R}_{\mathrm{e1}}\tilde{X}_{\mathrm{e1}} \pm \sin\left(\frac{n\pi}{Q}\right)\left(4\tilde{R}^2_{\mathrm{e1}} - 4\tilde{X}^2_{\mathrm{e1}} - 1\right)\right]^2 \end{aligned}. \tag{4.24}$$

Due to the complexity of this equation of that, it is recommended to enforce the condition of pure reactive metasurfaces ($\tilde{R}_{\mathrm{e1}} = \tilde{R}_{\mathrm{e2}} = 0$), to simplify the equation into

$$32\tilde{X}^4_{\mathrm{e1}} = \left[\cos\left(\frac{n\pi}{Q}\right)\left(1 + 4\tilde{X}^2_{\mathrm{e1}}\right) - 1\right]^2 + \left[\sin\left(\frac{n\pi}{Q}\right)\left(1 + 4\tilde{X}^2_{\mathrm{e1}}\right)\right]^2. \tag{4.25}$$

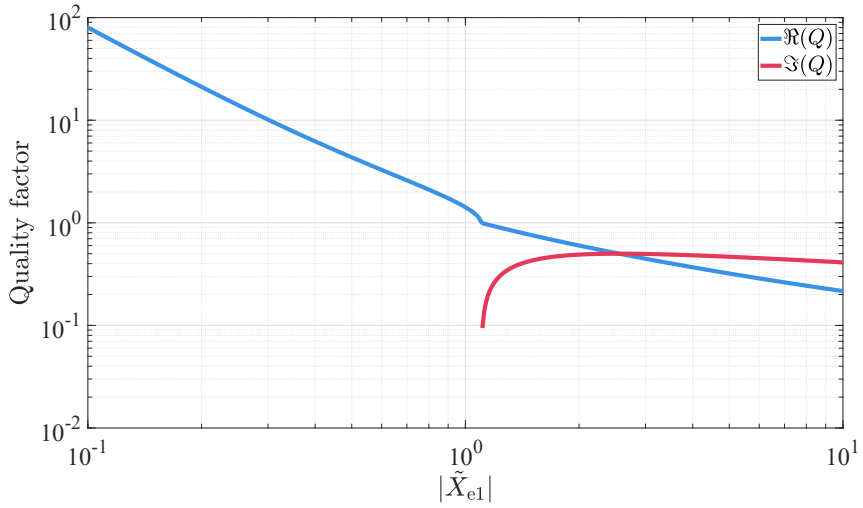

Figure 4.9. Quality factor as a function of the grid reactance for $n = 1$.

This equation is easier to solve, obtaining the expression for the quality factor:

$$Q = \frac{n\pi}{\operatorname{acos}\left(1 - \dfrac{8\tilde{X}_{e1}^4}{1 + 4\tilde{X}_{e1}^2}\right)}. \tag{4.26}$$

From the previous results, it can be found that the quality factor has a linear relation with respect to the Fabry-Perot number n. As an example, the quality factor can be increased 100% by doubling the distance between the metasurfaces. This property can be explained if we consider the field alignment between the forward and backward wave. At the resonance frequency, the forward and backward waves fields can add constructively creating standing waves. But if the frequency is changed, the distance between the metasurfaces and the ideal distance (where the forward and backward waves are contructively aligned) differ, reducing the standing fields produced inside the resonator and the transmitted wave. If the distance between the metasurfaces is large (with a high Fabry-Perot number), the resonator response will be narrower as the difference between the physical distance and the ideal distance also increases.

Also, as shown in Figure 4.9, the quality factor is affected by the grid reactance. Because the current in metasurfaces with high impedances is harder to induce, as they are more transparent, the quality factor decreases as the grid reactance increases. If we inspect Equation (4.26), we see that the quality factor reaches an inflection point when

$$\tilde{X}_{e1} = \pm\sqrt{\frac{1+\sqrt{2}}{2}}, \tag{4.27}$$

with an SWR of 2.4144, and the denominator becomes equal to π. Then, two effects happen: the quality factor becomes equal to n, and beyond this point

the quality factor becomes complex, as shown in Figure 4.9. In practical terms, the complex quality factor means that the structure transmits at all frequencies under the -3 dB level. This effect takes place because the bandwidths of the different resonant modes merge together (assuming frequency-independent grid impedances).

4.4 Influence of metasurfaces dissipation loss on resonator properties

Until now, we considered ideal metasurfaces and their conditions which grant invisibility while tailoring the fields inside the inner volume. But, real metasurfaces have intrinsic losses produced by the meta-atoms materials and metasurfaces substrates. In this study, we will use two assumptions: the losses produced by meta-atoms dominate over the other ones. The second assumption is that metasurfaces with equal absolute values of grid reactances have equal meta-atoms losses. Under these assumptions, let us define the lossy grid impedances for both metasurfaces:

$$\tilde{Z}_{\mathrm{e}1} = \tilde{R}_{\mathrm{loss}} + j\tilde{X}_{\mathrm{e}1}, \quad \tilde{Z}_{\mathrm{e}2} = \tilde{R}_{\mathrm{loss}} + j\tilde{X}_{\mathrm{e}2}, \tag{4.28}$$

where $\tilde{R}_{\mathrm{loss}}$ represents the normalized grid losses ($R_{\mathrm{loss}} = \eta_0 \tilde{R}_{\mathrm{loss}}$) and the normalized reactances $\tilde{X}_{\mathrm{e}1}$ and $\tilde{X}_{\mathrm{e}2}$ keep the relation $\tilde{X}_{\mathrm{e}1} = -\tilde{X}_{\mathrm{e}2}$ of Equation (3.27c). Using the redefined grid impedances, the transfer functions of Equation (3.26) (for a DER) can be reduced to

$$\Delta_{\mathrm{loss}} = (1 + 2\tilde{R}_{\mathrm{loss}})^2 + 4\tilde{X}_{\mathrm{e}1}^2 - 1, \tag{4.29a}$$

$$\Gamma_{\mathrm{loss}} = {\Delta_{\mathrm{loss}}}^{-1} \left[-4\tilde{R}_{\mathrm{loss}} \right], \tag{4.29b}$$

$$\tau_{\mathrm{loss}} = 4{\Delta_{\mathrm{loss}}}^{-1} \left[\tilde{R}_{\mathrm{loss}}^2 + \tilde{X}_{\mathrm{e}1}^2 \right], \tag{4.29c}$$

$$F_{\mathrm{loss}} = 2{\Delta_{\mathrm{loss}}}^{-1} \left[\tilde{R}_{\mathrm{loss}} + j\tilde{X}_{\mathrm{e}1} + 2\left(\tilde{R}_{\mathrm{loss}}^2 + \tilde{X}_{\mathrm{e}1}^2 \right) \right], \tag{4.29d}$$

$$B_{\mathrm{loss}} = -2{\Delta_{\mathrm{loss}}}^{-1} \left[\tilde{R}_{\mathrm{loss}} + j\tilde{X}_{\mathrm{e}1} \right]. \tag{4.29e}$$

Figure 4.10 shows the evolution of the electric fields inside and outside the resonator for different grid losses, assuming $\tilde{X}_{\mathrm{e}1} = -\tilde{X}_{\mathrm{e}2} = 0.101$ (corresponding to the case when $\mathrm{SWR} = 100$ and $\tilde{R}_{\mathrm{loss}} = 0$).

From Figure 4.10, three different behaviours can be identified depending on the ratio between metasurfaces resistance and reactance. The low-loss ($\tilde{R}_{\mathrm{loss}} \ll |\tilde{X}_{\mathrm{e}1}|$) region has waves close to the lossless case and the resonator is almost invisible. The high-loss ($\tilde{R}_{\mathrm{loss}} \gg |\tilde{X}_{\mathrm{e}1}|$) region is dominated by the meta-atoms losses. These high losses result in the fact that the currents in the metasurfaces are harder to induce, and the metasurfaces become transparent. The transition region, where

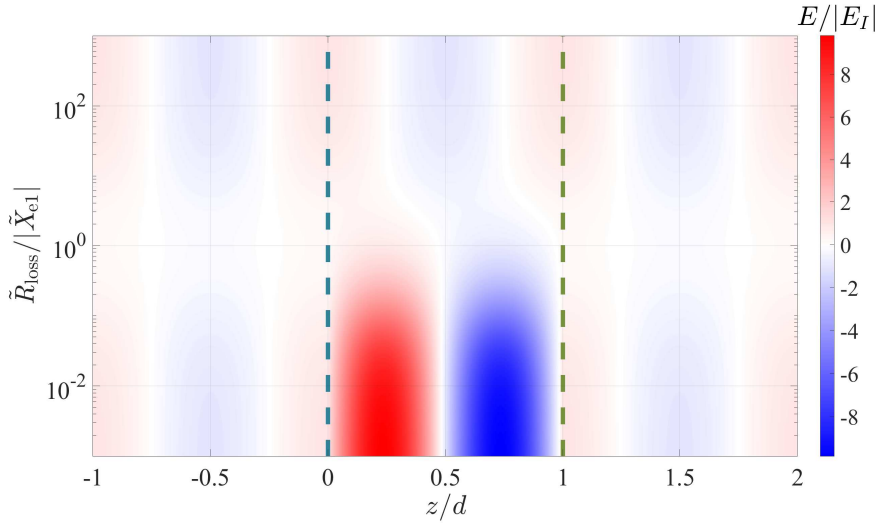

Figure 4.10. 1-D parametric sweep for the normalized electrical field for different losses, considering $d = \lambda$ and $\tilde{X}_{\text{e1}} = 0.101$ (SWR $= 100$ if $\tilde{R}_{\text{loss}} = 0$).

the loss resistances are comparable with the grid reactances, is characterized by high reflection and low transmission through the structure, while the inner fields have a low standing wave ratio.

Since the losses degrade the metasurfaces performance, it is compulsory to estimate the SWR under these new conditions. The SWR for lossy metasurfaces is obtained by applying the forward and backward transfer functions of (4.29) into the SWR definition of Equation (4.4):

$$\text{SWR}_{\text{loss}} = \frac{|2\tilde{R}_{\text{loss}} - 2j\tilde{X}_{\text{e1}} + 1| + 1}{|2\tilde{R}_{\text{loss}} - 2j\tilde{X}_{\text{e1}} + 1| - 1}. \tag{4.30}$$

As shown in Figure 4.11, the SWR decreases as the losses increase since the resonance is extinguished as the induced currents vanish. This effect is clearly seen also with the transmittance $|\tau|^2$, reflectance $|\Gamma|^2$, and absorbance $|\text{A}|^2 = 1 - |\tau|^2 - |\Gamma|^2$. It is important to remark that the phase of transmission coefficient τ and the reflection coefficient Γ are not affected by the grid losses.

During this part of the analysis, the grid reactances were considered as the same for an ideal SWR of 100 ($|\tilde{X}_{\text{e1}}| = 0.101$) and how the grid losses affect the structure performance. To expand the knowledge related with grid losses, Figure 4.12 becomes useful. The SWR is affected negatively as the grid losses increases; but this effect can be reduced by increasing the grid reactance, with the drawback of degradating the structure's performance in terms of ideal SWR.

Due of the degradation in resonator's performance due to grid losses, it is important to characterize these losses with a realistic model. In our case, we selected to model a metallic plate (which can be seen as a slab mad of a given medium), useful to determine the grid losses of different metals. For the analysis, we will consider

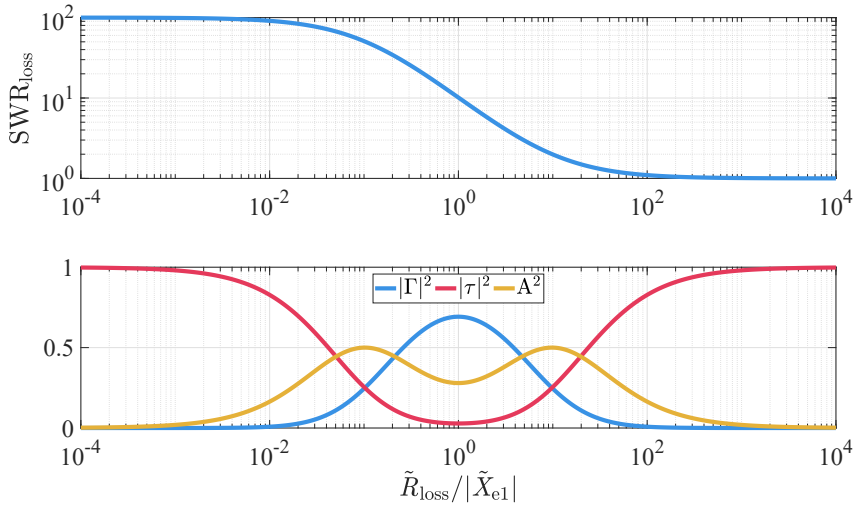

Figure 4.11. DER performance as a function of the normalized grid resistance for the case $\tilde{X}_{e1} = 0.101$ (SWR $= 100$ if $\tilde{R}_{loss} = 0$): top - SWR, bottom - transmittance, reflectance and absorbance

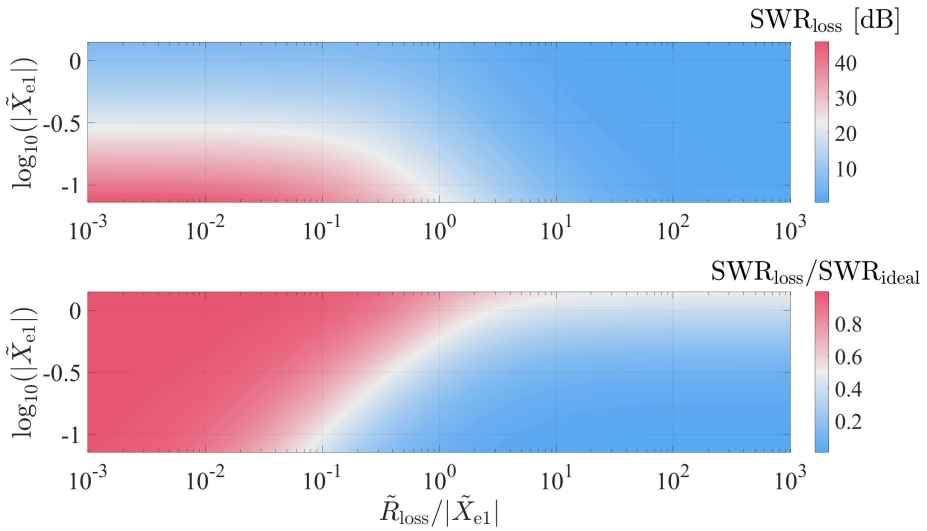

Figure 4.12. SWR as a function of the grid resistance and grid reactance): top - SWR in dB scale, bottom - Normalized SWR respect to the ideal case.

the scenario shown in Figure 4.13, where an infinite surface with thickness Δd, composed by a medium (like gold or silver) with complex characteristic impedance η and complex propagation constant γ, is normally illuminated by a plane wave. The scattered fields are denoted as it was shown in Equation (2.9); but in the inner fields of (3.1), the propagation constant component jk must be replaced by γ.

Considering the Maxwell equations, the boundary conditions at $z = 0$ and $z = \Delta d$

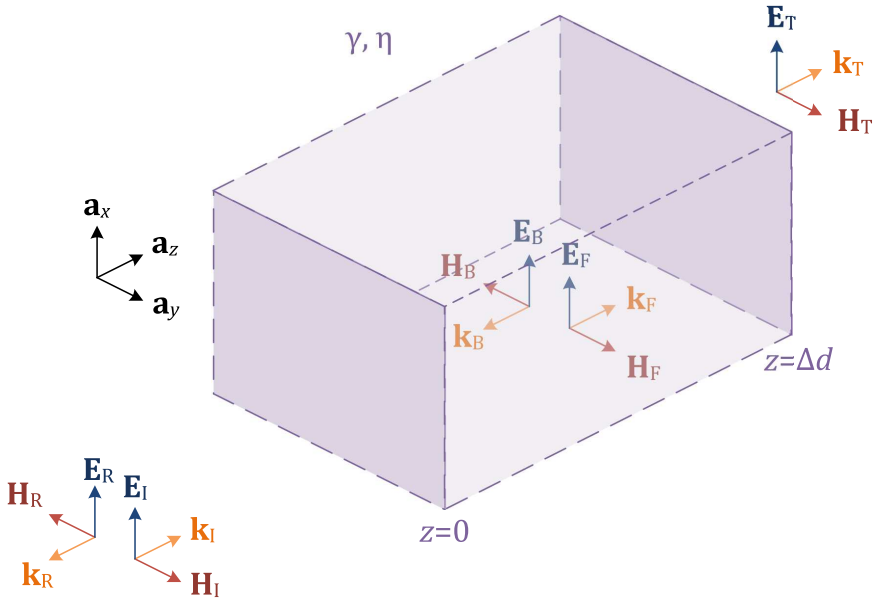

Figure 4.13. Electromagnetic fields across a generic material.

do not contain surface currents and can be written as

$$\mathbf{E}_{\mathrm{I}}(0) + \mathbf{E}_{\mathrm{R}}(0) = \mathbf{E}_{\mathrm{F}}(0) + \mathbf{E}_{\mathrm{B}}(0), \tag{4.31a}$$

$$\mathbf{H}_{\mathrm{I}}(0) + \mathbf{H}_{\mathrm{R}}(0) = \mathbf{H}_{\mathrm{F}}(0) + \mathbf{H}_{\mathrm{B}}(0), \tag{4.31b}$$

$$\mathbf{E}_{\mathrm{F}}(\Delta d) + \mathbf{E}_{\mathrm{B}}(\Delta d) = \mathbf{E}_{\mathrm{T}}(\Delta d), \tag{4.31c}$$

$$\mathbf{H}_{\mathrm{F}}(\Delta d) + \mathbf{H}_{\mathrm{B}}(\Delta d) = \mathbf{H}_{\mathrm{T}}(\Delta d). \tag{4.31d}$$

By substituting the components of each field, the boundary conditions can be reduced to

$$E_{\mathrm{I}} + E_{\mathrm{R}} = E_{\mathrm{F}} + E_{\mathrm{B}}, \tag{4.32a}$$

$$\frac{E_{\mathrm{I}}}{\eta_0} - \frac{E_{\mathrm{R}}}{\eta_0} = \frac{E_{\mathrm{F}}}{\eta} - \frac{E_{\mathrm{B}}}{\eta}, \tag{4.32b}$$

$$E_{\mathrm{F}} e^{-\gamma \Delta d} + E_{\mathrm{B}} e^{\gamma \Delta d} = E_{\mathrm{T}} e^{-jk_0 \Delta d}, \tag{4.32c}$$

$$\frac{E_{\mathrm{F}}}{\eta} e^{-\gamma \Delta d} - \frac{E_{\mathrm{B}}}{\eta} e^{\gamma \Delta d} = \frac{E_{\mathrm{T}}}{\eta_0} e^{-jk_0 \Delta d}. \tag{4.32d}$$

The scattered fields can be solved as it was done for the bounded volume between two metasurfaces, by defining transfer functions for each variable. In this case, we are only interested in the transmission and reflection coefficients:

$$\tau_{\mathrm{loss}} = \frac{4 e^{j(k_0 - \gamma)\Delta_d} \eta \eta_0}{(\eta + \eta_0)^2 - e^{-2\gamma \Delta_d} (\eta - \eta_0)^2}, \tag{4.33a}$$

$$\Gamma_{\mathrm{loss}} = \frac{\left(1 - e^{-2\gamma \Delta_d}\right)\left(\eta^2 - {\eta_0}^2\right)}{(\eta + \eta_0)^2 - e^{-2\gamma \Delta_d} (\eta - \eta_0)^2}. \tag{4.33b}$$

Using these two transfer functions, and by using the Huygens equivalence princi-

ple, it is possible to define an equivalent current sheet which produces the same transfer functions. In this case, we can use the theory of EMPMs to obtain the equivalent grid impedances, as it was done in Equation (2.30). Therefore, the grid losses can be defined as

$$Z_{\mathrm{loss,e}} = \frac{\eta_0}{2}\frac{1+\tau_{\mathrm{loss}}+\Gamma_{\mathrm{loss}}}{1-\tau_{\mathrm{loss}}-\Gamma_{\mathrm{loss}}}, \tag{4.34a}$$

$$Z_{\mathrm{loss,m}} = 2\eta_0\frac{1-\tau_{\mathrm{loss}}+\Gamma_{\mathrm{loss}}}{1+\tau_{\mathrm{loss}}-\Gamma_{\mathrm{loss}}}. \tag{4.34b}$$

One problem with the lossy slab model is that it is based on an EMPM, which considers electrical and magnetic grid impedance, required to model the discontinuities in electric and magnetic fields. These two grid impedances cannot be compared directly with the EPM of the lossless case, since it only has the electric grid impedance. Because of that, it is necessary to find a different impedance, which can be used to compare EPMs and EMPMs under the same conditions. The impedance matrix for an EMPM was described in Equation(2.39). In that case, the Z-impedance element Z_{11} is a suitable parameter to compare the metallic slab's model with the lossless metasurfaces. Therefore, the impedance for the metallic slab $Z_{11,\mathrm{loss}}$ and for the lossless EPMs ($Z_{11,\mathrm{e1}}$ and $Z_{11,\mathrm{e2}}$, respectively) can be written as

$$Z_{11,\mathrm{loss}} = Z_{\mathrm{loss,e}} + \frac{Z_{\mathrm{loss,m}}}{4}, \tag{4.35a}$$

$$Z_{11,\mathrm{e1}} = -Z_{11,\mathrm{e2}} = Z_{\mathrm{e1}}. \tag{4.35b}$$

Losses in the microwave range

For practical implementations, four materials (gold, silver, aluminium and copper) are considered for the microwave range analysis ($[1-20]\,[\mathrm{GHz}]$). In this range, all the selected metals can be considered as good conductors, whose propagation constant γ and the characteristic impedance η can be written as

$$\gamma = (1+j)\sqrt{\frac{2\pi f\mu\sigma_e}{2}}, \tag{4.36a}$$

$$\eta = (1+j)\sqrt{\frac{2\pi f\mu}{2\sigma_e}}, \tag{4.36b}$$

where σ_e is the metal conductance, f is the operational frequency and μ is the metal permeability (being equal to μ_0, vacuum's permeability, for the selected metals) [42]. For this analysis, the slab thickness is equal to $17\,[\mu\mathrm{m}]$ (approximately 0.05% of the wavelength in free space at the frequency of 9 [GHz]), and the metals conductivities were taken from Reference [42]. The slab resistance R_{11} as a

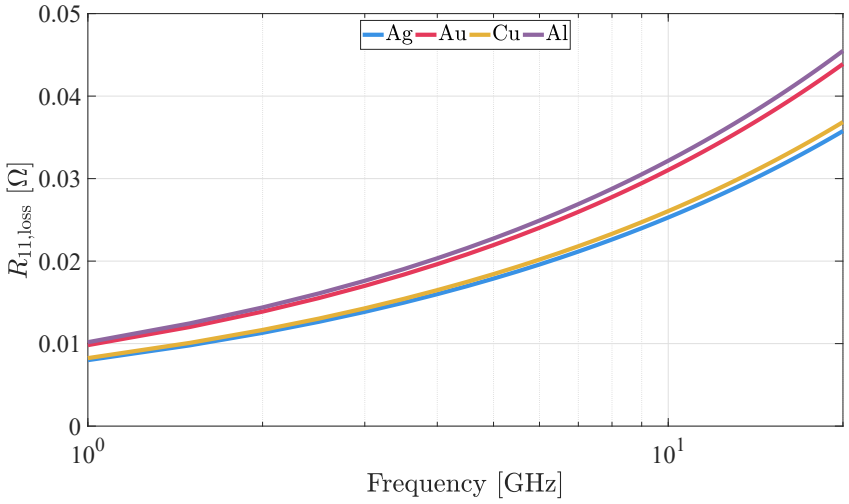

Figure 4.14. Resistance R_{11} for different materials in microwave range (1-20[GHz]) using a slab with thickness $\Delta_d = 17\,[\mu\text{m}]$.

function of the incident wave frequency is shown in Figure 4.14.

Based on these results, we can conclude that the design of a DER in the microwave range is feasible since the resistance R_{11} of the metallic slab is quite small compared to the grid reactance for a high-SWR lossless resonator. For example, the grid reactance for a lossless resonator with $\text{SWR} = 100$ is equal to $|X_{\text{e1}}| \approx 40\,[\Omega]$, while in the worst case (at 20 [GHz] for aluminium) the resistance $R_{11,\text{loss}} = \text{Re}\{Z_{11,\text{loss}}\}$ is smaller than $0.05\,[\Omega]$. With this information, let us consider an example of a copper slab of thickness $\Delta_d = 17\,[\mu\text{m}]$ illuminated by a plane wave at $f = 9\,[\text{GHz}]$. In that case, the resistance $R_{11,\text{loss}}$ is equal to $0.0243\,[\Omega]$. If we compare with the grid reactance for a lossless DER with $\text{SWR} = 100$, which was mentioned to be close to $40\,[\Omega]$, the equivalent lossy resonator will have an SWR_{loss} of 99.44. Additionally, the transmittance of this resonator $|\tau_{\text{loss}}|^2$ is equal to 98.82% of the incident power, the absorbance $|\text{A}_{\text{loss}}|^2$ is around 1.18% and the reflectance $|\Gamma_{\text{loss}}|^2$ is negligible.

Losses in the near-infrared region

In the near-infrared region (more specifically between $[1 - 1.7]\,[\mu\text{m}]$), metals such as silver, gold, copper and aluminium cannot be considered as good conductors anymore, and the propagation constant and characteristic impedance can be obtained from the experimental data on their relative permittivity available in Reference [44]. For generic materials [42], the propagation constant and the medium impedance can be written as

$$\gamma = j2\pi f\sqrt{\mu\varepsilon}, \tag{4.37a}$$

$$\eta = \sqrt{\frac{\mu}{\varepsilon}}. \tag{4.37b}$$

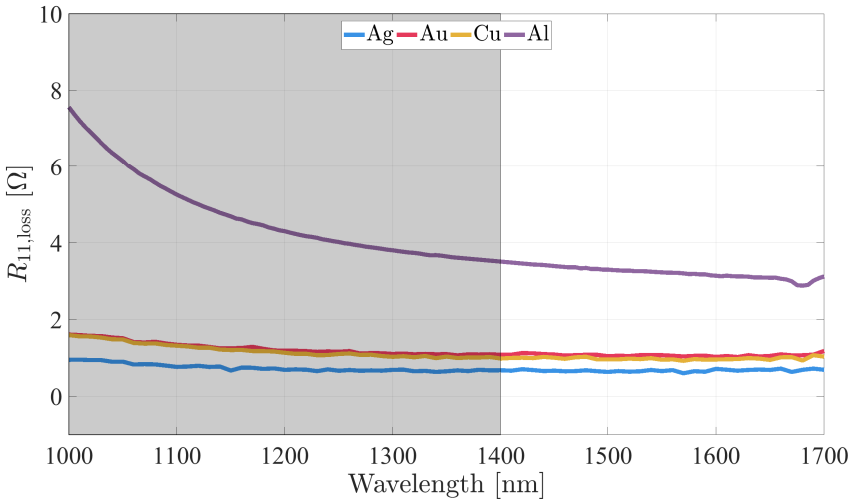

Figure 4.15. Resistance R_{11} for different materials in infrarred range ($1000 - 1700\,[\text{nm}]$) using a slab with thickness $\Delta_d = 30\,[\text{nm}]$. The usable range for this model is located between $1400 - 1700\,[\text{nm}]$.

For this analysis, the slab thickness is equal to $\Delta_d = 30\,[\text{nm}]$ (approximately 2% of $\lambda = 1550\,[\text{nm}]$). Under these conditions, the resistance R_{11} as a function of the wavelength for different materials is shown in Figure 4.15.

In this case, the results shown that the resistance R_{11} in the near-infrared region are greater than in microwave range, especially for aluminium which resistance is 20% the required grid reactance for a lossless resonator with $\text{SWR} = 100$. Let us consider as example a silver slab with thickness of $30\,[\text{nm}]$ at $\lambda = 1550\,[\text{nm}]$. In this case, the resistance $R_{11,\text{loss}}$ is equal to $0.657\,[\Omega]$, which corresponds to an SWR_{loss} of 86.16 (when a grid reactance of $\tilde{X}_{\text{e1}} = 0.101$ is used). In terms of power, this lossy structure has transmittance $|\tau_{\text{loss}}|^2$ of 73.77%, absorbance $|\text{A}_{\text{loss}}|^2$ of 24.24% with a reflectance $|\Gamma_{\text{loss}}|^2$ of approximately 2%. Based on these results, the concept of using a metallic slab to estimate the metasurface loss resistance is still valid; but simulations of actual metasurface designs will determine the grid losses more accurately. The error increases at higher frequencies, where metals start resonating at their plasma frequency. This increase of loss resistance can be seen in the shaded region of Figure 4.15.

5. Applications of invisible resonators

At this point, different properties of invisible cavity resonators were analysed based on the interaction of the resonator with an external plane wave. But, in order to reveal possible applications of this new type of resonators, it is important to develop more complex analysis. In this chapter, several scenarios when there are objects inside the resonator, will be considered. At first, the case when a radiant source is located inside the resonator (called the "reciprocal" case) is under study. Next, a mathematical model for a structure made of multiple metasurfaces is developed. Based on this new framework, the case when a planar sensor will be studied. At the end of this chapter, some more complex resonators will be analysed.

5.1 Reciprocity of the structure

Thanks to the analysis performed in previous chapters, we can understand how an invisible cavity resonator behaves when it is illuminated by an external plane wave. When the adequate conditions are achieved, the resonator is invisible (zero reflections with total transmission) while there are standing waves inside it. At this point, one question appears: what would happen if we position an electromagnetic source inside the resonator? Answering this question not only requires to find out the electromagnetic fields inside the structure, but it also requires to understand the different phenomena that are produced in this new fascinating scenario. From the previous chapter we know that inside the resonator there are regions where the electric field is stronger or weaker compared to the incident wave. According to the Lorentz reciprocity theorem, placing the source in the locations where there was field enhancement, the fields outside the resonator must be amplified by the same number of times. But this statement implies that more power would be radiated outside the structure. This conclusion must be valid even for pure-reactive metasurfaces (neither lossy nor active), which could suggest

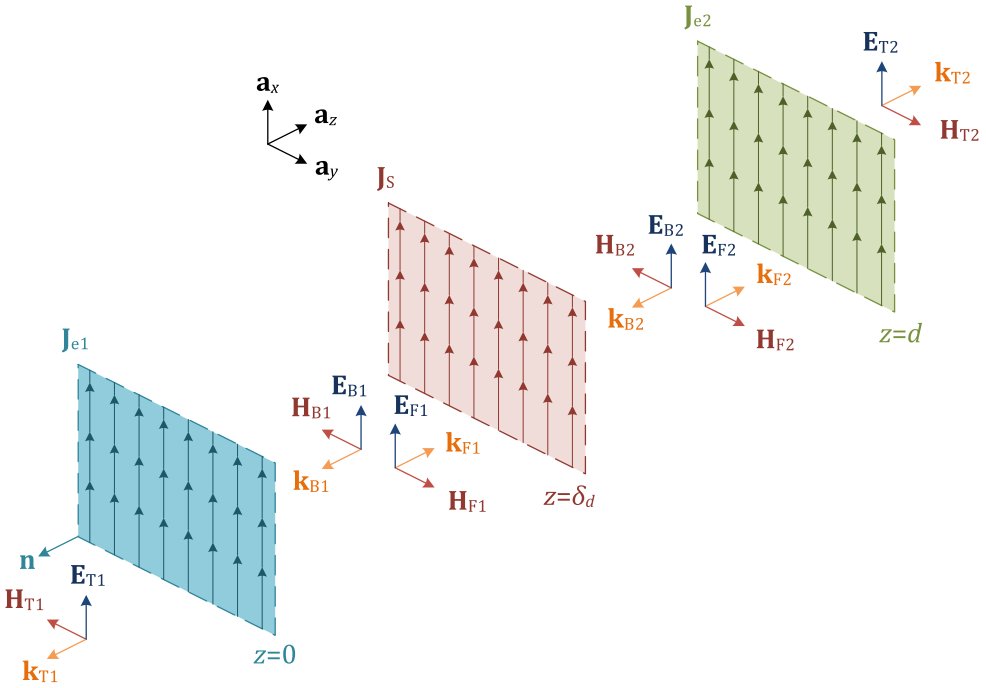

Figure 5.1. Electromagnetic fields across a DER in free space, when a current source is placed inside it.

that there is some violation of the law of conservation of energy. Also, what is the relation between the fields outside the resonator and the ones inside it? Is it possible that the location of the source affects the overall fields distribution? Due to these questions, it is important to analyse how reciprocity works for an invisible cavity resonator.

Consider the scenario where an infinitesimally thin current sheet is placed between two electrically polarizable metasurfaces, at a distance $z = \delta_d$ from the first metasurface. The metasurfaces are separated by a distance d and the source is inside the resonator at location $0 < \delta_d < d$. In order to compare the previous results with this case, the current in this sheet must radiate electromagnetic fields with the same amplitude as the plane wave used in studies of normal incidence from outside. Based on this statement, boundary conditions for a current sheet placed at the origin can be formulated, obtaining

$$\mathbf{J}_{\mathrm{s}} = -\frac{2E_{\mathrm{rad}}}{\eta_0}\mathbf{a}_{\mathrm{x}}, \tag{5.1}$$

where $\mathbf{J}_{\mathrm{S}}$ is the source electrical current density, which produces forward (propagation in $+z$ half space) and backward (propagation in $-z$ half space) waves with their magnitudes equal to E_{rad}. Due to the insertion of the source inside the resonator, the whole space can be divided into four regions, as shown in Figure 5.1, where different standing waves are produced inside the resonator, a transmitted wave $\mathbf{E}_{\mathrm{T1}}$ propagates into $z < 0$ half-space and another transmitted wave $\mathbf{E}_{\mathrm{T2}}$

propagates into $z > d$ half-space:

$$\mathbf{E}_{\mathrm{T1}} = E_{\mathrm{T1}} e^{jk_0 z}\mathbf{a}_{\mathrm{x}}, \qquad \mathbf{H}_{\mathrm{T1}} = -H_{\mathrm{T1}} e^{jk_0 z}\mathbf{a}_{\mathrm{y}}, \tag{5.2a}$$

$$\mathbf{E}_{\mathrm{T2}} = E_{\mathrm{T2}} e^{-jk_0 z}\mathbf{a}_{\mathrm{x}}, \qquad \mathbf{H}_{\mathrm{T2}} = H_{\mathrm{T2}} e^{-jk_0 z}\mathbf{a}_{\mathrm{y}}, \tag{5.2b}$$

$$\mathbf{E}_{\mathrm{F1}} = E_{\mathrm{F1}} e^{-jk_0 z}\mathbf{a}_{\mathrm{x}}, \qquad \mathbf{H}_{\mathrm{F1}} = H_{\mathrm{F1}} e^{-jk_0 z}\mathbf{a}_{\mathrm{y}}, \tag{5.2c}$$

$$\mathbf{E}_{\mathrm{B1}} = E_{\mathrm{B1}} e^{jk_0 z}\mathbf{a}_{\mathrm{x}}, \qquad \mathbf{H}_{\mathrm{B1}} = -H_{\mathrm{B1}} e^{jk_0 z}\mathbf{a}_{\mathrm{y}}, \tag{5.2d}$$

$$\mathbf{E}_{\mathrm{F2}} = E_{\mathrm{F2}} e^{-jk_0 z}\mathbf{a}_{\mathrm{x}}, \qquad \mathbf{H}_{\mathrm{F2}} = H_{\mathrm{F2}} e^{-jk_0 z}\mathbf{a}_{\mathrm{y}} \tag{5.2e}$$

$$\mathbf{E}_{\mathrm{B2}} = E_{\mathrm{B2}} e^{jk_0 z}\mathbf{a}_{\mathrm{x}}, \qquad \mathbf{H}_{\mathrm{B2}} = -H_{\mathrm{B2}} e^{jk_0 z}\mathbf{a}_{\mathrm{y}}. \tag{5.2f}$$

In this scenario, the scattered fields around each metasurface can be solved using the scattering matrix (based on Equation (2.38), considering the free-space scenario), and taking into account the displacement of the second metasurface with the results shown in Equation (3.5). The relations between the fields around each metasurface can be reduced into

$$E_{\mathrm{T1}} = \tilde{\tau}_1 E_{\mathrm{B1}}, \tag{5.3a}$$

$$E_{\mathrm{F1}} = \tilde{\Gamma}_1 E_{\mathrm{B1}}, \tag{5.3b}$$

$$E_{\mathrm{T2}} = \tilde{\tau}_2 E_{\mathrm{F2}}, \tag{5.3c}$$

$$E_{\mathrm{B2}} e^{jk_0 d} = \tilde{\Gamma}_2 E_{\mathrm{F2}} e^{-jk_0 d}. \tag{5.3d}$$

For the current sheet, the best strategy is to use the boundary conditions previously shown in Equation (2.7), obtaining

$$E_{\mathrm{F1}} e^{-jk_0\delta_d} + E_{\mathrm{B1}} e^{jk_0\delta_d} = E_{\mathrm{F2}} e^{-jk_0\delta_d} + E_{\mathrm{B2}} e^{jk_0\delta_d}, \tag{5.4a}$$

$$E_{\mathrm{F2}} e^{-jk_0\delta_d} - E_{\mathrm{B2}} e^{jk_0\delta_d} = E_{\mathrm{F1}} e^{-jk_0\delta_d} - E_{\mathrm{B1}} e^{jk_0\delta_d} + 2E_{\mathrm{rad}}. \tag{5.4b}$$

The equation system can be solved by defining the transfer functions:

$$\tau_1 = \frac{E_{\mathrm{T1}}}{E_{\mathrm{rad}}} = \frac{\tilde{\tau}_1 e^{-jk_0\delta_d}\left(e^{2jk_0d} + \tilde{\Gamma}_2 e^{2jk_0\delta_d}\right)}{e^{2jk_0d} - \tilde{\Gamma}_1\tilde{\Gamma}_2}, \tag{5.5a}$$

$$F_1 = \frac{E_{\mathrm{F1}}}{E_{\mathrm{rad}}} = \frac{\tilde{\Gamma}_1 e^{-jk_0\delta_d}\left(e^{2jk_0d} + \tilde{\Gamma}_2 e^{2jk_0\delta_d}\right)}{e^{2jk_0d} - \tilde{\Gamma}_1\tilde{\Gamma}_2}, \tag{5.5b}$$

$$B_1 = \frac{E_{\mathrm{B1}}}{E_{\mathrm{rad}}} = \frac{e^{-jk_0\delta_d}\left(e^{2jk_0d} + \tilde{\Gamma}_2 e^{2jk_0\delta_d}\right)}{e^{2jk_0d} - \tilde{\Gamma}_1\tilde{\Gamma}_2}, \tag{5.5c}$$

$$\tau_2 = \frac{E_{\mathrm{T2}}}{E_{\mathrm{rad}}} = \frac{\tilde{\tau}_2 e^{jk_0(2d-\delta_d)}\left(e^{2jk_0\delta_d} + \tilde{\Gamma}_1\right)}{e^{2jk_0d} - \tilde{\Gamma}_1\tilde{\Gamma}_2}, \tag{5.5d}$$

$$F_2 = \frac{E_{\mathrm{F2}}}{E_{\mathrm{rad}}} = \frac{e^{jk_0(2d-\delta_d)}\left(e^{2jk_0\delta_d} + \tilde{\Gamma}_1\right)}{e^{2jk_0d} - \tilde{\Gamma}_1\tilde{\Gamma}_2}, \tag{5.5e}$$

$$B_2 = \frac{E_{\mathrm{B2}}}{E_{\mathrm{rad}}} = \frac{\tilde{\Gamma}_2 e^{-jk_0\delta_d}\left(e^{2jk_0\delta_d} + \tilde{\Gamma}_1\right)}{e^{2jk_0d} - \tilde{\Gamma}_1\tilde{\Gamma}_2}, \tag{5.5f}$$

which dependent of each metasurface transmission and reflection coefficients, and the position of the source.

The solution of (5.5) applies to any combination of metasurfaces, but in this particular case a DER will be considered. So, by replacing the scattering coefficients for each metasurface, according to Equation (2.13) with their respective grid impedances, the transfer functions are simplified into

$$\Delta = e^{2jk_0d}(2\tilde{Z}_{\mathrm{e1}} + 1)(2\tilde{Z}_{\mathrm{e2}} + 1) - 1, \tag{5.6a}$$

$$\tau_1 = 2\tilde{Z}_{\mathrm{e1}} e^{-jk_0\delta_d}\left((2\tilde{Z}_{\mathrm{e2}} + 1)e^{2jk_0d} - e^{2jk_0\delta_d}\right)\Delta^{-1}, \tag{5.6b}$$

$$F_1 = -e^{-jk_0\delta_d}\left((2\tilde{Z}_{\mathrm{e2}} + 1)e^{2jk_0d} - e^{2jk_0\delta_d}\right)\Delta^{-1}, \tag{5.6c}$$

$$B_1 = e^{-jk_0\delta_d}(2\tilde{Z}_{\mathrm{e1}} + 1)\left((2\tilde{Z}_{\mathrm{e2}} + 1)e^{2jk_0d} - e^{2jk_0\delta_d}\right)\Delta^{-1}, \tag{5.6d}$$

$$\tau_2 = 2\tilde{Z}_{\mathrm{e2}} e^{jk_0(2d-\delta_d)}\left((2\tilde{Z}_{\mathrm{e1}} + 1)e^{2jk_0\delta_d} - 1\right)\Delta^{-1}, \tag{5.6e}$$

$$F_2 = e^{jk_0(2d-\delta_d)}(2\tilde{Z}_{\mathrm{e2}} + 1)\left((2\tilde{Z}_{\mathrm{e1}} + 1)e^{2jk_0\delta_d} - 1\right)\Delta^{-1}, \tag{5.6f}$$

$$B_2 = -e^{-jk_0\delta_d}\left((2\tilde{Z}_{\mathrm{e1}} + 1)e^{2jk_0\delta_d} - 1\right)\Delta^{-1}. \tag{5.6g}$$

In order to solve the reciprocal case, the invisibility conditions for a DER of Equation (3.27) must be applied; in that case, the transfer functions are reduced

to

$$\Delta = -4\tilde{Z}_{\mathrm{e1}}^2, \tag{5.7a}$$

$$\tau_1 = 2\tilde{Z}_{\mathrm{e1}} e^{-jk_0\delta_d}\left(1 - 2\tilde{Z}_{\mathrm{e1}} - e^{2jk_0\delta_d}\right)\Delta^{-1}, \tag{5.7b}$$

$$F_1 = -e^{-jk_0\delta_d}\left(1 - 2\tilde{Z}_{\mathrm{e1}} - e^{2jk_0\delta_d}\right)\Delta^{-1}, \tag{5.7c}$$

$$B_1 = e^{-jk_0\delta_d}(2\tilde{Z}_{\mathrm{e1}} + 1)\left(1 - 2\tilde{Z}_{\mathrm{e1}} - e^{2jk_0\delta_d}\right)\Delta^{-1}, \tag{5.7d}$$

$$\tau_2 = 2\tilde{Z}_{\mathrm{e1}} e^{-jk_0\delta_d}\left(1 - (2\tilde{Z}_{\mathrm{e1}} + 1)e^{2jk_0\delta_d}\right)\Delta^{-1}, \tag{5.7e}$$

$$F_2 = e^{-jk_0\delta_d}(1 - 2\tilde{Z}_{\mathrm{e1}})\left((2\tilde{Z}_{\mathrm{e1}} + 1)e^{2jk_0\delta_d} - 1\right)\Delta^{-1}, \tag{5.7f}$$

$$B_2 = e^{-jk_0\delta_d}\left(1 - (2\tilde{Z}_{\mathrm{e1}} + 1)e^{2jk_0\delta_d}\right)\Delta^{-1}. \tag{5.7g}$$

The reciprocity analysis will be performed in two stages: the first stage will focus on the fields inside the structure by performing an SWR analysis, while the second stage will focus on the fields outside the resonator by analysing the transmitted coefficients and the radiated power. If we consider the standing waves produced in front of ($z > \delta_d$) and behind ($z < \delta_d$) the current sheet, and the propagation sense of the induced fields, it is possible to define the standing wave ratios in both regions:

$$\mathrm{SWR}_1 = \frac{|B_1| + |F_1|}{|B_1| - |F_1|} = \frac{|2\tilde{Z}_{\mathrm{e1}} + 1| + 1}{|2\tilde{Z}_{\mathrm{e1}} + 1| - 1}, \tag{5.8a}$$

$$\mathrm{SWR}_2 = \frac{|F_2| + |B_2|}{|F_2| - |B_2|} = \frac{|2\tilde{Z}_{\mathrm{e1}} - 1| + 1}{|2\tilde{Z}_{\mathrm{e1}} - 1| - 1}. \tag{5.8b}$$

These SWR have similar expressions compared to Equation (4.6), which correspond to the “conventional case” where the resonator is illuminated from the outside. Notice that the difference between the SWR in the conventional case and SWR_1 presented for the region behind the current sheet is produced because the incident wave propagates in the opposite sense. In other words, the resonator is inverted and the terms are expressed in terms of the “second” metasurface instead of the “first” one by replacing $\tilde{Z}_{\mathrm{e1}}$ in (5.8a) with $\tilde{Z}_{\mathrm{e2}}$, which lead us to the expression of Equation (4.6).

As done in the conventional case, the standing waves transfer functions S_{e} can be defined as

$$S_{\mathrm{e},1}(z, \delta_d) = F_1 e^{-jk_0 z} + B_1 e^{jk_0 z}, \tag{5.9a}$$

$$S_{\mathrm{e},2}(z, \delta_d) = F_2 e^{-jk_0 z} + B_2 e^{jk_0 z}. \tag{5.9b}$$

The magnitude of both transfer functions can be deduced, considering pure-

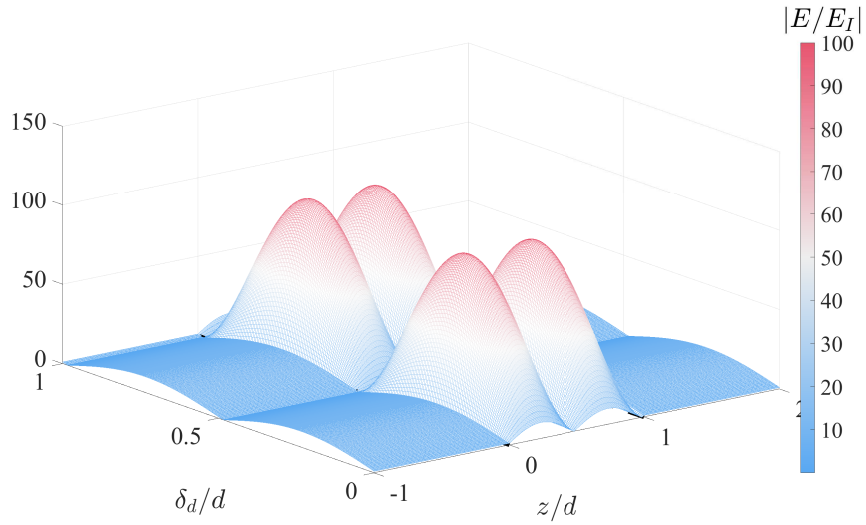

Figure 5.2. Electric field across a resonator with $\mathrm{SWR} = 100$ ($\tilde{X}_{\mathrm{e1}} = 0.101$) as a function of the position of the current sheet placed inside.

reactive metasurfaces:

$$|S_{\mathrm{e},1}(z,\delta_d)| = |S_{\mathrm{e},2}(z,\delta_d)| = |S_{\mathrm{e}}(z)||S_{\mathrm{e}}(\delta_d)|, \tag{5.10}$$

where $|S_{\mathrm{e}}(z)|$ is the same function as given in (4.10); $|S_{\mathrm{e}}(\delta_d)|$ is the same as $|S_{\mathrm{e}}(z)|$ but replacing z by δ_d:

$$|S_{\mathrm{e}}(\delta_d)| = \frac{1}{|\tilde{X}_{\mathrm{e1}}|}\sqrt{\tilde{X}_{\mathrm{e1}}^2 + \tilde{X}_{\mathrm{e1}}\sin(2k_0\delta_d) + \sin^2(k_0\delta_d)}. \tag{5.11}$$

In Chapter 4 was shown that $|S_{\mathrm{e}}(z)|$ (likewise, $|S_{\mathrm{e}}(\delta_d)|$) have maxima and minima. These values were proven to be located at fixed positions z_0 defined in Equation (4.8a). By extension, the locations δ_0, where $|S_{\mathrm{e}}(\delta_d)|$ reaches its maxima or minima, should follow the same conditions of (4.8). In conclusion, the locations of these extrema remain unchanged in the reciprocal case. Due to that, the absolute maximum of the standing wave is obtained when the source is placed in the maximum and the field is measured also in the maximum location. Likewise, the absolute minimum is obtained when the source is placed in the minimum and the field is also measured in the minimum. The exact values for these two extreme scenarios can be determined analytically:

$$|S_{\mathrm{e},1,2}|_{\max} = \mathrm{SWR}, \quad |S_{\mathrm{e},1,2}|_{\min} = \frac{1}{\mathrm{SWR}}. \tag{5.12}$$

To illustrate this behaviour, Figure 5.2 shows the effect of the current sheet position on the scattered fields across a resonator with $\mathrm{SWR} = 100$, using pure reactive metasurfaces with grid reactances $\tilde{X}_{\mathrm{e1}} = -\tilde{X}_{\mathrm{e2}} = 0.101$.

The next step is to analyse the fields radiated outside, characterized by τ_1 and

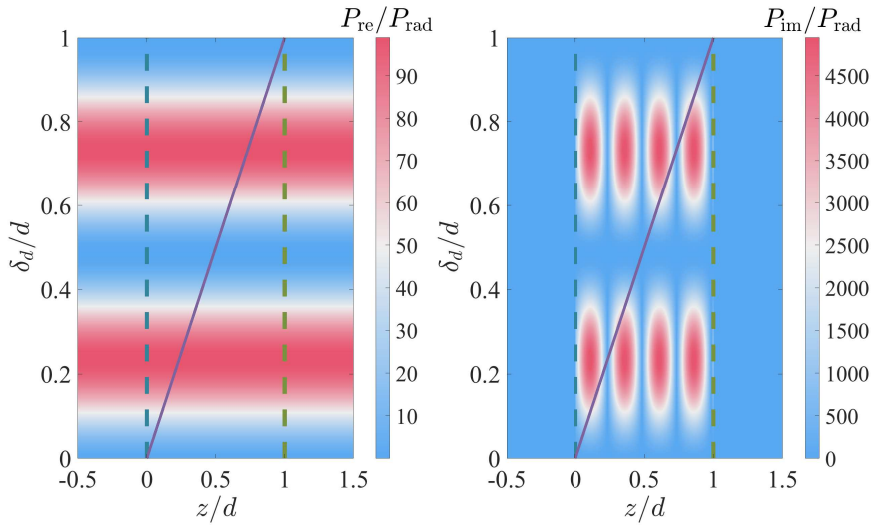

Figure 5.3. Normalized power distribution across a DER with $d = \lambda$ and $\mathrm{SWR} = 100$, as a function of the current sheet position (shown as a line): left - Normalized active power density, right - Normalized reactive power density.

τ_2. For both cases, it is possible to determine the magnitude of this two functions as a function of the source position:

$$|\tau_1| = |\tau_2| = |S_e(\delta_d)|, \tag{5.13}$$

where $|S_e(\delta_d)|$ is the same function described in (5.11); implying that the effect of the sheet position can be analysed separately from the general problem. In other words, the position of the radiant sheet only affects the magnitude of the scattered and transmitted fields, but not the position of standing waves nodes. Due to that, the active power P_{re} and the reactive power P_{im} (defined in Equation (5.14) and (5.15), respectively) can be understood also by this decoupling effect.

$$P_{re}(z) = \begin{cases} \frac{1}{2}|\mathrm{Re}\{\mathbf{E}_{T1} \times \mathbf{H}^*_{T1}\} \cdot \mathbf{a}_z| & z < 0 \\ \frac{1}{2}|\mathrm{Re}\{(\mathbf{E}_{F1} + \mathbf{E}_{B1}) \times (\mathbf{H}_{F1} + \mathbf{H}_{B1})^*\} \cdot \mathbf{a}_z| & 0 < z < \delta_d \\ \frac{1}{2}|\mathrm{Re}\{(\mathbf{E}_{F2} + \mathbf{E}_{B2}) \times (\mathbf{H}_{F2} + \mathbf{H}_{B2})^*\} \cdot \mathbf{a}_z| & \delta_d < z < d \\ \frac{1}{2}|\mathrm{Re}\{\mathbf{E}_{T2} \times \mathbf{H}^*_{T2}\} \cdot \mathbf{a}_z| & z > d \end{cases} \tag{5.14}$$

$$P_{im}(z) = \begin{cases} \frac{1}{2}|\mathrm{Im}\{\mathbf{E}_{T1} \times \mathbf{H}^*_{T1}\} \cdot \mathbf{a}_z| & z < 0 \\ \frac{1}{2}|\mathrm{Im}\{(\mathbf{E}_{F1} + \mathbf{E}_{B1}) \times (\mathbf{H}_{F1} + \mathbf{H}_{B1})^*\} \cdot \mathbf{a}_z| & 0 < z < \delta_d \\ \frac{1}{2}|\mathrm{Im}\{(\mathbf{E}_{F2} + \mathbf{E}_{B2}) \times (\mathbf{H}_{F2} + \mathbf{H}_{B2})^*\} \cdot \mathbf{a}_z| & \delta_d < z < d \\ \frac{1}{2}|\mathrm{Im}\{\mathbf{E}_{T2} \times \mathbf{H}^*_{T2}\} \cdot \mathbf{a}_z| & z > d \end{cases} \tag{5.15}$$

In fact, the sheet position affects the magnitude of the power radiated/stored but not the physical displacement of the stored energy, as shown in Figure 5.3, normalized using $P_{rad} = |E_{rad}|^2/2\eta_0$.

One last property of this scenario is the enhancing capabilities of the resonator.

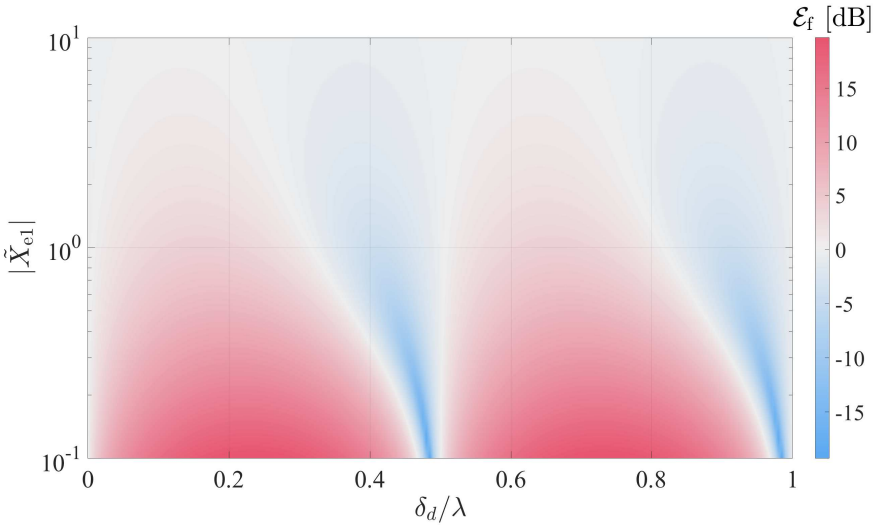

Figure 5.4. Enhancement factor as a function of current sheet position and the first metasurface grid reactance for a DER.

In this case it is convenient to define $\mathcal{E}_\mathrm{f}$ as the "enhancement factor", which is the ratio of the total radiated power by a current sheet placed inside the resonator and the radiated power by the same current sheet placed in free space. Mathematically, the enhancement factor can be written in terms of electromagnetic fields and in terms of transfer functions:

$$\mathcal{E}_\mathrm{f} = \frac{\frac{1}{2}\mathrm{Re}\{E_{\mathrm{T}1}H^*_{\mathrm{T}1}\} + \frac{1}{2}\mathrm{Re}\{E_{\mathrm{T}2}H^*_{\mathrm{T}2}\}}{2\left(\frac{1}{2}\mathrm{Re}\{E_\mathrm{rad}H^*_\mathrm{rad}\}\right)} = \frac{|\tau_1|^2 + |\tau_2|^2}{2}. \tag{5.16}$$

In this particular case, the enhancement factor can be simplified based on the results found in Equation (5.13):

$$\mathcal{E}_\mathrm{f} = |S_\mathrm{e}(\delta_d)|^2, \tag{5.17}$$

which shows that the current sheet radiated power can be modified in the range between $[1/\mathrm{SWR}\ ,\ \mathrm{SWR}]$. Figure 5.4 shows how the current sheet position and the grid reactance (which is related with the SWR) affect the enhancement factor.

The increment in the active power (Figure 5.3) and in the enhancement factor (5.4) is not a violation of the law of conservation of energy. In fact, the extra radiated power comes from the radiating source as the resonator improves its matching with the free space. With ideal currents sources, there is no limit of how much power they can radiate; but in the case of realistic radiating sources, the power will be increased until the source saturates.

5.2 Multiple-layer structures and the transfer matrix

Until now, different properties of a cavity resonator composed of two metasurfaces were considered, based on analyses which were performed based on the metasurfaces scattering matrices of Equations (2.34) and (2.37). In all of these cases, the solutions came from a four-equation system for the scattered fields at each metasurface. But, as seen in the reciprocity analysis, the addition of more layers increases the number of equations to be solved. Because of that, it is useful to define the relations between the fields around the metasurface, such that the fields located at one side are defined as functions of the fields of the other side, based on the T-parameter matrix [45–48]. In contrast to the most accepted notation, here the term "T-parameter matrix" corresponds to the version developed in Reference [45] because most of the analysis shown in this thesis considers that the source wave corresponds to the parameter $\mathbf{E}_{\mathrm{I}-}$ of Figure 2.5. Hence, the T-parameter matrix is defined as

$$\begin{bmatrix} E_{\mathrm{OUT}+} \\ E_{\mathrm{IN}+} \end{bmatrix} = \sqrt{\frac{\eta_+}{\eta_-}} \begin{bmatrix} T_{11} & T_{12} \\ T_{21} & T_{22} \end{bmatrix} \begin{bmatrix} E_{\mathrm{IN}-} \\ E_{\mathrm{OUT}-} \end{bmatrix}. \tag{5.18}$$

By comparing Equation (5.18) with Equation (2.34), it is possible to write the T-parameter matrix in terms of the scattering matrix components or vice-versa:

$$\begin{bmatrix} T_{11} & T_{12} \\ T_{21} & T_{22} \end{bmatrix} = \frac{1}{S_{12}} \begin{bmatrix} S_{12}S_{21} - S_{11}S_{22} & S_{22} \\ -S_{11} & 1 \end{bmatrix}, \tag{5.19}$$

$$\begin{bmatrix} S_{11} & S_{12} \\ S_{21} & S_{22} \end{bmatrix} = \frac{1}{T_{22}} \begin{bmatrix} -T_{21} & 1 \\ T_{11}T_{22} - T_{12}T_{21} & T_{12} \end{bmatrix}. \tag{5.20}$$

In the case of a non-bianisotropic metasurface (like EPMs, MPMs or EMPMs) placed in free-space, the T-parameters can be simplified to

$$\begin{bmatrix} T_{11} & T_{12} \\ T_{21} & T_{22} \end{bmatrix} = \frac{1}{\tilde{\tau}} \begin{bmatrix} \tilde{\tau}^2 - \tilde{\Gamma}^2 & \tilde{\Gamma} \\ -\tilde{\Gamma} & 1 \end{bmatrix}. \tag{5.21}$$

Also, it is possible to combine the results shown in Equation (3.5), such that the T-parameter matrix not only show the metasurface scattering coefficients, but also the effects of metasurface displacement:

$$\begin{bmatrix} T_{11} & T_{12} \\ T_{21} & T_{22} \end{bmatrix} = \frac{1}{\tilde{\tau}} \begin{bmatrix} \tilde{\tau}^2 - \tilde{\Gamma}^2 & \tilde{\Gamma}e^{2jk_0d} \\ -\tilde{\Gamma}e^{-2jk_0d} & 1 \end{bmatrix}. \tag{5.22}$$

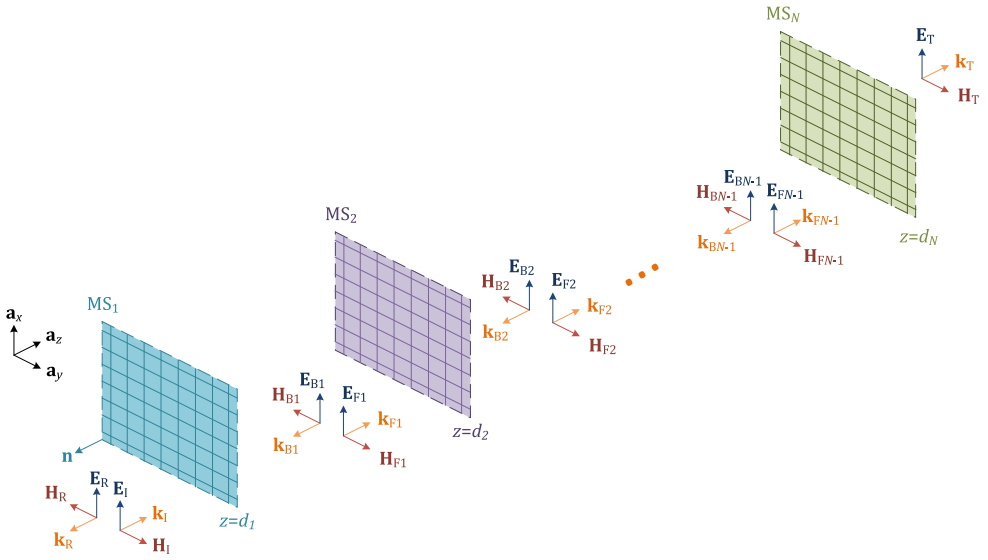

Figure 5.5. Electromagnetic fields produced by an electromagnetic wave incident onto a system made of N metasurfaces in free space.

Consider a system composed by N metasurfaces in free space, as shown in Figure 5.5, which is illuminated by a normally incident plane wave. The scattered waves can be grouped in such a way that after the i-th metasurface, with a transfer parameter matrix $[T_i]$ and located at position $z = d_i$, there is a forward wave ($\mathbf{E}_{\mathrm{F},i}$) and a backward wave ($\mathbf{E}_{\mathrm{B},i}$). The magnitudes of these forward and backward waves can be written as functions of the incident wave and the total reflected wave:

$$\begin{bmatrix} E_{\mathrm{F},i} \\ E_{\mathrm{B},i} \end{bmatrix} = [T_{\mathrm{comb},i}] \begin{bmatrix} E_{\mathrm{I}} \\ E_{\mathrm{R}} \end{bmatrix}, \tag{5.23}$$

where $[T_{\mathrm{comb},i}]$ is the i-th combined T-parameter matrix

$$[T_{\mathrm{comb},i}] = [T_i] * [T_{i-1}] * \ldots * [T_1] = \prod_{l=1}^{i} [T_l]\,. \tag{5.24}$$

It is important to remark that the total combined T-parameter matrix $[T_{\mathrm{tot}}]$, which corresponds to $[T_{\mathrm{comb},N}]$, relates the transmitted wave $\mathbf{E}_{\mathrm{T}}$ with the incident and reflected waves ($\mathbf{E}_{\mathrm{I}}$ and $\mathbf{E}_{\mathrm{R}}$, respectively). Due to that, it is important to transform this T-parameter matrix into the equivalent scattering matrix, using Equation (5.20), in order to obtain the reflected and transmitted waves in terms of the incident wave and the properties of the whole structure. In both cases, reflected and transmitted waves can be represented by their transfer functions:

$$\Gamma = \frac{E_{\mathrm{R}}}{E_{\mathrm{I}}} = -\frac{T_{\mathrm{tot},21}}{T_{\mathrm{tot},22}}, \tag{5.25a}$$

$$\tau = \frac{E_{\mathrm{T}}}{E_{\mathrm{I}}} = \frac{T_{\mathrm{tot},11}T_{\mathrm{tot},22} - T_{\mathrm{tot},12}T_{\mathrm{tot},21}}{T_{\mathrm{tot},22}}. \tag{5.25b}$$

In the case of three layers ($N = 3$), the transfer function of each scattered wave can be written as a function of each metasurfaces scattering coefficients and distances d_i:

$$\begin{aligned}\Delta =&\tilde{\Gamma}_1\tilde{\Gamma}_3\left(\tilde{\Gamma}_2^2-\tilde{\tau}_2^2\right)e^{2jk_0(d_1+d_2)}+\tilde{\Gamma}_1\tilde{\Gamma}_2\left(-e^{2jk_0(d_1+d_3)}\right)\\&+e^{2jk_0(d_2+d_3)}-\tilde{\Gamma}_2\tilde{\Gamma}_3e^{4jk_0d_2},\end{aligned}\tag{5.26a}$$

$$\tau=\frac{E_{\mathrm{T}}}{E_{\mathrm{I}}}=\Delta^{-1}\tilde{\tau}_1\tilde{\tau}_2\tilde{\tau}_3e^{2jk_0(d_2+d_3)},\tag{5.26b}$$

$$\begin{aligned}\Gamma=\frac{E_{\mathrm{R}}}{E_{\mathrm{I}}}=&\Delta^{-1}e^{-2jk_0d_1}\left[\tilde{\Gamma}_3\left(\tilde{\Gamma}_1^2-\tilde{\tau}_1^2\right)\left(\tilde{\Gamma}_2^2-\tilde{\tau}_2^2\right)e^{2jk_0(d_1+d_2)}\right.\\&\left.-\tilde{\Gamma}_2\left(\tilde{\Gamma}_1^2-\tilde{\tau}_1^2\right)e^{2jk_0(d_1+d_3)}+\tilde{\Gamma}_1e^{2jk_0(d_2+d_3)}-\tilde{\Gamma}_1\tilde{\Gamma}_2\tilde{\Gamma}_3e^{4jk_0d_2}\right],\end{aligned}\tag{5.26c}$$

$$F_1=\frac{E_{\mathrm{F1}}}{E_{\mathrm{I}}}=\Delta^{-1}\tilde{\tau}_1\left(e^{2jk_0(d_2+d_3)}-\tilde{\Gamma}_2\tilde{\Gamma}_3e^{4jk_0d_2}\right),\tag{5.26d}$$

$$B_1=\frac{E_{\mathrm{B1}}}{E_{\mathrm{I}}}=\Delta^{-1}\tilde{\tau}_1\left(\tilde{\Gamma}_2e^{2jk_0d_3}-\tilde{\Gamma}_3e^{2jk_0d_2}\left(\tilde{\Gamma}_2^2-\tilde{\tau}_2^2\right)\right),\tag{5.26e}$$

$$F_2=\frac{E_{\mathrm{F2}}}{E_{\mathrm{I}}}=\Delta^{-1}\tilde{\tau}_1\tilde{\tau}_2e^{2jk_0(d_2+d_3)},\tag{5.26f}$$

$$B_2=\frac{E_{\mathrm{B2}}}{E_{\mathrm{I}}}=\Delta^{-1}\tilde{\Gamma}_3\tilde{\tau}_1\tilde{\tau}_2e^{2jk_0d_2}.\tag{5.26g}$$

As seen from Equation (5.26), the transfer functions only depend on the metasurfaces scattering coefficients and positions. This is useful as the transfer functions do not depend directly on the meta-atoms which the metasurfaces are made of. In other words, these functions can be used for scenarios where one of the metasurfaces is replaced by any object which can be modelled using transmission and reflection coefficient. One scenario where these conclusions can be applied is when a sensor is placed inside an ICR.

5.3 Sensing with invisible resonators

In physics, the observer effect is the disturbance of a phenomenon produced by the act of measuring by an observer [49]. In the case of electromagnetics, different approaches were discussed in order to minimize the disturbances produced by a sensor. One of these approaches is based on the use of minimum-scattering antennas [50, 51]. The trade-off with this approach is the low power induced inside the antenna, reducing the sensibility of the sensor. Another approach is the use of spatial diversity (like the use of antenna arrays) to improve the sensor directivity [52–54]. In an one-dimensional case (as the invisible resonator), we have only two directions (forward and backward). Therefore, we need to make $\Gamma = 0$ and to balance the ratio between absorbed and transmitted powers. Due to these facts, it becomes of special interest how the scattering properties of a

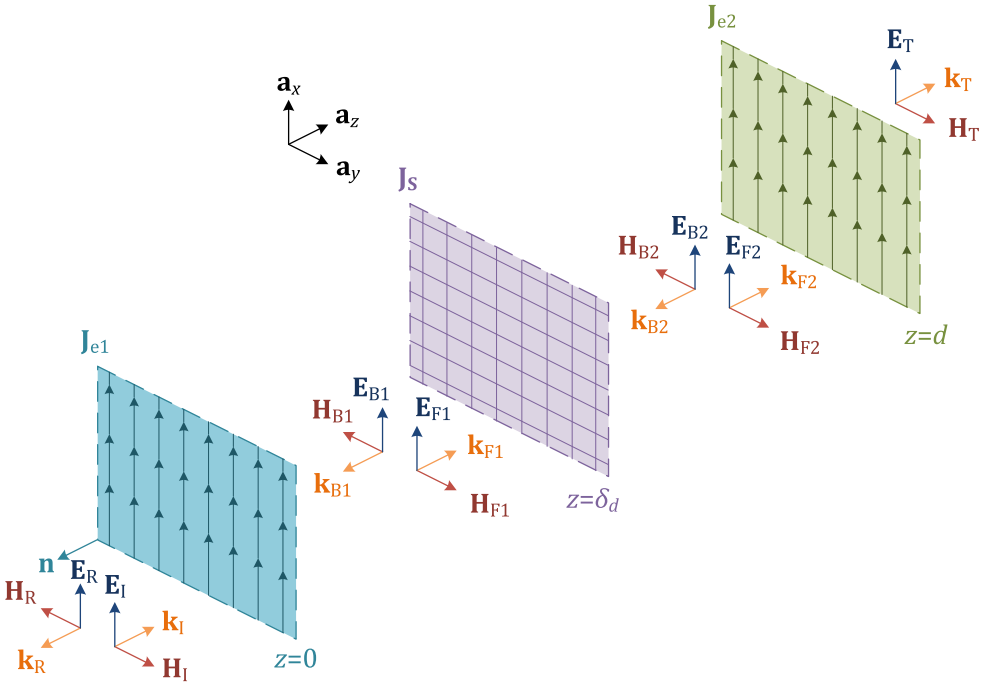

Figure 5.6. Electromagnetic fields produced by an electromagnetic wave incident onto a DER, when a planar sensor is placed between the metasurfaces.

particular sensor could be modified if it is placed inside a DER.

Now, consider the case, where a lossy object is placed inside an invisible cavity resonator, as shown in Figure 5.6. The resonator is formed by two metasurfaces, which fulfil the invisibility conditions of Equation (3.27) (with $d_3 - d_1 = \lambda_0$). The resonator is placed so that $d_1 = 0$ and the sensor is placed at $d_2 = \delta_d$. The sensor can be modelled as an EMPM, as this model can achieve total absorption, using the equations of (2.24), with electric and magnetic grid impedances Z_{es} and Z_{ms} (where "s" means "sensor") and scattering coefficients of Equation (2.29). The external scattered fields are defined as it was done in Equation (2.9), while the inner fields are defined as in Equation (5.2). With this information, the transfer functions can be solved from Equation (5.26), in terms of resonator and sensor grid impedances, as shown in Equation (5.27).

$$\begin{aligned}\Delta =&2e^{2jk_0\delta_d}\left(\tilde{Z}_{\mathrm{es}}\tilde{Z}_{\mathrm{ms}}+1-\tilde{Z}_{\mathrm{e1}}^2(2\tilde{Z}_{\mathrm{es}}+1)(\tilde{Z}_{\mathrm{ms}}+2)\right)\\&+e^{4jk_0\delta_d}(2\tilde{Z}_{\mathrm{e1}}+1)(\tilde{Z}_{\mathrm{es}}\tilde{Z}_{\mathrm{ms}}-1)+(2\tilde{Z}_{\mathrm{e1}}-1)(1-\tilde{Z}_{\mathrm{es}}\tilde{Z}_{\mathrm{ms}}),\end{aligned}\tag{5.27a}$$

$$\tau=\frac{E_{\mathrm{T}}}{E_{\mathrm{I}}}=2\Delta^{-1}\tilde{Z}_{\mathrm{e1}}^2e^{2jk_0\delta_d}(\tilde{Z}_{\mathrm{ms}}-4\tilde{Z}_{\mathrm{es}}),\tag{5.27b}$$

$$\begin{aligned}\Gamma=\frac{E_{\mathrm{R}}}{E_{\mathrm{I}}}=&\Delta^{-1}\left[2e^{2jk_0\delta_d}(2\tilde{Z}_{\mathrm{e1}}-1)(\tilde{Z}_{\mathrm{es}}\tilde{Z}_{\mathrm{ms}}+1)\right.\\&\left.+e^{4jk_0\delta_d}(1-\tilde{Z}_{\mathrm{es}}\tilde{Z}_{\mathrm{ms}})+(1-2\tilde{Z}_{\mathrm{e1}})^2(1-\tilde{Z}_{\mathrm{es}}\tilde{Z}_{\mathrm{ms}})\right],\end{aligned}\tag{5.27c}$$

$$\begin{aligned}F_1=\frac{E_{\mathrm{F1}}}{E_{\mathrm{I}}}=&\Delta^{-1}\tilde{Z}_{\mathrm{e1}}e^{2jk_0\delta_d}\left[2e^{2jk_0\delta_d}(\tilde{Z}_{\mathrm{es}}\tilde{Z}_{\mathrm{ms}}-1)\right.\\&\left.-(2\tilde{Z}_{\mathrm{e1}}-1)(2\tilde{Z}_{\mathrm{es}}+1)(\tilde{Z}_{\mathrm{ms}}+2)\right],\end{aligned}\tag{5.27d}$$

$$\begin{aligned}B_1=\frac{E_{\mathrm{B1}}}{E_{\mathrm{I}}}=&\Delta^{-1}\tilde{Z}_{\mathrm{e1}}\left[(2\tilde{Z}_{\mathrm{es}}-1)(\tilde{Z}_{\mathrm{ms}}-2)e^{2jk_0\delta_d}\right.\\&\left.-2(2\tilde{Z}_{\mathrm{e1}}-1)(\tilde{Z}_{\mathrm{es}}\tilde{Z}_{\mathrm{ms}}-1)\right],\end{aligned}\tag{5.27e}$$

$$F_2=\frac{E_{\mathrm{F2}}}{E_{\mathrm{I}}}=\Delta^{-1}\tilde{Z}_{\mathrm{e1}}e^{2jk_0\delta_d}(2\tilde{Z}_{\mathrm{e1}}-1)(\tilde{Z}_{\mathrm{ms}}-4\tilde{Z}_{\mathrm{es}}),\tag{5.27f}$$

$$B_2=\frac{E_{\mathrm{B2}}}{E_{\mathrm{I}}}=\Delta^{-1}\tilde{Z}_{\mathrm{e1}}e^{2jk_0\delta_d}(\tilde{Z}_{\mathrm{ms}}-4\tilde{Z}_{\mathrm{es}}).\tag{5.27g}$$

After obtaining the general transfer functions, the next step is to define the sensor properties in terms of grid impedances $\tilde{Z}_{\mathrm{es}}$ and $\tilde{Z}_{\mathrm{ms}}$.

Sensor modelled as an electrically and magnetically polarizable metasurface

In order to simplify the whole analysis, it is convenient to define a sensor model based on two criteria: sensor absorbance $|A_{\mathrm{s}}|^2$ and how transmissive/reflective the sensor is when it is in free space. For the first criterium, the sensor absorbance is defined as

$$|A_{\mathrm{s}}|^2=1-|\tilde{\tau}_{\mathrm{s}}|^2-|\tilde{\Gamma}_{\mathrm{s}}|^2,\tag{5.28}$$

where $|\tilde{\tau}_{\mathrm{s}}|^2$ and $|\tilde{\Gamma}_{\mathrm{s}}|^2$ corresponds to sensor transmittance and reflectance in free-space, respectively. The second criterium is harder to define since Equation (5.28) helps to solve partially the ratio of transmission and reflection coefficient (considering that both parameters had magnitude and phase). In order to simplify the model, the transmission and reflection coefficients are considered as real values ($\tilde{X}_{\mathrm{es}}=\tilde{X}_{\mathrm{ms}}=0$). Additionally, Equation (5.28) can be written in terms of Pythagorean theorem with an hypotenuse of $1-|A_{\mathrm{s}}|^2$ and both scattering coefficients as catheti. In that case, it is possible to define transmission and

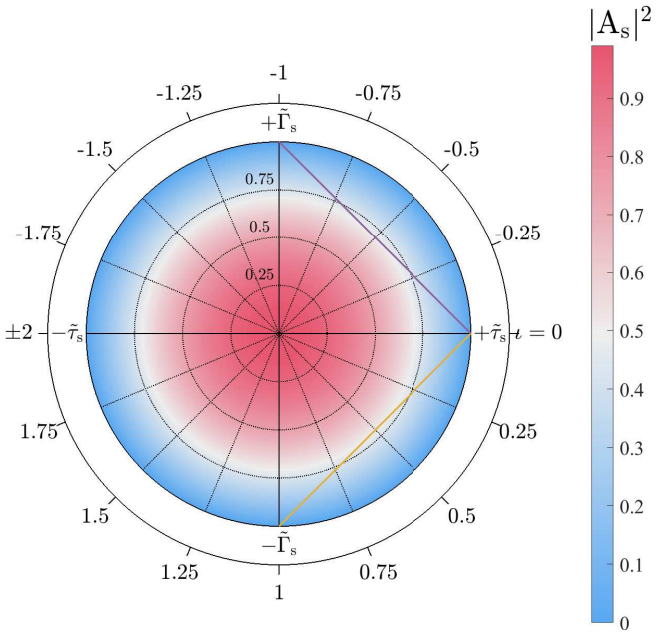

Figure 5.7. Grid sensor transmission and reflection coefficients as functions of absorbance (color) and parameter ι. Yellow line - lossy EP metasurfaces, Purple line - lossy MP metasurfaces.

reflection coefficients using trigonometric functions:

$$\tilde{\tau}_s = \sqrt{1-|A_s|^2}\cos\left(\frac{\pi}{2}\iota\right), \tag{5.29a}$$

$$\tilde{\Gamma}_s = -\sqrt{1-|A_s|^2}\sin\left(\frac{\pi}{2}\iota\right), \tag{5.29b}$$

where the parameter ι (iota) indicates how much backscattering is produced by the sensor (values of $|\iota|$ close to 1 correspond to high backscattering, while values closes to 0 or 2 correspond to low backscattering). Substuting these definitions of transmission and reflection coefficients in Equation (2.30), it is possible to obtain the electric and magnetic grid impedances as functions of the absorbance and parameter ι:

$$\tilde{Z}_{es} = \frac{1}{2}\frac{1+\sqrt{1-|A_s|^2}\left(\cos\left(\frac{\pi}{2}\iota\right)-\sin\left(\frac{\pi}{2}\iota\right)\right)}{1-\sqrt{1-|A_s|^2}\left(\cos\left(\frac{\pi}{2}\iota\right)-\sin\left(\frac{\pi}{2}\iota\right)\right)}, \tag{5.30a}$$

$$\tilde{Z}_{ms} = 2\frac{1-\sqrt{1-|A_s|^2}\left(\cos\left(\frac{\pi}{2}\iota\right)+\sin\left(\frac{\pi}{2}\iota\right)\right)}{1+\sqrt{1-|A_s|^2}\left(\cos\left(\frac{\pi}{2}\iota\right)+\sin\left(\frac{\pi}{2}\iota\right)\right)}. \tag{5.30b}$$

Under these definitions, it is possible to obtain all the transmission/reflection combinations, as shown in Figure 5.7, for $\iota = [-2, 2]$, but we will consider only the range of $\iota = [-1, 1]$.

Using this model, it is possible to obtain some cases where the sensor is an EPM or an MPM. The location of EPMs and MPMs are shown in Figure 5.7, where the yellow line represents lossy EPM (which fulfil Equation (2.11d)) and the purple line indicates lossy MPM (based on Equation (2.19d)). One observation related with the location of EPMs and MPMs in this model is that positive values of parameter ι correspond to metasurfaces with dominant electric behaviour, while negative parameter ι values imply a dominance of the magnetic properties of the sensor. Additionally, it is possible to define a region in Figure 5.7, limited by the axis of $\tilde{\tau}_{\mathrm{s}} = 0$ and the pure EPM and MPM lines, where both grid impedances are positive real values. In contrast, outside of this region one of the grid impedances have negative values (with active properties). It is true that there are values outside the triangle where the whole sensor is lossy, but because this active component can be excited by the resonant fields, it is convenient to use lossy grid impedances values.

Due to the number of degrees of freedom, it is convenient to perform some analysis in order to find the relations between different parameters: SWR of the resonator, position and scattering properties of the sensor. The parameters to consider through the analysis are the system transfer functions Γ and τ, and the system absorbance $|A|^2$ defined as

$$|A|^2 = 1 - |\tau|^2 - |\Gamma|^2. \tag{5.31}$$

This system absorbance is useful to determine how much the sensor can be cloaked, since the resonator without any object is lossless under invisibility conditions. The first analysis is focused on determining the effect of the sensor position δ_d and its absorbance $|A_{\mathrm{s}}|^2$. In that case, a resonator with an $\mathrm{SWR} = 100$ was considered; while the sensor parameter ι was defined to ensure equal magnitudes of the transmission and reflection coefficients, being the only difference the sign of the reflection coefficient. The results for this analysis is shown in Figure 5.8.

Both figures show similar results, but the fundamental difference between them is the location where the system absorbance is maximized. In the case of $\tilde{\Gamma}_{\mathrm{s}} < 0$, the absorption is maximized in locations where the electrical field of the standing wave is weak. Likewise, the absorption is maximum for $\tilde{\Gamma}_{\mathrm{s}} > 0$ when the sensor is placed at positions where the electrical field is strong (and the magnetic field is weak). This effect can be understood by the contributions of sensor electric and magnetic grid impedances. In the case of $\tilde{\Gamma}_{\mathrm{s}} < 0$, the sensor behaves more like an EMP affecting more the standing waves where the electrical field is stronger. On the other hand, for $\tilde{\Gamma}_{\mathrm{s}} > 0$, the sensor acts more like an MPM, affecting more the standing waves at locations where the magnetic field is maximal. Therefore,

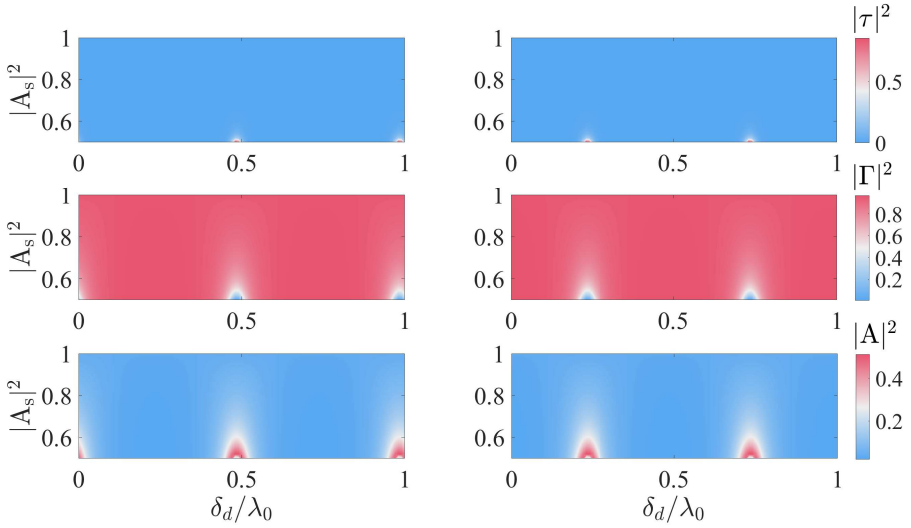

Figure 5.8. Transmittance, reflectance and absorbance of a DER with $\mathrm{SWR} = 100$ and a grid sensor placed inside, as a function of the sensor position and absorbance in free space: left - $\tilde{\Gamma}_s < 0$, right - $\tilde{\Gamma}_s > 0$.

the system absorption is maximized at locations where the sensor affects less the standing waves, but it still collects power as the sensor collects the energy from the forward and backward waves.

If we compare the system absorption in terms of sensor absorbance, it must be noticed that the system absorption is maximum for sensors with low absorption. Sensors with high absorption disturb more the standing waves created by the sensors. As the sensor absorption increases, the standing waves fade faster. This scenario implies that for high-SWR resonators, the use of high-absorption sensor should degenerate the standing waves even more. Due to that, it becomes important to perform a second analysis which compares the system transmittance, reflectance, and absorbance as a function of the resonator SWR and the sensor absorbance. The sensor has the same scattering properties as the previous analysis, but only in the case when $\tilde{\Gamma}_s < 0$ is considered. Also, the sensor is placed in an eletric field minimum, so the system absoprtion can be maximized. Meanwhile, the resonator metasurfaces are modified to realize different SWR, between 2 and 100. The results of this analysis is shown in Figure 5.9.

Based on the obtained results, the system behaviour can be divided into three regions as a function of the sensor absorbance: sensor attenuation, sensor matching, and resonance destruction. The first region, corresponding to the sensor attenuation, is when the sensor absorption is too small to disturb harmfully the standing wave. In that case, the location over a minimum is more determinant, and the sensor absorption is attenuated. In the second region, the sensor is partially matched to free space due to the scattering produced by both metasurfaces. In this region, the system absorption seems to be enhanced, by degradating the system transmission and reflection. In the third region, where the sensor has

high absorption, the standing wave is degradated and the system reflection is dominated by the first metasurface. In the other hand, the transmission is dominated by the sensor absorption. In this region, the system absorption is also degradated because the first metasurface is more opaque and the energy captured by the sensor is reduced. In terms of the SWR, as this parameter increases, the range of the resonance destruction region increases, while the range of the other two regions decreases. As a conclusion, it is not necessary to use high-absorption sensor inside the resonator since its properties degrade as the resonator SWR increases. Because of that, the next analysis will focus on low-absorption sensors.

Sensor modelled as an electrically polarizable or magnetically polarizable metasurface

In order to simplify the analysis, we will focus only on pure EPM and pure MPM sensors, following the yellow and purple lines of Figure 5.7. By using equations (2.11d) and (2.19d) with the definitions of transmission and reflection coefficients for our model in (5.29), it is possible to find the relation between the sensor absorbance and parameter ι for lossy EPMs and MPMs metasurfaces:

$$|A_\mathrm{s}|^2 = \frac{\sin(\pi|\iota|)}{1+\sin(\pi|\iota|)}. \tag{5.32}$$

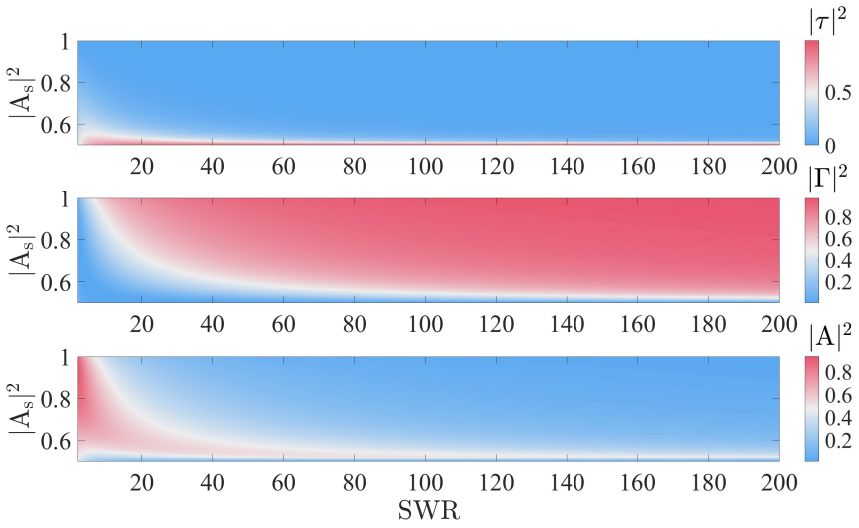

Figure 5.9. Transmittance, reflectance and absorbance of a DER and a grid sensor (with $\tilde{\Gamma}_\mathrm{s} < 0$) placed inside, as funcitons of the sensor absorbance and the resonator SWR. The sensor is placed in an electic field minimum.

Therefore, sensor transmission and reflection coefficients can be written only as functions of parameter ι:

$$\tilde{\tau}_{\mathrm{s}} = \frac{\cos\left(\frac{\pi}{2}\iota\right)}{\sqrt{1+\sin(\pi|\iota|)}}, \tag{5.33a}$$

$$\tilde{\Gamma}_{\mathrm{s}} = -\frac{\sin\left(\frac{\pi}{2}\iota\right)}{\sqrt{1+\sin(\pi|\iota|)}}. \tag{5.33b}$$

Figure 5.10 illustrates these relationships.

From the previous results, it is important to determine how the resonator SWR and the sensor absorbance (through parameter ι) affect the system performance (transmittance, reflectance and absorbance). In this analysis, only EPM-based sensor results will be presented, as the only difference between both models (EPM and MPM) is the location where the system absorption is maximized. Therefore, Figure 5.11 shows the system transmission, reflection and absorbance as functions of parameter ι and the resonator SWR, when the sensor is placed at electrical field maxima and minima.

From both figures, we can conclude that the absorption enhancement can be obtained for low-absorption sensors, but in two specific scenarios: placed at the corresponding maxima for low values of parameter $|\iota|$ (most transmittive); while for high values of parameter $|\iota|$ (close to one), the absorption enhancement is achieved when the sensor is placed at mimima locations. In both cases, the absorption enhancement (which maximum value is 0.5, corresponding with the limits of pure EPM/MPM-based sensors) degenerates the invisibility conditions (system transmission and reflection coefficients), as the energy captured by the sensor is not used by the metasurfaces to cancel their scattering. Notice that the nature of

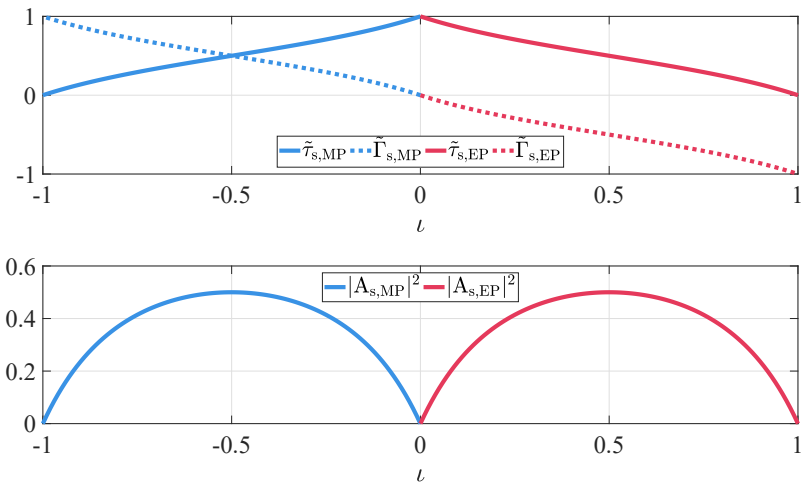

Figure 5.10. Sensor transmittance, reflectance and absorbance and absorbance for pure EPM-based and MPM-based models as functions of parameter ι.

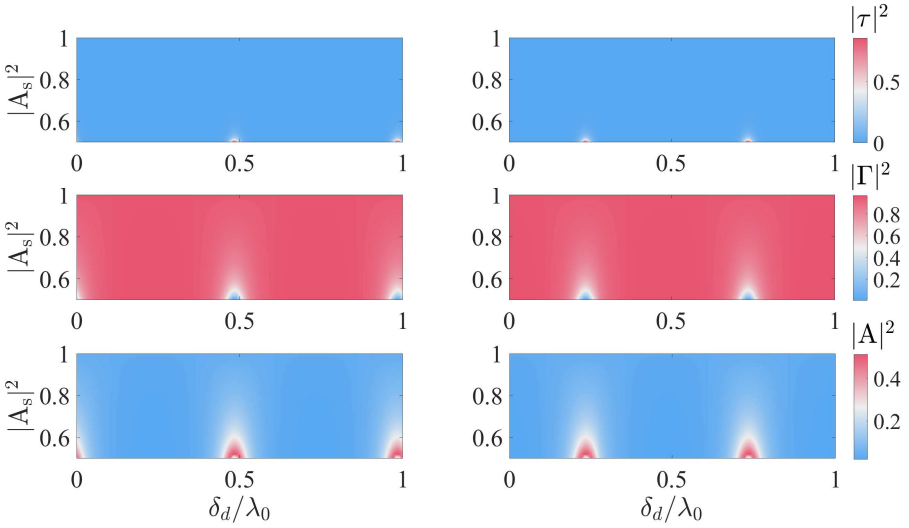

Figure 5.11. Transmittance, reflectance and absorbance of a DER and a grid sensor placed inside; as functions of the sensor parameter ι and the resonator SWR: left - At maxima of electrical field, right - At minima of electrical field.

the three regions (sensor attenuation, matching and resonance destruction) is the same as explained in the previous analysis. In fact, the matching region becomes narrower as the resonator SWR increases, but also displaces to regions where the sensor has small absorption. When the sensor is placed at an electric field maximum, as in Figure 5.11, this matching region is achieved when the sensor transmission coefficient is close to 1. This can be useful to enhance the sensibility of nearly-transparent sensor, but affecting the system scattering.

For the last analysis, we reconsider the relationship between the sensor position and its parameter ι, using pure EP and MP models. We consider a resonator with $d = \lambda_0$ and $\mathrm{SWR} = 100$. Also, the system transmission, reflection and absorbance are compared with their respective parameters of the sensor in free space (without the resonator). All of this information is shown in Figures 5.12 and 5.13.

Analysing these two figures, we can achieve some conclusions. In terms of absorption enhancement: The optimal location for most-transmittive sensors is at their corresponding field maxima, while most-reflective sensors should be placed at field minima. A more interesting result can be seen from Figure 5.13, where a region where an object can be cloaked appears. This region is located near the field minima corresponding to the nature of the object (electric field if the object is like an EPM, and the magnetic field for an MPM-like object). In this region, the transmission and reflection coefficients of the whole system are closer to ideal invisibility compared to the original scattering properties of the object. Due to the fact that this region is tolerant to variations of parameter ι, it can be used for sensor cloaking.

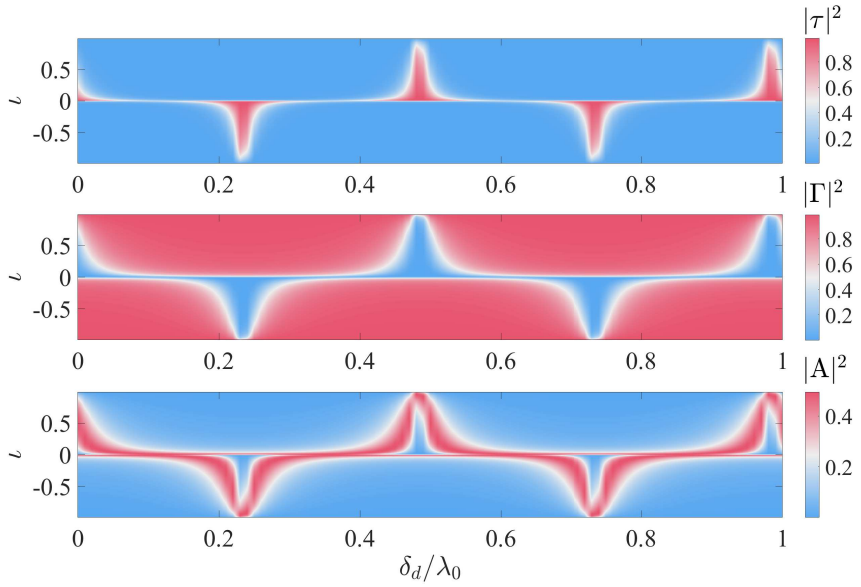

Figure 5.12. System transmission and reflection coefficients, and absorbance for lossy EPM or MPM based sensors using a resonator with $\mathrm{SWR} = 100$ as functions of sensor positon.

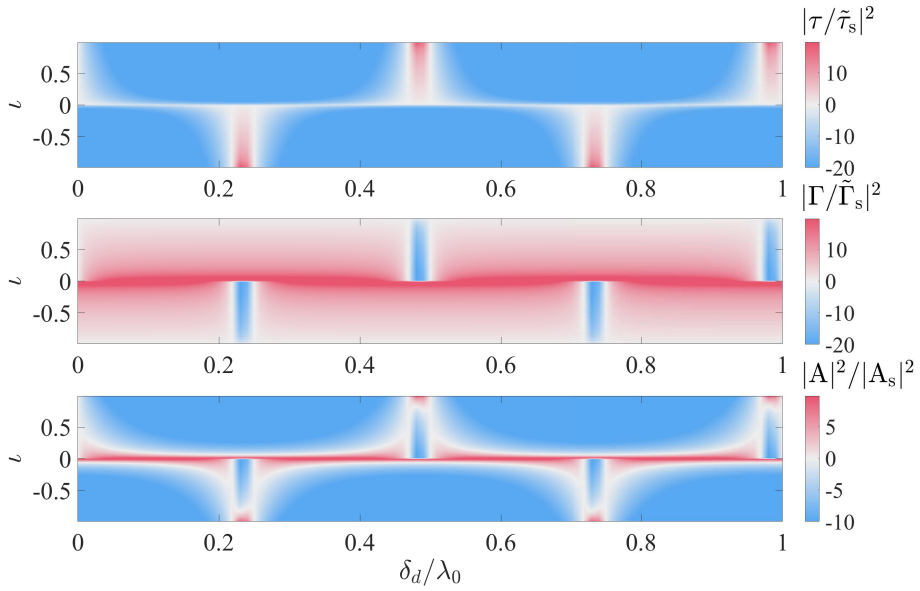

Figure 5.13. Comparision between transmission and reflection coefficients, and absorbance between the sensor inside the resonator and the sensor in free space (without the resonator). A resonator with $\mathrm{SWR} = 100$ was considered. The results are shown in dB scale.

5.4 Analysis of invisible resonators through transmission-line theory

Let us re-examine the invisibility conditions obtained in Chapter 3 for a DER in free space:

$$e^{2j\phi} = 1 \tag{5.34a}$$

$$d = \frac{n\lambda}{2} \tag{5.34b}$$

$$\tilde{Z}_{e1} = -\tilde{Z}_{e2} \tag{5.34c}$$

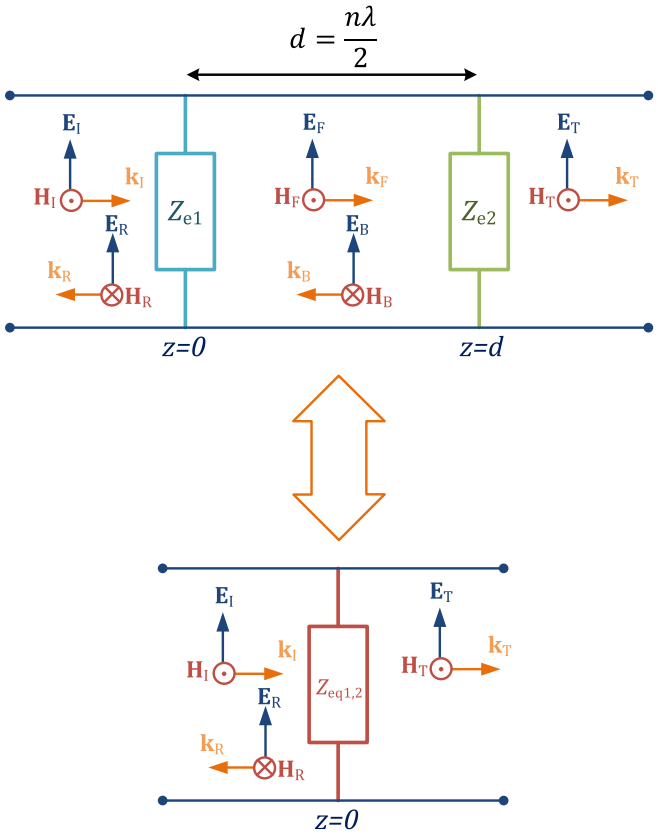

Figure 5.14. Equivalent schematics for a DER.

If we consider each metasurface as a lumped element (as in Figure 2.7a) in a transmission line, the DER will look like in Figure 5.14.

From the transmission-line theory [43], the equivalent shunt impedance of the second metasurface seen at the location of the first metasurface $\tilde{Z}_{\text{eq2}}$ can be obtained through

$$\tilde{Z}_{\text{eq2}} = \frac{\tilde{Z}_{\text{e2}} + j\tan(k_0 d)}{1 + j\tilde{Z}_{\text{e2}}\tan(k_0 d)}. \tag{5.35}$$

If we consider that the distance between the metasurfaces is the same as in (5.34b), then the equivalent impedance of the second metasurface is equal to its grid impedance ($\tilde{Z}_{\text{eq2}} = \tilde{Z}_{\text{e2}}$). Then, the equivalent normalized impedance of the whole resonator is equal to the expression

$$\tilde{Z}_{\text{eq1,2}} = \left[\frac{1}{\tilde{Z}_{\text{e1}}} + \frac{1}{\tilde{Z}_{\text{eq2}}}\right]^{-1} = \frac{\tilde{Z}_{\text{e1}}\tilde{Z}_{\text{e2}}}{\tilde{Z}_{\text{e1}} + \tilde{Z}_{\text{e2}}}. \tag{5.36}$$

If we apply the impedance condition for an invisible resonator of Equation (5.34c), then the equivalent impedance goes to infinity, like if there were nothing there. In other words, the resonator is completely invisible since its equivalent impedance goes to infinity. This result can be extended to different kinds of resonators, for example if we decide to add a third EPM, as shown in Figure 5.15.

To avoid the use of the equivalent impedance equation of (5.36), and use only

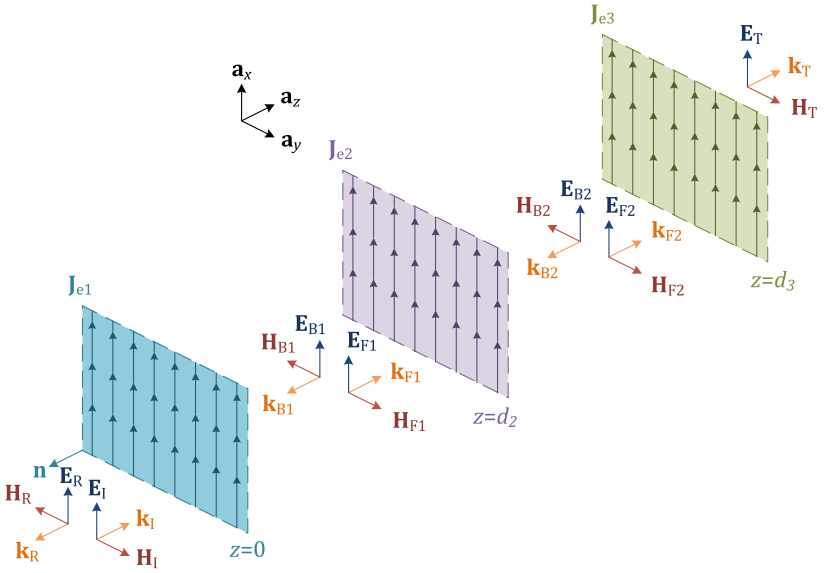

Figure 5.15. Electromagnetic fields produced by an electromagnetic wave incident onto a resonator made of three EP metasurfaces.

the grid impedance, each metasurface is placed at a distance d_i, multiple of $\lambda_0/2$. In this case, the equivalent normalized shunt admittance can be written as

$$\tilde{Y}_{\text{eq}} = \frac{1}{\tilde{Z}_{\text{eq1,2}}} = \frac{1}{\tilde{Z}_{\text{e1}}} + \frac{1}{\tilde{Z}_{\text{e2}}} + \frac{1}{\tilde{Z}_{\text{e3}}} \tag{5.37}$$

To achieve invisibility, the equivalent normalized admittance must be equal to zero, which is useful to determine the required grid impedance of one metasurface as a function of the other two:

$$\tilde{Z}_{\text{e2}} = -\frac{\tilde{Z}_{\text{e1}}\tilde{Z}_{\text{e3}}}{\tilde{Z}_{\text{e1}} + \tilde{Z}_{\text{e3}}}. \tag{5.38}$$

Notice that if we select positive grid impedances $\tilde{Z}_{\text{e1}}$ and $\tilde{Z}_{\text{e3}}$, then the grid impedance $\tilde{Z}_{\text{e2}}$ will be always negative. This result implies that there must be always metasurfaces with opposite signs (active/lossy and/or capacitive/inductive) of surface resistance and/or reactance. Using these conditions (the distance between metasurfaces and Equation (5.38)), it is possible to reduce the transfer functions

of (5.26) to

$$\Gamma = 0, \tag{5.39a}$$

$$\tau = 1, \tag{5.39b}$$

$$F_1 = 1 - \frac{1}{2\tilde{Z}_{\mathrm{e}1}}, \tag{5.39c}$$

$$B_1 = \frac{1}{2\tilde{Z}_{\mathrm{e}1}}, \tag{5.39d}$$

$$F_2 = 1 + \frac{1}{2\tilde{Z}_{\mathrm{e}2}}, \tag{5.39e}$$

$$B_2 = -\frac{1}{2\tilde{Z}_{\mathrm{e}2}}. \tag{5.39f}$$

From these transfer functions, it is possible to notice that this three-EPM resonator (or Triple Electric Resonator - TER) behaves like if two DER were put together and two adjacent metasurfaces were combined. Under this point of view, the properties of the standing waves inside each half can be understood using the analysis found in Chapter 4.

The next step is to determine how $\tilde{Z}_{\mathrm{e}1}$ and $\tilde{Z}_{\mathrm{e}2}$ affect the standing waves in each subresonator. Let us take the extreme case when $\tilde{Z}_{\mathrm{e}1} \to \infty$ (the first metasurface becomes invisible). In that case, through Equation (5.38) we can find that $\tilde{Z}_{\mathrm{e}2} = -\tilde{Z}_{\mathrm{e}3}$; which corresponds to a DER. If we do the same analysis via $\tilde{Z}_{\mathrm{e}3}$, we can choose the dynamic range of the first and third metasurfaces grid impedance are between $-\tilde{Z}_{\mathrm{e}2}$ and $-\infty$. Outside of this range, the resonator still works but the distribution of positive and negative grid impedances will change. Considering these facts, Figure 5.16 shows how the balance in the standing waves can be modified between each subresonator, considering that we fix the grid impedance $\tilde{X}_{\mathrm{e}2} = 0.101$ and use the dynamic range for the other two metasurfaces between $\tilde{X}_{\mathrm{e}1}, \tilde{X}_{\mathrm{e}3} = [-\tilde{X}_{\mathrm{e}2}; -\infty]$.

One particular scenario in Figure 5.16 is when $\tilde{X}_{\mathrm{e}1} = \tilde{X}_{\mathrm{e}3}$, where both subresonators have the same SWR. In that case, the relation between the grid impedance and the transfer functions for the standing waves can be written as

$$\tilde{Z}_{\mathrm{e}1} = \tilde{Z}_{\mathrm{e}3} = -2\tilde{Z}_{\mathrm{e}2}, \tag{5.40a}$$

$$F_1 = 1 - \frac{1}{2\tilde{Z}_{\mathrm{e}1}}, \tag{5.40b}$$

$$B_1 = \frac{1}{2\tilde{Z}_{\mathrm{e}1}}, \tag{5.40c}$$

$$F_2 = 1 + \frac{1}{2\tilde{Z}_{\mathrm{e}1}}, \tag{5.40d}$$

$$B_2 = -\frac{1}{2\tilde{Z}_{\mathrm{e}1}}. \tag{5.40e}$$

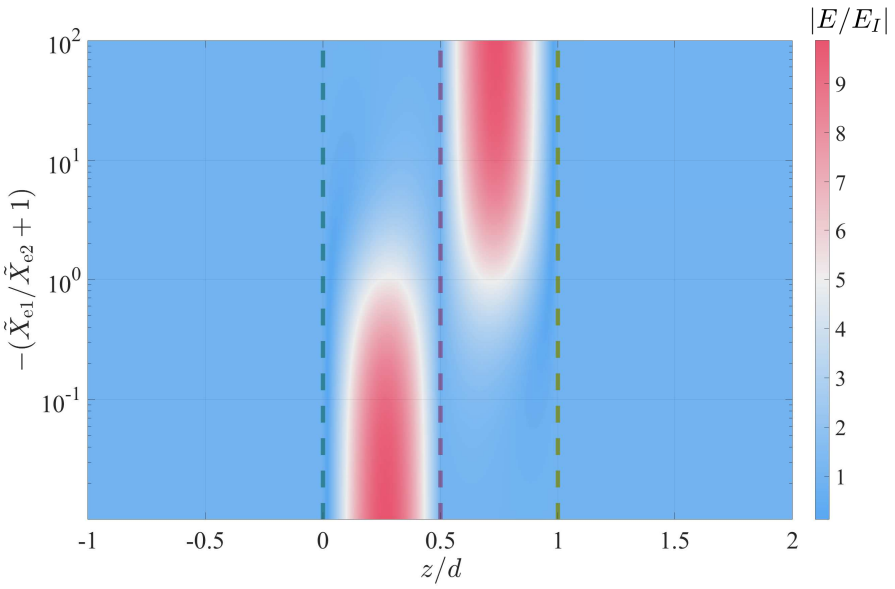

Figure 5.16. Electic field across a three-EP resonator for different combinations of $\tilde{X}_{e1}$ and $\tilde{X}_{e2}$ in the range $[-\tilde{X}_{e2}; -\infty]$ using $\tilde{X}_{e2} = 0.101$.

This specific case will be taken into account for introducing the next, and last, kind of invisible cavity resonators to be studied in this thesis.

5.5 Matryoshka-like invisible cavity resonators

The structure analysed in the previous section can also be seen as an arrangement of two resonators, where one of the metasurfaces of the first resonator overlaps with one of the second resonator. In that case, we can divide the grid impedance of the second metasurface to obtain two independent DERs. Considering that each resonator is invisible by itself, we can interchange the metasurfaces positions of the second resonator without altering the total reflection and transmission of the whole system. If the distance between the resonators is large enough, the "inner" metasurfaces (the closest ones) will start to resonate. At this point, these two metasurfaces can be seen as a resonator, and the combination of the external metasurfaces can be seen as another one. Also, each new resonator can be tuned to be invisible. In other words, this structure is equivalent to a resonator inside another one, while both maintain the invisibility conditions. This concept of placing a resonator inside another one resembles a certain Russian doll-toy. Due to that, it is convenient to call this new kind of structures as "Matryoshka-like invisible cavity resonator", abbreviated as "MLR". One representation of this novel structure is shown in Figure 5.17.

Due to the complexities involved to the analysis of a four-metasurface structure, it is convenient to choose resonators with similar properties. In this analysis,

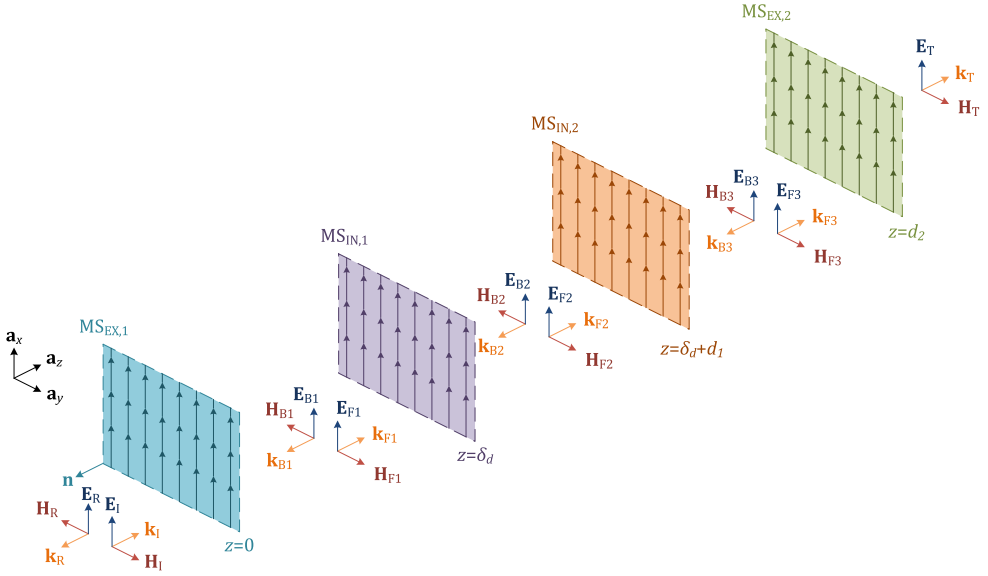

Figure 5.17. Electromagnetic fields produced by an incident electromagnetic wave into a matryoshka-like invisible resonator, using only DERs.

both resonators are based on a DER topology with the same SWR and using only reactive grid impedances. The only difference between the inner resonator and the external one is the separation between their metasurfaces, such that the inner resonator is smaller than the external one:

$$d_1 = \frac{n_1 \lambda_0}{2}, \quad \tilde{Z}_{\mathrm{IN},1} = -\tilde{Z}_{\mathrm{IN},2} = \tilde{Z}_{\mathrm{e}}, \tag{5.41a}$$

$$d_2 = \frac{n_2 \lambda_0}{2}, \quad \tilde{Z}_{\mathrm{EX},1} = -\tilde{Z}_{\mathrm{EX},2} = \tilde{Z}_{\mathrm{e}}, \tag{5.41b}$$

where n_1 and n_2 are positive integer values with the relation $n_2 > n_1$. In this case, there are only two parameters that can be used to tune the structure: the grid impedance $\tilde{Z}_{\mathrm{e}}$ and the displacement of the inner resonator compared to the external one δ_d. The transfer functions for this MLR were solved by replacing the transmission and reflection coefficients of each EPM into the T-parameter matrix of Equation (5.22) and using the i-th combined T-parameter matrix of Equation (5.24) to find out the i-th forward and backward waves. Additionally, Equations (5.25) were used to verify that this MLR has zero reflection with total zero-phase transmission.

The expression for the transfer functions are written as

$$\tau = 1, \tag{5.42a}$$

$$\Gamma = 0, \tag{5.42b}$$

$$F_1 = F_3 = 1 - \frac{1}{2\tilde{Z}_\mathrm{e}}, \tag{5.42c}$$

$$B_1 = B_3 = \frac{1}{2\tilde{Z}_\mathrm{e}}, \tag{5.42d}$$

$$F_2 = \frac{(2\tilde{Z}_\mathrm{e} - 1)^2 - e^{2jk_0\delta_d}}{4\tilde{Z}_\mathrm{e}^2}, \tag{5.42e}$$

$$B_2 = \frac{(2\tilde{Z}_\mathrm{e} - 1)e^{-2jk_0\delta_d} + 2\tilde{Z}_\mathrm{e} + 1}{4\tilde{Z}_\mathrm{e}^2}. \tag{5.42f}$$

Equations (5.42) show that the fields inside the external resonator but outside the internal one have the same transfer functions as of Equation (4.5); therefore, the behaviour of the standing waves in these two regions can be explained from the DER analysis presented in Chapter 4. Due to the invisibility properties of the inner resonators, the standing waves outside it remains unchanged as we change the position δ_d of the inner resonator inside the external one. On the other hand, the expression for the forward and backward waves inside the inner resonator are more complex, depending of the grid impedance and the resonator displacement. For this inner standing wave, it is convenient to determine its SWR:

$$\mathrm{SWR}_2 = \frac{|(2\tilde{Z}_\mathrm{e} - 1)^2 e^{-2jk_0\delta_d} - 1| + |(2\tilde{Z}_\mathrm{e} - 1)e^{-2jk_0\delta_d} + 2\tilde{Z}_\mathrm{e} + 1|}{|(2\tilde{Z}_\mathrm{e} - 1)^2 e^{-2jk_0\delta_d} - 1| - |(2\tilde{Z}_\mathrm{e} - 1)e^{-2jk_0\delta_d} + 2\tilde{Z}_\mathrm{e} + 1|}, \tag{5.43}$$

which correspond to the case where pure reactive metasurfaces were used ($\tilde{Z}_\mathrm{e} = j\tilde{X}_\mathrm{e}$).

Figure 5.18 shows the electric field distribution inside a MLR with $d_1 = \lambda_0/2$, $d_2 = 3\lambda_0/2$ and $\tilde{X}_\mathrm{e} = 0.101$, versus the position of the inner resonator δ_d. The fields inside the inner resonator increase or decrease according to the resonator displacement, and it becomes of special interest to determine the peak value of the SWR. To maximize the inner SWR, it is necessary to solve the first and second derivative of the expression found in Equation (5.43) as a function of δ_d. The locations of the maxima and minima δ_0 are

$$\delta_0 = \frac{\lambda_0}{4}\left(p - \frac{1}{\pi}\arctan\left(\frac{4\tilde{X}_\mathrm{e}}{1 - 4\tilde{X}_\mathrm{e}^2}\right)\right), \tag{5.44}$$

where p is a positive integer value and λ_0 is the resonance wavelength. Due to the complexity related to the curvature analysis, the values of p and the exact values of SWR_2 were solved numerically. For this structure, an odd p value leads to a

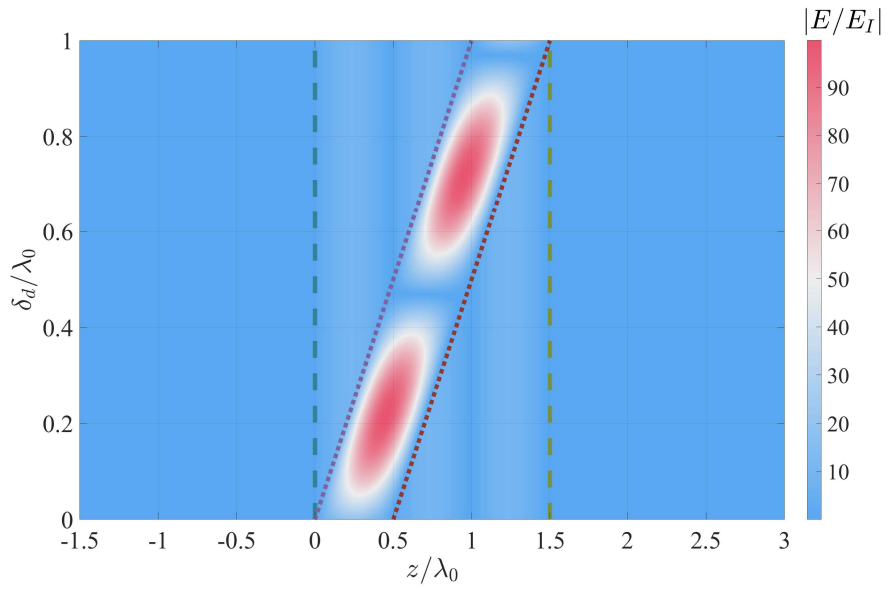

Figure 5.18. Electric field across a matryoshka-like invisible resonator as a function of the internal resonantor displacement δ_d. Both resonators were designed to have an individual $\mathrm{SWR} = 100$ ($\tilde{X}_\mathrm{e} = 0.101$).

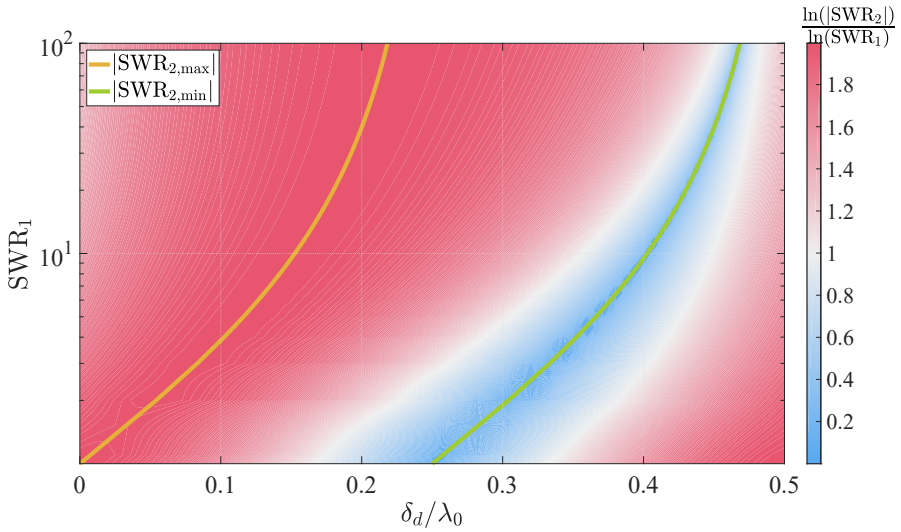

Figure 5.19. The normalized value of the internal resonator SWR as a function of the resonator displacement for different values of SWR_1. The yellow line shows where SWR_2 reaches its maximum value, likewise, the green line denotes the minima of SWR_2. Notice that this is a periodical plot (with the period $\lambda_0/2$).

SWR maxima equal to SWR_1^2, where SWR_1 is the SWR created by the external resonator. On the other hand, an even value of p leads to a minimum value of $\mathrm{SWR}_2 = 1$; the same as for a plane wave in free space.

All of these results can be sumarized as shown in Figure 5.19, where the SWR of the internal resonator SWR_2 is plotted as a function of the resonator displacement δ_d and the SWR of the external resonator SWR_1(which is the same as in the case when there is no internal resonator).

From Figure 5.19 it is possible to notice that as SWR_1 increases, the location of SWR_2 maxima (and minima) shifts to values multiples of $\lambda_0/2$. Also the region where $\mathrm{SWR}_2 > \mathrm{SWR}_1$ becomes wider as SWR_1 increases, meaning that the SWR

enhancement becomes less dependent of the inner resonator position. These results can be useful in scenarios where it is required to obtain a high-SWR resonator with metasurfaces whose grid impedances cannot be made very small.

6. Discussion and conclusions

This thesis analyses the design requirements and the properties of one-dimensional invisible cavity resonators. In the first chapters, a theoretical background was developed to characterize different kinds of metasurfaces in terms of their impedances under normal incidence. With this background, it is possible to analyse the interaction between two metasurfaces separated by a given distance, without using the generalized sheet transition conditions. Using this information, the conditions for different combinations of metasurfaces, such that there is no scattering, were obtained. For resonators with a dielectric slab, the requirements of invisibility indicate that the distance between the metasurfaces must be fixed fractions of the wavelength, while their impedances must be complex conjugate. In the case of a resonator without dielectric filling, the distance between the metasurfaces is a multiple of half of the resonance wavelength; meanwhile, the grid impedance of one metasurface must be equal to the negative of the other one.

In the fourth chapter, some characteristics of these resonators were studied, focused mostly on a double electric resonator based on pure-reactive metasurfaces. The analysis of the standing waves inside the resonator revealed that the standing wave ratio can be increased by using metasurfaces with low impedances. Additionally, it was determined how to obtain the reactance required for a specific standing wave ratio. This design rule is useful for creation of invisible resonators with regions where the electric field is enhanced or suppressed, which can be exploited for sensor enhancement or sensor cloaking. The multiple-reflections analysis revealed that as the standing wave ratio increases, the resonator requires more time to reach its steady-state regime. This analysis can be used to understand how the resonator will work in the time domain. In terms of the frequency response, it was shown that invisible cavity resonators can achieve large quality factors by increasing the standing wave ratio or the distance between the metasurface. The last sections of the fourth chapter were focused on determining the effect of metasurface losses. It was found that the resonator performance does not degrade

when metasurfaces with low level of losses are used. In terms of realistic implementations, it is shown that losses is a minor issue when the resonator is designed for the microwave range. On the other hand, for the visible and near-infrared ranges, effect of losses must be taken into account and studied separately (e.g., via full-wave simulations).

The last chapter can be divided into two parts: the interaction between a resonator with an object placed inside it, and the extension of the invisibility conditions for multiple-metasurfaces structures. In the first part, the scenario when an active source is placed inside the resonator was considered. The analysis of this case shows that the resonator can be used to improve or to decrease the matching between the source and the free space. This is done by placing the source at specific locations inside the resonator, such that it is able to radiate more or less power. Similar matching properties were found for the scenario when a lossy sheet (modelling a sensor) is placed inside the resonator. In that case, the resonator can be used to increase the harvested energy by the sensor with the disadvantage that the whole system becomes more visible. On the other hand, when the resonator is used to improve the matching of the lossy sheet, it is shown that the resonator can decrease the scattering of the sheet in order to make the whole system more invisible (compared to the same sheet in free space). In this case, the analysis reveals that the resonator creates a region where the sheet scattering can be reduced. In other words, the proposed ICR can be used as a cloaking device under certain conditions (except for extreme cases like cloaking a perfect electric conductor).

The second part of Chapter 5 developed the mathematical model for a three-metasurfaces structure, such that it can be extended for multiple-metasurfaces structure. An approach based on the transmission-line theory was used to define a triple electric resonator starting from a double electric resonator. In that case, it was shown that this resonator can be seen as two resonators placed in a cascade. Finally, this triple electric resonator was used as a basis for one specific case of a resonator made of four metasurfaces, called matryoshka-like invisible resonator, as it follows the principle of placing one resonator inside another one. The analysis of matryoshka-like resonators were focused on giving us an idea of their properties and application possibilities.

To summarize, this thesis is an attempt to explore electromagnetic properties and physical principles of invisible cavity resonators. Also, it analyses the advantages and disadvantages of these structures and some possible applications. Future work related with this thesis includes the characterization of a resonator with actual metasurfaces. In order to achieve a better understanding of these novel

structures, it is suggested to analyse alternative scenarios (e. g., oblique incidence) and to extend the previous analyses to a more general case (with two electrically and magnetically polarizable metasurfaces) or to more complex structures like matryoshka-like resonators.

Bibliography

[1] E. Abbott, *Flatland: Romance of Many Dimensions*. Roberts Brothers, 1885.

[2] R. Rucker, *The Fourth Dimension: Toward a Geometry of Higher Reality*. Dover Publications Inc., 2014.

[3] L. S. Dolin, "To the possibility of comparison of three-dimensional electromagnetic systems with non-uniform anisotropic filling," *Izvestiya Vysshikh Uchebnykh Zavedeniĭ. Radiofizika*, vol. 4, no. 5, pp. 964–967, 1961.

[4] J. B. Pendry, D. Schurig, and D. R. Smith, "Controlling electromagnetic fields," *Science*, vol. 312, no. 5781, pp. 1780–1782, 2006.

[5] U. Leonhardt, "Optical conformal mapping," *Science*, vol. 312, no. 5781, pp. 1777–1780, 2006.

[6] D. Schurig, J. J. Mock, B. J. Justice, S. A. Cummer, J. B. Pendry, A. F. Starr, and D. R. Smith, "Metamaterial Electromagnetic Cloak at Microwave Frequencies," *Science*, vol. 314, no. 5801, pp. 977–980, 2006.

[7] M. Kerker, "Invisible bodies," *J. Opt. Soc. Am.*, vol. 65, no. 4, pp. 376–379, Apr 1975.

[8] A. J. Devaney, "Nonuniqueness in the inverse scattering problem," *Journal of Mathematical Physics*, vol. 19, no. 7, pp. 1526–1531, 1978.

[9] E. Wolf and T. Habashy, "Invisible Bodies and Uniqueness of the Inverse Scattering Problem," *Journal of Modern Optics*, vol. 40, no. 5, pp. 785–792, 1993.

[10] C. W. Hsu, B. Zhen, A. D. Stone, J. D. Joannopoulos, and M. Soljačić, "Bound states in the continuum," *Nature Reviews Materials*, vol. 1, no. 9, p. 16048, jul 2016.

[11] J. von Neuman and E. Wigner, "Über merkwürdige diskrete Eigenwerte. Über das Verhalten von Eigenwerten bei adiabatischen Prozessen," *Physikalische Zeitschrift*, vol. 30, pp. 467–470, 1929.

[12] Y. Yang, C. Peng, Y. Liang, Z. Li, and S. Noda, "Analytical Perspective for Bound States in the Continuum in Photonic Crystal Slabs," *Phys. Rev. Lett.*, vol. 113, p. 037401, Jul 2014.

[13] M. V. Rybin, K. L. Koshelev, Z. F. Sadrieva, K. B. Samusev, A. A. Bogdanov, M. F. Limonov, and Y. S. Kivshar, "High-Q supercavity modes in subwavelength dielectric resonators," *Phys. Rev. Lett.*, vol. 119, p. 243901, Dec 2017.

[14] A. Albo, D. Fekete, and G. Bahir, "Electronic bound states in the continuum above (Ga,In)(As,N)/(Al,Ga)As quantum wells," *Phys. Rev. B*, vol. 85, p. 115307, Mar 2012.

[15] C. Linton and P. McIver, "Embedded trapped modes in water waves and acoustics," *Wave Motion*, vol. 45, no. 1, pp. 16 – 29, 2007, special Issue on Localization of Wave Motion.

[16] F. H. Stillinger and D. R. Herrick, "Bound states in the continuum," *Phys. Rev. A*, vol. 11, pp. 446–454, Feb 1975.

[17] V. Bortolani, A. M. Marvin, F. Nizzoli, and G. Santoro, "Theory of Brillouin scattering from surface acoustic phonons in supported films," *Journal of Physics C: Solid State Physics*, vol. 16, no. 9, p. 1757, 198.

[18] Y. Plotnik, O. Peleg, F. Dreisow, M. Heinrich, S. Nolte, A. Szameit, and M. Segev, "Experimental Observation of Optical Bound States in the Continuum," *Phys. Rev. Lett.*, vol. 107, p. 183901, Oct 2011.

[19] D. S. J. Ballantine, R. M. White, S. J. Martin, A. J. Ricco, G. C. Frye, E. T. Zellars, and H. Wohltjen, *Acoustic Wave Sensors - Theory, Design, and Physico-Chemical Applications*. Elsevier, 1997.

[20] V. Laine, *Photonic Crystals: Fabrication, Band Structure, and Applications*, ser. Physics research and technology. Nova Science Publishers, 2011.

[21] P. W. Milonni and J. H. Eberly, *Laser Physics*. John Wiley & Sons, 2010.

[22] C. Fabry and A. Perot, "Theorie et applications d' une nouvelle methods de spectroscopie intereferentielle," *Ann. Chim. Ser. 7*, vol. 16, pp. 115–144, 1899.

[23] A. Perot and C. Fabry, "On the Application of Interference Phenomena to the Solution of Various Problems of Spectroscopy and Metrology," *Astrophysical Journal*, vol. 9, p. 87, Feb. 1899.

[24] V. Kochergin, *Omnidirectional Optical Filters*, 1st ed. Springer US, 2003.

[25] W. L. Wolfe, "Fabry-Perot Interferometer Spectrometers," in *Introduction to Imaging Spectrometers*. SPIE, 1997.

[26] "Rockman X: The Day of Sigma," OVA, 2005.

[27] METAMORPHOSE VI AISBL, "Metamaterials definition," http://www.metamorphose-vi.org/index.php/metamaterials, accessed: 2018-04-19.

[28] S. A. Maier, *World Scientific Handbook of Metamaterials and Plasmonics*. World Scientific Publishing Company, 2017.

[29] C. Pfeiffer and A. Grbic, "Bianisotropic Metasurfaces for Optimal Polarization Control: Analysis and Synthesis," *Phys. Rev. Applied*, vol. 2, p. 044011, Oct 2014.

[30] S. A. Schelkunoff, "Some Equivalence Theorems of Electromagnetics and Their Application to Radiation Problems," *Bell System Technical Journal*, vol. 15, no. 1, pp. 92–112, jan 1936.

[31] S. Schelkunoff, "On Diffraction and Radiation of Electromagnetic Waves," *Physical Review*, vol. 56, no. 4, pp. 308–316, aug 1939.

[32] S. Silver, *Microwave Antenna Theory and Design*, ser. Electromagnetics and Radar Series. P. Peregrinus, 1949.

[33] K.-M. Chen, "A mathematical formulation of the equivalence principle," *IEEE Transactions on Microwave Theory and Techniques*, vol. 37, no. 10, pp. 1576–1581, 1989.

[34] C. A. Balanis, *Antenna Theory: Analysis and Design, 3rd Edition*. Wiley-Interscience, 2005.

[35] S. J. Orfanidis, *Electromagnetic Waves and Antennas*, 2010. [Online]. Available: http://eceweb1.rutgers.edu/~orfanidi/ewa/

[36] W. L. Stutzman and G. A. Thiele, *Antenna Theory and Design*. Wiley, 2012.

[37] M. Idemen and A. Serbest, "Boundary conditions of the electromagnetic field," *Electronics Letters*, vol. 23, no. 13, p. 704, 1987.

[38] S. Tretyakov, *Analytical Modeling in Applied Electromagnetics*. Artech House, 2003.

[39] S. B. Glybovski, S. A. Tretyakov, P. A. Belov, Y. S. Kivshar, and C. R. Simovski, "Metasurfaces: From microwaves to visible," *Physics Reports*, vol. 634, pp. 1–72, May 2016.

[40] N. I. Landy, S. Sajuyigbe, J. J. Mock, D. R. Smith, and W. J. Padilla, "Perfect Metamaterial Absorber," *Physical Review Letters*, vol. 100, no. 20, may 2008.

[41] K. Kurokawa, "Power Waves and the Scattering Matrix," *IEEE Transactions on Microwave Theory and Techniques*, vol. 13, no. 2, pp. 194–202, Mar 1965.

[42] D. M. Pozar, *Microwave Engineering*. J. Wiley & Sons, Inc, 2011.

[43] F. T. Ulaby, *Fundamentals of Applied Electromagnetics (5th Edition)*. Prentice Hall, 2006.

[44] K. M. McPeak, S. V. Jayanti, S. J. P. Kress, S. Meyer, S. Iotti, A. Rossinelli, and D. J. Norris, "Plasmonic Films Can Easily Be Better: Rules and Recipes," *ACS Photonics*, vol. 2, no. 3, pp. 326–333, 2015, pMID: 25950012.

[45] C. Montgomery, R. Dicke, and E. Purcell, *Principles of Microwave Circuits*, ser. Electromagnetics and Radar Series. Institution of Engineering & Technology, 1987.

[46] R. Mavaddat, *Network Scattering Parameters*, ser. Advanced series on circuits and systems. World Scientific, 1996.

[47] M. Resso and E. Bogatin, *Signal Integrity Characterization Techniques*. International Engineering Consortium, 2009.

[48] A. Khan, *Microwave Engineering: Concepts and Fundamentals*, ser. Chapman & Hall/CRC Computational Science. Taylor & Francis, 2014.

[49] M. Sassoli de Bianchi, "The Observer Effect," *Foundations of Science*, vol. 18, no. 2, pp. 213–243, Jun 2013.

[50] W. Kahn and H. Kurss, "Minimum-scattering antennas," *IEEE Transactions on Antennas and Propagation*, vol. 13, no. 5, pp. 671–675, September 1965.

[51] S. A. Tretyakov, S. Maslovski, and P. A. Belov, "An analytical model of metamaterials based on loaded wire dipoles," *IEEE Transactions on Antennas and Propagation*, vol. 51, no. 10, pp. 2652–2658, Oct 2003.

[52] A. Alù and N. Engheta, "Cloaking a Sensor," *Physical Review Letters*, vol. 102, no. 23, Jun 2009.

[53] N. Mohammadi Estakhri and A. Alù, "Minimum-scattering superabsorbers," *Phys. Rev. B*, vol. 89, p. 121416, Mar 2014.

[54] S. Tretyakov, “Maximizing Absorption and Scattering by Dipole Particles,” *Plasmonics*, vol. 9, no. 4, pp. 935–944, Aug 2014.